3

180 DEGREE DOMAIN WALLS AS A SOURCE OF MAGNETOACOUSTIC EMISSION

by

THOMAS WILLIAM ALTSHULER

B.S. Rensselaer Polytechnic Institute
(1983)

S.M. Massachusetts Institute of Technology
(1988)

Submitted to the Physics
Department in Partial Fulfillment of
the Requirements for the
Degree of

DOCTOR OF PHILOSOPHY
at the

Massachusetts Institute of Technology

August 1993

Signature of Author_____
Physics Department
August 1993

Certified by_____
Professor Robert M. Rose
Department of Material Science and Engineering
Thesis Supervisor

Accepted by_____
Professor George Koster
Chairman Graduate Comittee

180 DEGREE DOMAIN WALLS AS

A SOURCE OF MAGNETOACOUSTIC EMISSION

by

THOMAS WILLIAM ALTSHULER

Submitted to the Physics Department
on August 30, 1993 in partial fulfillment of the requirements
of the degree of Doctor of Philosophy in
Physics

ABSTRACT

Magnetoacoustic emission from 180 degree domain walls in magnetic materials is investigated. The result is a theoretical model which predicts that the 180 degree domain wall is a source of elastic radiation. This is contrary to accepted theory. The emission from a planar moving 180 degree domain wall is modeled using a micromagnetic approach to determine the spin distribution within the domain wall. The continuum spin distribution within the wall has a small component in the direction of motion of the domain wall. The component in the direction of motion is directly proportional to the velocity of the domain wall for velocities small compared to the Walker limiting velocity. Using the spin distribution, a continuum elastic model is developed where the motion of domain walls couples into the crystal lattice via magnetostriction. It is shown that the 180 degree domain wall emits elastic radiation upon acceleration. This is the necessary condition for elastic radiation, i.e., the convective derivative of the non-elastic strain is non-zero.

A transducer is developed to measure the elastic radiation from the accelerating 180 degree domain wall. The transducer is based on a Scanning Tunneling Microscope modified to have sensitivity to surface motion on the order of 10^{-12} meter with a 5 MHz bandwidth. The tunneling transducer is used to attempt to measure small shear elastic emission from domain walls in a SiFe picture frame single crystal. The magnitude of the emission based on the theoretical model developed in the thesis is approximately the same as the noise limit of the tunneling transducer. Thus no magnetoacoustic emission is measured. Experimental modifications are discussed to enhance the ability to isolate elastic radiation from a moving 180 degree domain wall.

Thesis Supervisor: Professor Robert M. Rose
Department of Materials Science and Engineering

Table of Contents

List of Figures

List of Tables

Acknowledgement

I wish to thank all the people who have contributed directly and indirectly to this thesis. There are many members of the M.I.T. community who have donated their time and equipment to enable its completion.

I would like to thank: David Robinson in the undergraduate physics laboratories for all his help over the past years. The members of the Uhlig Corrosion Laboratory for all the tid bits borrowed. The members of the graduate physics office, and especially Peggy Berkovitz for all her help. Dr. Robert O'Handely, of the Material Science and Engineering Department for helping to initiate my interest in magnetism and then supplementing my education and reading parts of the theoretical background for this thesis.

I wish to acknowledge the help of the magnetics community in assisting this research. Especially I'd like to thank: Mr. Jim Salsgiver of Allegheny Ludlum Corp. for helping me find the samples for experimentation. Dr. Robert Krause of Magnetic International for the SiFe picture frame single crystal used to test the theoretical model and the tunneling transducer.

I would like to thank the past and present members of the Specialty Material Laboratory at M.I.T. including: Louise Harrigan for all her help. My colleagues, Ron Gans and Mira Misra for their interest and contributions to my research and their friendship during the day to day existence at M.I.T. Dr. Bruce Jette for the challenge to keep up with him, and the technical assistance offered whenever I needed it. Dr. James Bellingham, who has been my friend and peer for almost all my years at M.I.T. Professor Margaret L.A. MacVicar for her constant support and dedication to me as a scientist. I wish that she was here to see the finished product.

I'd like to thank Leslie Lawrence for her unwavering dedication to Professor MacVicar's students. All of us feel that she is one of the most special people we have had the pleasure of working with. I would like to thank Dr. Kevin Rhoads for his technical assistance and friendship. His constant reassurance and advice allowed me to bring my work to a level I never thought I could reach. Thanks to all the other people working for Professor Robert Rose who were always willing to help. Professor Robert Rose for his guidance and support through the hard years of this thesis. It is no wonder that Professor MacVicar left us in his hands. There are none better at M.I.T.

Finally I would like to thank my family: To my father for permitting me to use his facility at the Advanced Materials Laboratory, and his assistance throughout my years at M.I.T. Thanks to my son Joshua for showing me what is important in life. And most of all my wonderful wife Kara, she has supported me with love throughout. She has made this thesis work tolerable. I could not have done it without her.

Chapter I: Introduction

I.1 Background

A ferromagnetic material emits elastic radiation during the magnetization process. This type of emission was first theoretically proposed and subsequently measured by Lord [1967 and 1975] and Lord et al. [1974]. Elastic radiation is a traveling stress wave propagating in an elastic medium. In general, emission of elastic radiation in any material, termed an acoustic emission because the frequency is typically in the audible or ultrasonic range, is directly related to sudden changes in the internal strain distribution of the material [Malén and Bolin 1974]. Many possible sources of elastic radiation exist in materials, e.g., dislocation motion [James and Carpenter 1971], and growth of cracks in brittle materials [Evans and Linzer 1977]. For each of these possible sources there is a local change in the internal strain field, and stress field, which emits the elastic radiation. In a magnetic material a number of possible sources of elastic radiation exist [Higgins and Carpenter 1978, Ono 1986, Jiles 1988, and Guyot and Cagan 1991]. Magnetic sources of acoustic emission are discussed in this thesis with emphasis on the emission in the initial stages of magnetization, when domain wall motion is the dominant mechanism for the magnetization process.

I.2 Magnetoacoustic Emission: Background

Lord [1967] initiated interest in acoustic emission from ferromagnetic materials during magnetization with his theoretical investigation of elastic radiation from an oscillating 180° domain wall. This theory is based on a planar 180° domain wall, a region separating two magnetic domains in which the magnetization rotates through an angle of 180°, whose amplitude modulates sinusoidally, while the wall remains spatially stationary. This is really a dynamic model for creation/annihilation because of the temporal modulation of the domain wall amplitude. Lord theorized that an oscillating, or

in his case a modulating, magnetic domain wall is a source of elastic radiation because of the changing strain field during the oscillations. The local strain field undergoes oscillations caused by a magnetoelastic coupling of the domain wall to the crystal lattice.

Lord et al. [1974] extended the theory, qualitatively, to include experimentally observed acoustic emission, referred to as magnetoacoustic emission when arising from magnetoelastic sources [Jiles 1988 and 1991], during magnetization of nickel. These later measurements were made such that isolation of elastic radiation from a unique source was not possible. The material geometry and microstructure did not permit the determination of the emission source. They concluded that since the magnetization changes discontinuously in a changing external applied magnetic field (this behavior is called the magnetic Barkhausen effect) the accompanying magnetoacoustic emissions can be attributed to the same discontinuous domain wall motion that is responsible for the Barkhausen effect.

I.3 Magnetoacoustic Emission: Models for Emission

Subsequent investigations of elastic radiation produced during magnetization of ferromagnetic materials have resulted in a number of emission models. None of these emission models accurately describe all the phenomena associated with magnetoacoustic emission. The main similarity among almost all models is that they disregard 180° domain walls as sources of magnetoacoustic emission.

I.3a Magnetoacoustic Emission: Magnetoelastic Energy Model

The most commonly used models are based on the work of Kusanagi et al. [1979a] which utilizes the conclusion by Lord et al. [1974] that magnetoacoustic emission during magnetization is caused by discontinuous domain wall motion. Kusanagi et al. attempt to determine the net change in total elastic energy, ΔE_{el}, from a

combination of magnetoelastic and elastic strain energy densities of the material before and after the discontinuous motion of a domain wall. The dynamics of domain wall motion are not included, only the net change in the magnetization is used. They postulate that at least some of the net change in total elastic energy is emitted as elastic radiation. Kusanagi et al. propose that only non-180° domain walls, a region separating two magnetic domains in which the magnetization rotates through an angle less than 180°, can contribute to the magnetoacoustic emission. This is because there is a negative net change in the total elastic energy of a magnetic material after non-180° domain wall motion in a material with cubic magnetocrystalline anisotropy, where as there is no net change in the total elastic energy for 180° domain wall motion. Kusanagi et al. have made a number of incorrect assumptions in their calculation. This work is discussed in Chapter III.2a.

Further evidence for the dismissal of 180° domain wall motion as a possible source of magnetoacoustic emission is a comparison of the intensity of elastic radiation from material with cubic magnetocrystalline anisotropy, which contain many non-180° domain walls, and uniaxial magnetocrystalline anisotropy, which contain very few non-180° domain walls. In cobalt (uniaxial), Kusanagi et al. [1979a] measure lower levels of magnetoacoustic emission than those in iron (cubic). Since there are far fewer non-180° domain walls in cobalt, they postulate that non-180° domain walls must be the source of magnetoacoustic emissions. The relative difference in the magnetoacoustic emission for cobalt and iron or nickel is not presented by Kusanagi et al. Their general conclusion, which is widely accepted, is that 180° domain walls cannot play a role in magnetoacoustic emission observed during magnetization.

In addition to the type of domain wall responsible for magnetoacoustic emission in magnetic materials, Kusanagi et al. [1979a] list a number of other predictions by their model. These include:

1) The intensity of the magnetoacoustic emissions should be related to the magnetoelastic constants and the number of energy emission sites n(H), where H is the applied magnetic field.

2) The intensity of magnetoacoustic emission should depend on both applied stress and residual stress since n(H) is dependent on these stresses.

3) The intensity of magnetoacoustic emission should depend on internal strains.

It is the relation between applied stress, internal strain and the intensity of magnetoacoustic emission that can be tested experimentally.

I.3b Magnetoacoustic Emission: Effects of Applied Stress and Internal Strain

The effects of stress on magnetoacoustic emission are reported by Kusanagi et al. [1979a and 1979b]. It was observed that, in general, increased applied stress, either tensile or compression, causes a decrease in the amplitude of the magnetoacoustic emission. Kusanagi et al. did report a maximum, or two maxima in the case of nickel, in the region close to, but not exactly at, the zero load point. Their general results have been verified by a number of authors [Ono and Shibata 1980 and 1981, Shibata and Ono 1981, Burkhardt et al. 1982, Kwan 1983, Ono 1986, Buttle et al. 1986, Edwards and Palmer 1987, Kim and Kim 1989, Namkung et al. 1989 and 1991, and Ng et al. 1992a]. Edwards and Palmer determined that some of the rapid decrease in magnetoacoustic emission could be caused by the experimental setup used to apply the external stress. The relative degree of clamping during application of the applied stress can alter the fundamental resonance frequency and the magnitude of resonance, thus altering the magnetoacoustic emission measured by a piezoelectric transducer. More recently Ng et al. have measured an increase in the magnetoacoustic emission for nickel, under tension, for applied magnetic fields both parallel and orthogonal to the applied stress.

The observed dependence of the intensity of magnetoacoustic emission on applied stress is explained using magnetoelastic energy [Jiles 1991, Kwan 1983, Edwards and

Palmer 1987, and Ng et al. 1992a]. For materials with positive magnetostriction the ratio of 180° to non-180° domain walls increases when that material is under tension. Thus the magnetoacoustic emission should decrease. Likewise for materials with negative magnetostriction the ratio of 180° to non-180° domain walls decreases when that material is under tension. So here the magnetoacoustic emission should increase (possibly the increase observed by Ng et al. [1992a]). More troubling is the effect compressive stress should have on the magnetoacoustic emission using this type of explanation. In this case, the change in non-180° domain walls is opposite to the case during tension, and thus the intensity of magnetoacoustic emission of a material under compression should change accordingly. This is not observed [Jiles 1991, Kusanagi 1979a, Ono and Shibata 1981, Burkhardt et al. 1982, Ono 1986]. The dependence of magnetoacoustic emission on applied stress is more complicated than a simple change in the relative area of non-180° to 180° domain walls. In a dynamic model of magnetoacoustic emission, the effects of the applied stress on the actual motion of domain walls is also critical. Inclusion of domain wall motion is suggested by Namkung et al [1989 and 1991] for materials under uniaxial stress.

The response of magnetoacoustic emission in materials under biaxial stress has also been investigated [Buttle et al. 1990, and Ng et al. 1992b]. In a cross shaped steel specimen, Buttle et al. report that the intensity of magnetoacoustic emission does not appear to depend directly on the level of tensile stress applied orthogonally to the applied magnetic field. This is inconsistent with a model in which non-180° domain walls are the unique source of magnetoacoustic emission at low magnetic fields. The opposite result is observed by Ng et al. [1992b]. In a cross shaped nickel specimen, in which the majority of domain walls are non-180° domain walls (actually either 71° or 109°), they report a strong dependence of magnetoacoustic emission on the level of applied stress. The difference could stem from the existence of different dominant magnetoacoustic emission mechanism in these materials with very different domain wall configurations.

The dependence of magnetoacoustic emission on internal strain is also contradictory to that hypothesized by Kusanagi et al. [1979a]. It has been determined that cold working, increasing internal strain, causes a decrease in the intensity of magnetoacoustic emission [Ono and Shibata 1981, Kwan 1983, Ono 1986, and Buttle 1986 and 1987]. On the other hand the same studies indicate that annealing increased the intensity of magnetoacoustic emission. This is inconsistent with the concept that the intensity of magnetoacoustic emission is directly proportional to the internal strain, and likewise inconsistent with the concept that the increased number of active emitting sites occurs with increased internal strain. As is shown in Chapter III.2a, Kusanagi et al. have incorrectly accounted for the internal strain. The corrected model suggests that the change in total elastic energy is not *directly* dependent on internal strain. If the volume of material involved at each individual site is increased with decreased strain, the increase in the intensity of magnetoacoustic emission upon annealing can be accounted for.

I.3c Magnetoacoustic Emission: Dynamic Inelastic Strain Model

In order to deal with the direct problems associated with the model proposed by Kusanagi et al. [1979a], Ono and Shibata [1981] have attempted to look at the emission of the elastic radiation from a dynamic point of view. This model uses an approach formulated by Malén and Bolin [1974] and Ono [1978] for acoustic emission by a moving dislocation where the equations of motion for a linear elastic media are solved after introducing an inelastic strain associated with the dislocation. Malén and Bolin determine that for a step change in inelastic strain, Δe^*, the amplitude of elastic radiation emitted should be proportional to Δe^* and the volume associated with the change. Ono and Shibata employ this dynamic model for the motion of the non-180° domain wall. They again conclude that since there is no net static Δe^* after motion of a 180° domain wall, there can be no magnetoacoustic emission from 180° domain wall. Such a

conclusion ignores any possible dynamic changes in the strain field within the 180° domain wall. This model does not specifically give information about the magnitude or functionality of the change in inelastic strain. Thus the observed effects of applied stress and residual strain can not be directly addressed.

I.3d Magnetoacoustic Emission: Creation/Annihilation Model

The model of Ono and Shibata [1981] suggests a direct relation between the Δe^* and the saturation magnetostriction constants, λ_s. Kwan [1983] and Kwan et al.[1984] conclude that depending on the type of material, and the dominant mechanisms for magnetization, the level of magnetoacoustic emission should be linear with saturation magnetostriction λ_s, in a moderate applied magnetic field. Kwan and Kwan et al. observe a linearity in nickel based alloys used in these experiments, but not in iron based alloys.

Such a relation was not observed by Guyot et al. [1990a, 1990b and 1991]. In the experiments performed by Guyot et al., yttrium iron garnet based ferrimagnetic compounds were investigated. Significant amounts of magnetoacoustic emission is reported even for a polycrystalline material with manganese substitution such that the saturation magnetostriction constant is zero. Guyot et al. propose that domain wall motion models cannot account for the observed emission from this material. In addition, they point out that the shape demagnetizing effect of the sample can significantly alter the magnetoacoustic emission. Guyot et al. [1987, 1988, 1990a, 1990b and 1991] find a direct proportionality between magnetoacoustic emission and hysteresis loss in the ferrite, amorphous and mu-metal samples. Thus Guyot et al. propose that a domain wall annihilation/creation mechanism is more appropriate as a source of magnetoacoustic emission.

Although a domain wall creation/annihilation mechanism cannot be discounted as a contributor to the magnetoacoustic emission, the conclusion that the magnetostriction coefficient does not play a role is not proven. Guyot et al. [1990a, 1990b and 1991] discount the lack of magnetoacoustic emission seen by Kwan [1983] and Kwan et al. [1984] for certain nickel-iron alloys, where λ_{100}, λ_{111} and the saturation magnetostriction coefficient, λ_s, are all zero, as an artifact of other magnetic parameters. On the other hand Guyot et al. use $Y_3Fe_{4.92}Mn_{0.08}O_{12}$ with a zero λ_s, but non-zero λ_{100} and λ_{111} [Dionne and Goodenough 1972]. It is unknown whether the value of λ_s is determined using the standard formula for an anisotropic material [Jiles 1991] or the corrected formula for polycrystalline aggregates [Callen and Goldberg 1965]. If a model for magnetoacoustic emission includes a term dependent on individual magnetostriction constants, then magnetoacoustic emission for the ferrite tested by Guyot et al. should be finite, as was found. The determination that magnetostriction does not play any role in emission of elastic radiation in a ferromagnet during magnetization is not proven by Guyot et al.

Another domain wall creation/annihilation has been proposed by Kim and Kim [1989]. This model couples the creation/annihilation of the domain wall to magnetoacoustic emission via the magnetostriction. Although the premise of the argument is not inaccurate, the method for determination of the strain field is incorrect (this is discussed in Chapter III). Thus the results of this model cannot be accepted.

I.3e Magnetoacoustic Emission: 180° Domain Wall Model

Many proposed mechanisms exist for magnetoacoustic emission in a ferromagnetic material. Other than early work by Lord [1967 and 1975], Lord et al. [1974] and Burkhardt, et al. [1982] and a more recent review by Kuleev et al. [1986], the possibility that 180° domain wall motion is a source of emission has been discounted.

Such a conclusion is based on a non-dynamic and non-realistic model of the magnetization process. A true dynamic model must include the emission by 180° domain wall motion, along with non-180° domain wall motion and domain wall creation/annihilation.

Experimental evidence suggest that 180° domain walls can cause measurable magnetoacoustic emission in single crystal silicon-iron. Kwan [1983] observed significant magnetoacoustic emission in a single crystal. She suggested that the source might be 180° domain walls. But later, in order to demonstrate that the observed magnetoacoustic emission from a single crystal is consistent with her proposal of a direct relation between the intensity of magnetoacoustic emission and saturation magnetostriction, she concludes that this is unlikely. Gorkunov et al. [1986] also measured large magnetoacoustic emission in silicon-iron oriented in the [100] direction. They observed reasonable correlation between the Barkhausen effect and magnetoacoustic emission at the early stages of magnetization. Since the majority of Barkhausen jumps at this stage of magnetization are caused by 180° domain walls, especially in their particular single crystal orientation, they concluded that the motion of 180° domain walls must be related directly to the motion of non-180° domain walls. This conclusion was drawn to overcome their difficulty in explaining how 180° domain walls could be a magnetoacoustic emission source. The claim that the 180° domain walls drag the non-180° domain walls along in the early stages of magnetization is also suggested by Namkung et al. [1991].

I.4 Scope of Thesis

This thesis extends the original calculations by Lord [1967] and Kuleev et al. [1986] to a model in which a spatially moving 180° domain wall emits elastic radiation in a ferromagnetic material. This model shows that it is the local change in the magnetization distribution within the domain wall which alters the strain field of the

domain wall. It is this change in the magnetization distribution within the domain wall, which is required for motion [Landau and Lifshitz 1935, and O'Dell 1981], that produces the magnetoacoustic emission from the 180° domain wall. The model proposed in this thesis, in which the acceleration of a 180° domain wall is a source of elastic radiation, can then be added to the list of mechanisms for magnetoacoustic emission.

In order to model the elastic radiation emitted from 180° domain wall motion, the magnetization within the domain wall is needed. Chapter II discusses models of a static 180° domain wall in the cubic material. The cubic material is chosen since attempts at experimental verification are performed on a cubic 3% SiFe single crystal. A number of inconsistencies found in the literature describing the 180° domain wall are discussed.

Chapter III is a review of the current models and descriptions of magnetoacoustic emission. This is background for Chapter IV, in which the static domain wall model developed in Chapter II is extended to a simple dynamic model for the 180° domain wall. A model for the magnetization distribution within a moving domain wall is presented. The basis of the model follows the presentation of O'Dell [1981], but extends his postulates to determine a self consistent solution to the Landau and Lifshitz equation of motion including Gilbert damping [Gilbert 1955]. The magnetization distribution derived in this thesis is shown in Appendix C to be a lower energy state than that of the Walker solution commonly used [Dillon 1963 and Schryer and Walker 1974]. The magnetization distribution is used to find the elastic interaction of the moving domain wall with the magnetic crystal. This interaction produces magnetoacoustic emission if the domain wall is accelerating.

The model presented follows the approach used by Lord [1967] and Kuleev et al. [1986]. This literature is based on a number of assumptions about the symmetry of the magnetic system and the elastic displacement vectors which are only approximate for magnetic materials containing domain walls. Both papers are based on the premise that the stress tensor is symmetric and that the rotation tensor plays no role in the magnetic

system. As pointed out by Auld [1968] and Brown [1965 and 1966], these are two of a number of incorrect assumptions commonly made when dealing with deformable ferromagnetic materials. Auld specifically deals with the elastic effects in ferrimagnetic materials undergoing electron spin resonance, but does not deal with domain walls.

Since a corrected formalism has not been attempted when modeling the dynamics of the domain wall, the accuracy of the model presented in this thesis is only approximate. But the model is of value because it introduces a clear conceptual basis for the elastic coupling of a 180° domain wall to the magnetic material which produces magnetoacoustic emission. The corrections required to accurately model the magnetoelastic coupling at the domain wall do not invalidate the conclusion made in this thesis using the simpler model that there is magnetoacoustic emission from 180° domain walls.

Experimental techniques for the measurement of magnetoacoustic emission are discussed Chapter V. The standard techniques are presented. Next the design of a high frequency tunneling acoustic emission transducer developed for this thesis is discussed. The tunneling transducer has high sensitivity to local surface motion. The transducer can detect surface motion of approximately 0.5Å at a bandwidth of greater than 5MHz before any signal processing or averaging. This sensitivity can be used with material geometries to attempt to isolate magnetoacoustic emission from 180° domain walls.

Using the tunneling transducer, the validity of the prediction that a 180° domain wall can be the source of magnetoacoustic emission is then tested experimentally by measurement of magnetoacoustic emission in an imperfect picture-frame single crystal of iron with 3% silicon. If the picture frame is perfect, the geometry isolates 180° domain walls allowing isolation of emission from other possible sources. Since the crystal is slightly out of alignment a more complex domain structure exists which can obfuscate the experimental results. The results of experimentation on SiFe presented in Chapter IV

indicate that any emission in the crystal is below limit of detection of the tunneling transducer.

In Chapter VII the consequences of the model and the experimental results are discussed along with a presentation of future experiments that should circumvent the experimental difficulties encountered in this thesis. These experiments are designed to enhance the understanding of magnetoacoustic emission in ferromagnetic materials.

Chapter II: Magnetic Domain Walls

II.1 Introduction

An investigation of the elastic interaction of a moving 180° Bloch wall in a ferromagnetic material requires, as a foundation, a theoretical description of a static Bloch wall. The Bloch wall is referred to simply as a domain wall; all other types of interdomain regions are referred to by using specific names. The theoretical aspects of this thesis employ domain wall theory, published by Landau and Lifshitz [1935], which models the statics and dynamics of magnetization in a material, using the Landau-Lifshitz equation. The Landau-Lifshitz equation can be used to determine both the static and dynamic structure of a domain wall. The use of the Landau-Lifshitz equation is discussed in greater depth in Chapter IV of this thesis.

The approach used here to model characteristics of domain walls is similar to that of O'Dell [1981]. O'Dell's postulate is expanded upon and compared to the Walker solutions to the Landau and Lifshitz equation [Dillon 1963 and Schryer and Walker 1974]. Although it is easier to determine the thickness of and magnetization distribution in a domain wall using an energy argument, by using the Landau and Lifshitz approach the dynamic characteristic of the domain wall can be found. The Landau-Lifshitz equation is needed to develop a model for the magnetization distribution within a domain wall to be employed in the modeling of emission of elastic radiation caused by the motion of a 180° domain wall. Thus the groundwork for the later calculations should be presented in this formalism.

This chapter presents the description of a 180° domain wall used in the model for magnetoacoustic emission. The appropriate magnetization distribution is determined for this domain wall. The magnetization distribution is found using a classical continuum approximation to the magnetic system. In addition, some of the fundamentals of domain wall theory are presented. This is done to elucidate a number of approximations and

assumptions made by earlier authors that are not valid. The result of these approximations and assumptions does not significantly alter the accepted structure of the domain wall [Landau and Lifshitz 1935, Kittel 1949, O'Dell 1981, and Chikazumi 1986], but does change the interpretation of the cause of the 180° domain wall in cubic materials.

II.2 Overview

The defining characteristic of a 180° domain wall is that, when static, there is no component of magnetization normal to the wall. Instead the magnetization rotates entirely within the plane of the wall (tangential to the wall). Such a domain wall configuration is experimentally observed in materials with either cubic or uniaxial magnetocrystalline anisotropy. In this thesis a material is considered as having cubic magnetocrystalline anisotropy if it has cubic crystal symmetry and thus magnetocrystalline anisotropy energy which has cubic symmetry (i.e. iron, which has body centered cubic symmetry). A material is considered to have uniaxial magnetocrystalline anisotropy if it does not have cubic crystal symmetry and thus the magnetocrystalline anisotropy energy has only one easy axis (i.e. cobalt, which has hexagonal crystal symmetry) [Chikazumi 1986]. Although cubic material is the focal point of this thesis the theoretical parts of this work also include some discussion of uniaxial material.

Lifshitz [1944] first pointed out that the energy terms needed to form a 180° domain wall in a cubic material differ from those required for a uniaxial case. A 180° domain wall in a uniaxial material can be derived with only exchange and magnetocrystalline anisotropy terms. This is not the case for the cubic crystal. The difference stems from the fact that, since cubic material has six easy, orthogonal directions, a rotation of the magnetization from an easy direction through 90° can leave the magnetization pointing in a different easy direction. The uniaxial system has only two easy directions 180° apart, so the anisotropy energy is lowest when the magnetization is

in either of the two easy directions. Uniaxial material has only one dominant domain wall configuration, the 180° domain wall, if only magnetocrystalline anisotropy energy is considered. In the cubic material the magnetocrystalline anisotropy permits the formation of either 90° or 180° domain walls. If the same approach is used to calculate the domain wall structure of cubic material, assuming an infinite, perfect crystal, as is used for the uniaxial case, the 180° domain wall is not a consistent solution to the Landau-Lifshitz equation. The only achievable solution is a 90° domain wall, with no magnetization normal to the domain wall. Such a wall is referred to as a tangential 90° domain wall. The configuration of magnetization in the vicinity of three types of domain walls is shown in Figure II.1a-c.

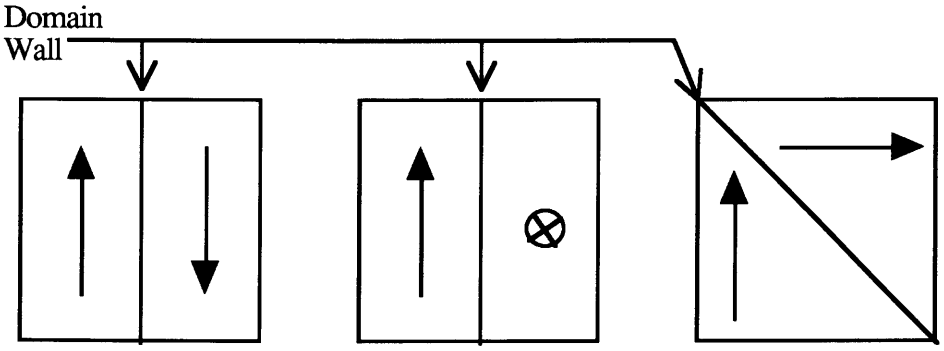

Figure 1a) Figure 1b) Figure 1c)

Figures II.1a-c. The direction of magnetization (marked by the arrow) on either side of a domain wall. 1a) The 180° domain wall with magnetization rotation in the plane of the wall. 1b) The tangential 90° domain wall with magnetization rotation in the plane of the wall. 1c) The normal 90° domain wall with a component of magnetization normal to the plane of the wall.

Observations of real cubic materials have found both tangential 180° domain walls and normal 90° domain walls [Chikazumi 1986, Kittel 1949, and Kittel and Galt 1956]. The observed static normal 90° domain wall has a component of magnetization normal to the domain wall, while the observed static 180° domain wall does not have a component

of magnetization normal to the wall. It is not immediately apparent why both tangential 90° and 180° domain walls should not exist. Details of this are presented in this chapter.

II.3 The Static Domain Wall Equilibrium Equation

A static domain wall can be modeled as an equilibrium between the total magnetic field and the magnetization of a material on a point by point basis. This method for determining the magnetic characteristics of a material is the basis of micromagnetics, first developed by Brown [1963]. The equilibrium condition is given by the Landau-Lifshitz equation for the static case,

$$\mathbf{M} \times \mathbf{H} = 0, \tag{II.1}$$

where appropriate magnetization **M** and magnetic field **H** for the system investigated in this thesis are given later in this chapter. Equation (II.1) states that the magnetic torque at any point in a medium in equilibrium must be zero. If all the appropriate contributions to the magnetic field are included in **H**, the magnetization of the medium is described by the solution of equation (II.1). An analytic solution seldom exists without approximation to the magnetic field terms. This is typically done to permit determination of the approximate magnetization distribution within the domain wall.

The standard calculation of the structure of the domain wall is to minimize energies by balancing magnetic exchange and magnetocrystalline anisotropy [Landau and Lifshitz 1935]. This approach does not use the Landau-Lifshitz equation directly. A more accurate picture must account for six magnetic energies, or when using the Landau-Lifshitz equations, the corresponding six magnetic field terms, which influence the magnetic domain wall. These fields, in addition to the two already named, are the magnetostatic self field, the magnetoelastic field, magnetic surface anisotropy, and the externally applied field [Kittel 1949, Kittel and Galt 1956, Maugin 1979, O'Dell 1981 and Scheinfein et al. 1991]. Surface anisotropy is ignored throughout this thesis.

The magnetic field terms, except the externally applied field, are typically presented in terms of magnetic energies. Each magnetic field term, $\mathbf{H}_k$, is related to the appropriate magnetic energy term as follows,

$$E_k = -\mathbf{M} \cdot \mathbf{H}_k. \tag{II.2}$$

In a ferromagnetic material the magnetic field terms, $\mathbf{H}_k$, can be determined from each magnetic energy term:

$$\mathbf{H}_k = -\frac{1}{M_s}\left(\frac{\partial E_k}{\partial \alpha_i}\right)\mathbf{i}, \tag{II.3}$$

where E_k is expressed in cartesian coordinates, M_s is the saturation magnetization, and $(\alpha_1, \alpha_2, \alpha_3)$ are the three direction cosines in the coordinate system. Equation (II.3) is valid only under the approximation that the magnetic material is rigid (no magnetic strains are permitted). In a deformable medium an additional term is present in equation (II.3) [How et al. 1989, Maugin and Miled 1986, and Motigi and Maugin 1984a and 1984b]. Appendix A describes three of the magnetic energy contributions: exchange energy, magnetocrystalline anisotropy energy, and magnetoelastic energy. The applied magnetic field, normally taken to be zero for the static wall, comes into the Landau-Lifshitz equation directly and will not be needed until domain wall dynamics is discussed in Chapter IV.

II.4 The Static Domain Wall

The domain wall is modeled as a transition layer which separates two large (compared to the domain wall) uniformly magnetized regions. The simplest model, which will be used throughout this thesis is that of an infinite material with a central x-z planar domain wall (Figure II.2). The normal to the domain wall is in the y-direction. The magnetization is M_s, taken to be in the positive z-direction at $y = -\infty$ and in the

negative z-direction at $y = +\infty$. The consequences of choosing these conditions at $\pm\infty$ will be discussed later in this chapter. The magnetization, **M**, in the static domain wall is assumed to rotate smoothly (a continuum model) only in the x-z plane from -z to +z. The continuum approximation is used to simplify the modeling of the domain wall. The dominant energy contributions in reality come from quantum mechanical spin-spin and spin-orbit interactions. But since the domain wall extends of a large number of lattice sites, these interactions can be approximated by continuous classical energy expression even though their source is purely quantum mechanical (see Appendix A).

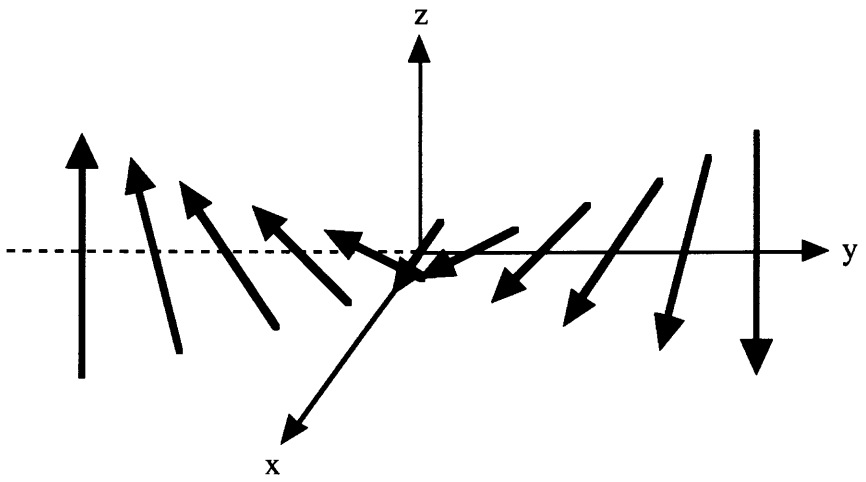

Figure II.2 The region of magnetization rotation, where **M** switches from $+M_s$ to $-M_s$ is the domain wall. Arrows represent the magnetization vector.

The magnetization is given by $M_x = M_s \sin\theta$ and $M_z = M_s \cos\theta$. There are a number of domain wall and material geometries for which there is a component of the magnetization in the normal direction to the static domain wall: i.e. the Néel wall [Malozemoff and Slonczewski 1979], at a surface where the domain wall terminates [Krinchik and Benidze 1974, Scheinfein et al. 1989 and 1991], at a closure domain

[Kittel 1949, and Kittel and Galt 1956]. These types of domain walls will not be dealt with in detail in this thesis.

II.4a The Static Domain Wall: Magnetic Field Terms

Three magnetic field terms needed to calculate the static equilibrium of the magnetization configuration, and thus domain wall structure in an infinite rigid material, can be determined using equation (II.3) and the energy terms from Appendix A. These are magnetic exchange, magnetocrystalline anisotropy and magnetostatic self energies. The magnetic exchange energy for material with cubic crystal symmetry is

$$E_{ex} = -\frac{2A}{M_s^2}\,\mathbf{M}\cdot\nabla^2\mathbf{M}\,, \tag{II.4}$$

where A is the exchange constant (this is considered a material constant) [O'Dell 1981]. This expression is a classical continuum approximation of the quantum mechanical exchange interaction which cause ferromagnetism. The exchange constant for each of the three types of cubic crystal structures is the same to within a constant which is dependent on the number and configuration of nearest neighbors to any particular atom. This expression for magnetic exchange energy is discussed in Appendix A. It should be noted that this expression and the more typical expression for exchange energy in a continuous medium are equivalent [Chikazumi 1986 and Kittel 1949]. The choice of this expression is made for convenience when applying the dynamic equations for the magnetization.

From the exchange energy given above the exchange field can be calculated:

$$\mathbf{H}_{ex} = \frac{2A}{M_s^2}\,\nabla^2\mathbf{M}\,. \tag{II.5}$$

Although the exchange field for a non-cubic crystal structure differs from that of the cubic crystal structure, the general form of the exchange field for the hexagonal crystal structure (the only non-cubic being used in this thesis) is the same as (II.5), only with a different exchange constant for each direction [Landau and Lifshitz 1982].

The magnetocrystalline anisotropy field is the second term needed to determine the structure of the domain wall. This energy can be written as a classical continuum approximation to a quantum mechanical spin-orbit interaction. Here there are significant differences between expressions for the fields of the cubic crystal and no-cubic crystal symmetries. For a cubic material the magnetocrystalline anisotropy energy to lowest (non-constant) order in the magnetization is given by

$$E_{an} = K_1 [\alpha_i^2 \alpha_j^2], \tag{II.6}$$

where K_1 is the magnetocrystalline anisotropy constant, $(\alpha_1, \alpha_2, \alpha_3)$ are the direction cosines between the actual and easy directions of magnetization, and $i \neq j$. A material with this type of magnetocrystalline anisotropy is called a cubic material in this thesis. For a material with non-cubic crystal symmetry the lowest (non-constant) order term in the magnetocrystalline anisotropy energy is given by

$$E_{an} = K_{u1} [\alpha_1^2 + \alpha_2^2], \tag{II.7}$$

where K_{u1} is the uniaxial magnetocrystalline anisotropy constant and (α_1, α_2) are direction cosines between the actual and the easy directions of magnetization, which in this case is in the 3-direction. A material with this type of magnetocrystalline anisotropy is referred to as a uniaxial material in this thesis.

From these energy terms the anisotropy fields can be calculated using equation (II.3). They are, assuming the wall geometry depicted in Figure II.2,

$$\mathbf{H}_{an} = -\frac{K_1}{M_s} \nabla_{\alpha_i} [\alpha_i^2 \alpha_j^2] \mathbf{i}, \tag{II.8}$$

for cubic ($\mathbf{i}$ is the unit vector in i-direction) and

$$\mathbf{H}_{an} = -\frac{2 K_{u1}}{M_s} [\alpha_1 \mathbf{x} + \alpha_2 \mathbf{y}], \tag{II.9}$$

for uniaxial (**x** and **y** are the unit vectors in the x- and y-directions respectively). In both these cases the anisotropy field is zero if magnetization is in an easy direction. It is typical to write the anisotropy field such that it is parallel to the easy direction in a uniaxial material [Chikazumi 1986, Jiles 1991]. But as pointed out by Landau and Lifshitz [1935] and O'Dell [1981], the representation with the anisotropy field orthogonal to an easy axis is equivalent to within a scalar constant. This representation, with H_a orthogonal to an easy axis, is used by O'Dell.

The final energy term needed to determine the structure of the domain wall is the magnetostatic self energy. This energy is the most difficult to deal with because it is non-local. The expression for the magnetostatic self field can be found from the general form of the magnetic scalar potential to be

$$\mathbf{H}_{st} = \frac{1}{4\pi} \nabla \left[\int_v \frac{\nabla \cdot \mathbf{M}}{r_{ik}} dV + \int_s \frac{\mathbf{M} \cdot \mathbf{n}}{r_{ik}} dS \right], \qquad \text{(II.10)}$$

where r_{ik} is the distance between the point of integration, i, and the point, k, where $\mathbf{H}_{st}$ is evaluated and **n** is the unit vector normal to the surface of integration [Jackson 1975, O'Dell 1981]. In the standard approach, when investigating domain walls, one attempts to choose a geometry, magnetization distribution, and surface conditions so as to eliminate the magnetostatic self field, and thus simplify the model. Landau and Lifshitz [1935] achieve this by closure domains and restrictions on the rotation of the direction of magnetization within the domain wall. They then investigate the domain wall far from the closure domains. A discussion of this is presented below for the uniaxial material. Extension to the cubic material is also presented below.

II.4b The Static Domain Wall: Closure Domains and the Infinite Crystal

Landau and Lifshitz [1935] were the first to attempt an investigation of the domain structure in a finite uniaxial material by postulating the existence of closure domains at two of the surfaces of the material (Figure II.3). The introduction of these closure domains is an attempt to minimize the magnetic energy of the crystal by eliminating the free poles on the surface, $M_n = 0$, and forcing the div(**M**) = 0 inside the material. Their model covered uniaxial materials exclusively.

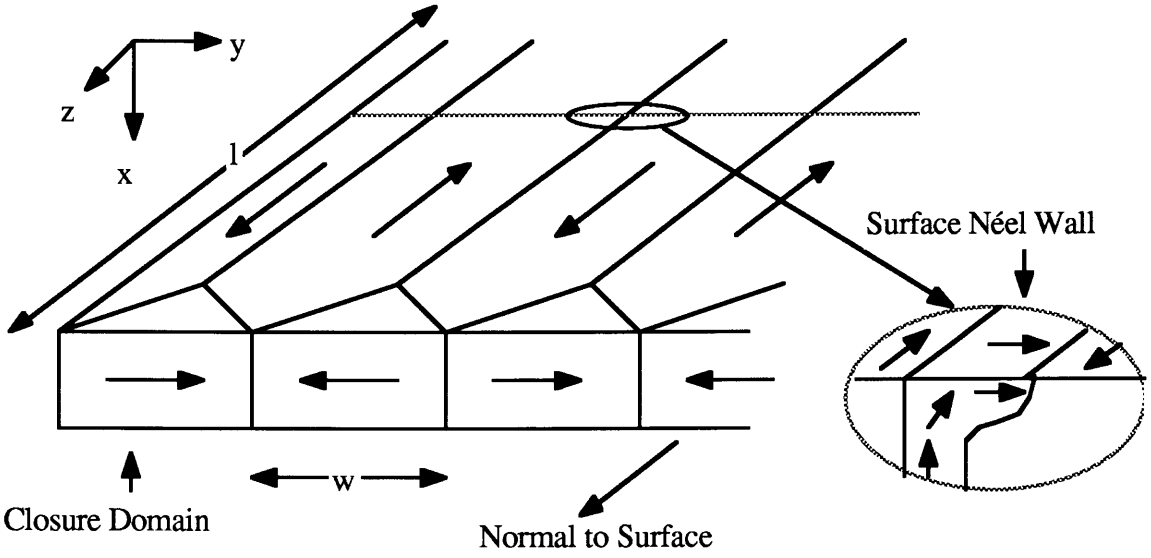

Figure II.3 Example of closure domains at the surface of a magnetic material. The closure domains assure that $M_n = 0$. The cross-sectional view is that of a surface Néel wall of the form reported by Scheinfein et al. [1989 and 1991].

From this model Landau and Lifshitz [1935] were able to estimate domain structure within the material as a function of the size of the material. They showed that the width of the long domains are proportional to the square root of their length, $w = C_1 l^{1/2}$, where C_1 is a constant, (Figure II.3). This relationship is a result of the fact that

the closure domains in the uniaxial material have a large anisotropy energy, since they are magnetized in a hard direction. The domain wall configuration is a trade-off between the energy of the domain wall and the energy of the closure domains. The number of long domains and closure domains is determined by the size of the material.

This model was extended to cubic materials by Lifshitz [1944] who postulated the existence of cubic closure domains. The closure domains in cubic materials were observed by Williams et al. [1949]. In the cubic material the closure domains are magnetized in an easy direction. Thus the closure domains are energetically favorable. Lifshitz determined that in cubic material the width of the long domains is again proportional to the square root of their length, $w = C_2 l^{1/2}$, where C_2 is a constant. But in this case it is magnetoelastic energy which limits the size of the closure domains relative to the long domains.

Lifshitz [1944] has determined that for large enough uniaxial materials a more complicated domain structure, with domain wall branching, can occur. He determined that in the uniaxial material Co, that this branch should occur as soon as the linear dimension is of the order of 10^{-5} cm. The branching is also a result of the large anisotropy energy associated with the closure domains. This type of complicated domain structure is observed in uniaxial materials [Takata 1963 and Chikazumi 1986].

A thermodynamic investigation into the existence of closure domains is reported by Privorotskii [1971 and 1976]. He claims that in a uniaxial material it is thermodynamically unstable to form closure domains of the form postulated by Landau and Lifshitz [1935]. Instead a more complicated branching structure similar to that suggested by Lifshitz [1944] and Takata [1963] must be present. In either case the magnetization distribution at the surface is such that the magnetic energy is minimized.

When the linear dimensions of the cubic material become large enough Lifshitz [1944] postulated that branching should occur in a similar manner to that predicted for

uniaxial materials. The magnetoelastic energy is the driving force for this branching. Such branch should not be observed experimentally in most real cubic materials because the relative size of the magnetoelastic energy is quite small. The predicted splitting should occur in iron when the length of a single domain exceeds 10^4 cm.

So far the model does not look at the surface of the material orthogonal to the plane of the long domain wall (a surface parallel to the y-z plane in Figure II.3). On this surface there will be a normal component of magnetization unless the magnetization distribution in the domain wall is modified from that of the domain wall far from the surface. Such a normal component has been measure in cubic materials [Krinchik and Benidze 1974] and predicted using a micromagnetic model by Scheinfein et al. [1989 and 1991] for both uniaxial and cubic materials. Scheinfein et al. [1989 and 1991] have demonstrated that the magnetization distribution undergoes a rearrangement at this surface to include a surface Néel wall to act as a microclosure, see Figure II.3. This configuration permits M_n to remain zero at the surface, but results in a non-zero div(**M**). This contributes to the total magnetostatic self field in the magnetic material.

The infinite material approximation is used in modeling the domain wall in an attempt to ignore the effects of the magnetostatic self field. The success of such a model depends on what happens to closure and branching domains in the vicinity of the surfaces as well as the surface Néel walls as the surfaces are extended to infinity. Using Landau and Lifshitz [1935] configuration for the uniaxial material and Lifshitz [1944] for the cubic material the closure domains would continue to exist, although their size would be dependent on the relationship $w = C_l l^{1/2}$. Even the branching domains located at the surface [Lifshitz 1944, Takata 1963 and Privorotskii 1971 and 1976] large would continue to exist as l approaches infinity. The same is true for the surface Néel walls, although their size does not change as that surface extends to infinity [Scheinfein 1989 and 1991 and Aharoni and Jakubovics 1991]. Thus in some materials it may be

acceptable to assume the different surfaces effects do not play a significant role in the domain wall configuration, but this is not assured. In fact the magnetostatic self field caused by the surface effects can be ignored in modeling the uniaxial material which is much thicker than the domain wall width [Scheinfein et al. 1989 and 1991]. But in the cubic material the effect of the surfaces, or more exactly the magnetostatic self field, are significant for finite materials as demonstrated by Scheinfein et al. [1989 and 1991]. As shown in this thesis this should also be the case for infinite materials.

II.4c The Static Domain Wall: Uniaxial Material

The domain wall structure for the uniaxial material is determined by the micromagnetic equilibrium condition (II.1). It is appropriate to assume, for the uniaxial material, that the magnetostatic self field does not make a significant contribution to the structure of the domain wall. For an infinite material the surfaces shown in Figure II.3 must be pushed to infinity. Doing this does not remove the surface domain structure [Landau and Lifshitz 1935] or the surface Néel walls. But in a large uniaxial material far from all surfaces, magnetostatic self field has little affect on the domain wall. The same can be concluded for the surface Néel walls. This is observed in the numerical models of Scheinfein et al. [1991] and Aharoni and Jakubovics [1991].

The magnetization distribution in the domain wall far from the closure domains and the surface Néel walls can be found if it is assumed that M_y is zero (The only non-trivial term in (II.1) is $M_xH_z - M_zH_x = 0$, where M_x and M_z are defined in Chapter II.4). H_x and H_z can be found from the magnetic field expressions (II.5) and (II.9),

$$H_x = -\frac{2K_{u1}}{M_s}\sin\theta + \frac{2A}{M_s}\frac{d^2\sin\theta}{dy^2}, \qquad \text{(II.11)}$$

and

$$H_z = \frac{2A}{M_s}\frac{d^2\cos\theta}{dy^2}, \qquad \text{(II.12)}$$

where, since **M** is only dependent on y, the Laplacian becomes a second derivative with respect to y. Using the expressions for M_x, and M_y and θ as the dependent variable, the equilibrium differential equation is determined to be

$$\frac{d^2\theta}{dy^2} - \frac{K_{u1}}{A} \sin\theta \cos\theta = 0. \tag{II.13}$$

If the substitution $d\theta/dy = u$ is made, the equation can be solved in terms of $u(\theta)$. Since the magnetization is antiparallel at $y = \pm\infty$, $d\theta/dy$ can be assumed to approach zero at $\pm\infty$. This forces the constant of integration to be zero and a simple first order differential equation can be found

$$\frac{d\theta}{dy} = \left(\frac{K_{u1}}{A}\right)^{1/2} \sin\theta. \tag{II.14}$$

Solving this for $y(\theta)$ yields

$$y = \left(\frac{A}{K_{u1}}\right)^{1/2} \ln\left(\pm \tan\left(\frac{\theta}{2}\right)\right) + C. \tag{II.15}$$

Here C, the constant of integration, is zero since at $y = 0$, $\theta = \pm \pi/2$. The general expressions for the magnetization as a function of y can be found from (II.15) to be

$$M_z = - M_s \tanh\left(\frac{y}{\Delta}\right), \tag{II.16}$$

and

$$M_x = \pm M_s \operatorname{sech}\left(\frac{y}{\Delta}\right), \tag{II.17}$$

where Δ is domain wall width parameter $(A/K_{u1})^{1/2}$. The solution has both a positive and negative sign for the values of M_x. This is because the direction of rotation (clockwise or counterclockwise) relative to the normal direction to domain wall can not be

predetermined in this geometry. Either direction is equally energetically favorable, and both solutions are physically realizable.

II.4d The Static Domain Wall: Cubic Material

The static structure of the domain wall in an infinite cubic material will be calculated in the same manner as is presented in Chapter II.4c. It is assumed that the closure domains and the surface Néel walls are far from the region in which the domain wall is being investigated and thus have little effect on the magnetization distribution. As is noted in the last section these two surface effects do not disappear if one assume that a finite material is extended to infinity [Landau and Lifshitz 1935]. For this calculation the cubic field expressions must be used. The direction cosines (α_1, α_2, α_3) are given by (sin θ, 0, cos θ). Thus the magnetic field equations are

$$H_x = -\frac{2K_1}{M_s}\sin\theta\cos^2\theta + \frac{2A}{M_s}\frac{d^2\sin\theta}{dy^2}, \tag{II.18}$$

and

$$H_z = -\frac{2K_1}{M_s}\sin^2\theta\cos\theta + \frac{2A}{M_s}\frac{d^2\cos\theta}{dy^2}. \tag{II.19}$$

These field equations can be used to find the equilibrium condition (II.1)

$$\Delta^2\frac{d^2\theta}{dy^2} + \left[\sin^3\theta\cos\theta - \sin\theta\cos^3\theta\right] = 0. \tag{II.20}$$

Using the substitution for dθ/dy the resulting linear differential equation is

$$\frac{d\theta}{dy} = \Delta^{-1}\sin\theta\cos\theta. \tag{II.21}$$

Here the integration constant is zero if the extent of the wall is finite. This equation can be solved to determine y(θ) to within a constant,

$$y = \Delta \ln (\pm \tan \theta) + C. \qquad \text{(II.22)}$$

If the condition that the domain wall is centered at $y = 0$ with the magnetization entirely in the x-direction, then the constant of integration must be infinite. A closer look at the system using the boundary conditions ($y = -\infty$, $\theta = 0$) and ($y = \infty$, that $\theta = +\pi$) helps illuminate the inconsistency. At $y = -\infty$, $\theta = 0$ forces the constant of integration to be zero. The constraint at $y = \infty$ can now only be satisfied if $\theta = \pm \pi/2$ (assuming that the rotation does not complete more than one full cycle). In other words a 180° domain wall is not the stable equilibrium configuration. Instead a tangential 90° domain wall with magnetization only in the plane of the domain wall (Figure II.1b) is formed. From a qualitative energy argument this is expected if only the exchange and magnetocrystalline anisotropy energies are considered, because as discussed earlier easy directions exist at 90° increments in the cubic crystal symmetry. Thus the lowest energy state which contains a region of rotation (a domain wall) will be one that requires the least amount of exchange energy, which is related to the amount of rotation, and falls in an easy direction because of anisotropy energy. This is the tangential 90° domain wall, not the 180° domain wall.

II.5 Effects of the Magnetoelastic Field on a Domain Wall in a Cubic Material

Lifshitz [1944] was the first to point out that it is impossible to model a 180° domain wall in an infinite cubic material using only exchange and magnetocrystalline anisotropy energies. He proposed that the observation of 180° domain walls in real materials is caused by additional energy terms in the formulation, suggesting the standard magnetoelastic and elastic strain energy. The standard magnetoelastic energy is the energy connected with the phenomenon of magnetostriction, and is based on the magnetic anisotropy energy in a deformable medium. Lifshitz continued to assume the

magnetostatic self energy is zero because of the infinite material approximation and thus plays no role in the configuration of the domain wall.

Kittel [1949] later presented a qualitative description of the effect of magnetostriction calculated by Lifshitz [1944] in a general review of the theory of domains in ferromagnetic materials. In Kittel's discussion the magnetization is constrained at the boundaries to be antiparallel. He contends that magnetostriction permits the existence of a 180° domain wall at the center of the material. Kittel then uses the strain fields determined by Lifshitz for the infinite material to calculate the structure of the domain wall. These strain fields are calculated using a number of invalid approximations; e.g., all physical quantities associated with magnetization are unidirectional, the displacement vector is related to the strain in the infinitesimal strain approximation, and the standard magnetoelastic energy is the only coupling between magnetic and elastic properties of the material. Thus conclusions drawn from these approximations are suspect.

Although magnetostriction does change the domain wall structure (a non-physical example is that of the cubic material with uniaxial anisotropy [How et al. 1989, Maugin and Miled 1986, and Motigi and Maugin 1984a and 1984b]), its addition to field expressions (II.18) and (II.19) does not insure by itself the existence of the 180° domain wall in the infinite crystal. In fact the addition of magnetoelastic energy in the uniaxial case causes the wall to contract only slightly [Maugin and Miled 1986, and Motigi and Maugin 1984a and 1984b]. It is not immediately apparent why this is different for the cubic case. Both Lifshitz's quantitative and Kittel's qualitative arguments assume that the magnetoelastic energy causes a significant change in the stable domain wall configuration for a cubic material. A review of Lifshitz's [1944] and Kittel's [1949] discussions is presented below and the consequences of the assumption made are presented.

II.5a Magnetostrictive Coalescence of the 180° Domain Wall

Lifshitz [1944] has calculated the strain field in a cubic magnetic material, in order to predict the effects magnetostriction has on a domain wall. He asserts that the strain tensor, which describes the strain field, can only be a function of the coordinate normal to the domain wall in the infinite material. The domain wall symmetry for this discussion is the same as in Figure II.2 where the y-direction is normal to the domain wall. The y dependence comes from the symmetry of the magnetic system. Using the infinitesimal strain approximation, where u_i's are the components of the displacement vector,

$$e_{ij} = \frac{1}{2}\left(\frac{\partial u_i}{\partial x_j} + \frac{\partial u_j}{\partial x_i}\right). \tag{II.23}$$

There are two standards for defining strain. The first which will be used throughout this thesis is the tensoral strain [Segel 1977] equation (II.23). The second which is in the classic work by Love [1944] defines the shear components of strain as twice the shear components given in equation (II.23). Lifshitz contends that the only non-constant components of the strain tensor are the $e_{yj}(y)$'s, which are functions only of the y coordinate. Lifshitz uses (II.23) to determine the strain tensor without any information about the magnetic state of the material, other than the restriction that the strain be a function of y only. By using the stress tensor, calculated from both elastic energies involved (standard magnetoelastic and elastic strain), the force equilibrium condition, and the requirement that the stress tensor is zero at infinity, he is able to determine that each component of the strain tensor, e_{ij}, is a constant. The values of the constants can then be determined by looking at the strain tensor an arbitrary distance from the domain wall. The conclusion that the strain tensor is a constant means that for a cubic material the strain field is independent of the existence of one or many domain walls. A complete description of Lifshitz' calculation, along with criticism is presented in Appendix B.

Recent experimental evidence suggests that there is a local strain field in the vicinity of a 180° domain wall. Mihara [1992] has observed the local strain field associated with a 180° domain wall in iron using X-ray transmission topography. The experiments were performed on 70 μm thick single crystals. This thickness is large compared to that of the domain wall and thus it is reasonable to assume that this is a bulk phenomenon. No direct measurement of deformation caused by the domain wall has been made.

The addition of the standard magnetoelastic energy, assuming the constant strain field determined by Lifshitz [1944], introduces an effective uniaxial anisotropy term into the differential equation II.18, which will be called the "magnetoelastic anisotropy". The general form of the equation is now

$$\Delta^2 \frac{d^2\theta}{dy^2} + \left[\sin^3\theta\cos\theta - \sin\theta\cos^3\theta + P\sin\theta\cos\theta\right] = 0, \qquad \text{(II.24)}$$

where P is a constant parameter for the normalized contribution of the uniaxial "magnetoelastic anisotropy" introduced by magnetoelastic effects. Solving this equation employing the same approach used in the previous sections yields

$$\frac{d\theta}{dy} = \Delta^{-1}\left[\sin^2\theta\cos^2\theta + P\sin^2\theta\right]^{1/2}. \qquad \text{(II.25)}$$

This has the solution [Gradshteyn and Ryzhik 1980]

$$y = \left(\frac{-\Delta}{2\left[1+P\right]^{1/2}}\right) \ln\left[\frac{\left[1-\frac{\sin^2\theta}{1+P}\right]^{1/2} + \cos\theta}{\left[1-\frac{\sin^2\theta}{1+P}\right]^{1/2} - \cos\theta}\right], \qquad \text{(II.26)}$$

where the integration constant is zero and the boundary conditions are satisfied. A general expressions for the components of the magnetization are then

$$M_z = M_s \left[\frac{-\left(\frac{P}{1+P}\right)^{1/2} \sinh\left(\frac{y(1+P)^{1/2}}{\Delta}\right)}{\left(1+\left(\frac{P}{1+P}\right)\sinh^2\left(\frac{y(1+P)^{1/2}}{\Delta}\right)\right)^{1/2}} \right], \tag{II.27}$$

and

$$M_x = \pm M_s \left(1+\left(\frac{P}{1+P}\right)\sinh^2\left(\frac{y(1+P)^{1/2}}{\Delta}\right)\right)^{-1/2}. \tag{II.28}$$

The magnetization distribution of the domain wall is depicted in Figures II.4a and 4b along with the magnetization distribution of a uniaxial material with the same wall width parameter, Δ. Note that the midsection of the wall exhibits an elongated region of magnetization in a direction approximately 90° to that of the domains. For Figures II.4a and 4b the value for $P = 2.4 \times 10^{-3}$, the value for iron determined by Lifshitz [1944].

There are number of weaknesses in the model Lifshitz presents. He has proposed that the strain and stress tensors depend only on the direction normal to the domain wall. This requirement is made under the assumption that the magnetization does not vary in any plane within the material which is parallel to the plane of the domain wall. This is valid only when the volume of material being investigated is an arbitrary distance from the surfaces which have closure domains or surface Néel walls. Near these surfaces, or in the infinite material at infinity, the symmetry is no longer valid, and care must be taken when determining restrictions on either the stress or strain fields there.

Lifshitz has used the force equilibrium condition, $\mathrm{div}(\sigma_{ij}) = 0$, and the surface force requirement that normal component of the stress tensor at the surfaces be zero, $n_i\sigma_{ij} = 0$, to establish restrictions on the stress tensor. The second condition, that $n_i\sigma_{ij} = 0$, does not mean that $\sigma_{ij} = 0$ at infinity as assumed by Lifshitz. Since the magnetization depends on x and z at the surfaces containing the closure domains and surface Néel walls, it is inaccurate to use the surface force restriction to determine the stress tensor at

these surfaces (or at infinity) and then apply the restriction to the y dependent stress tensor far form those surface effects. Only at $y = \pm \infty$ is the exclusive y dependence maintained. Thus it is possible to show, see Appendix B, that only five of the nine components of the stress tensor in the bulk are uniquely zero, not all the components as stated by Lifshitz [1944].

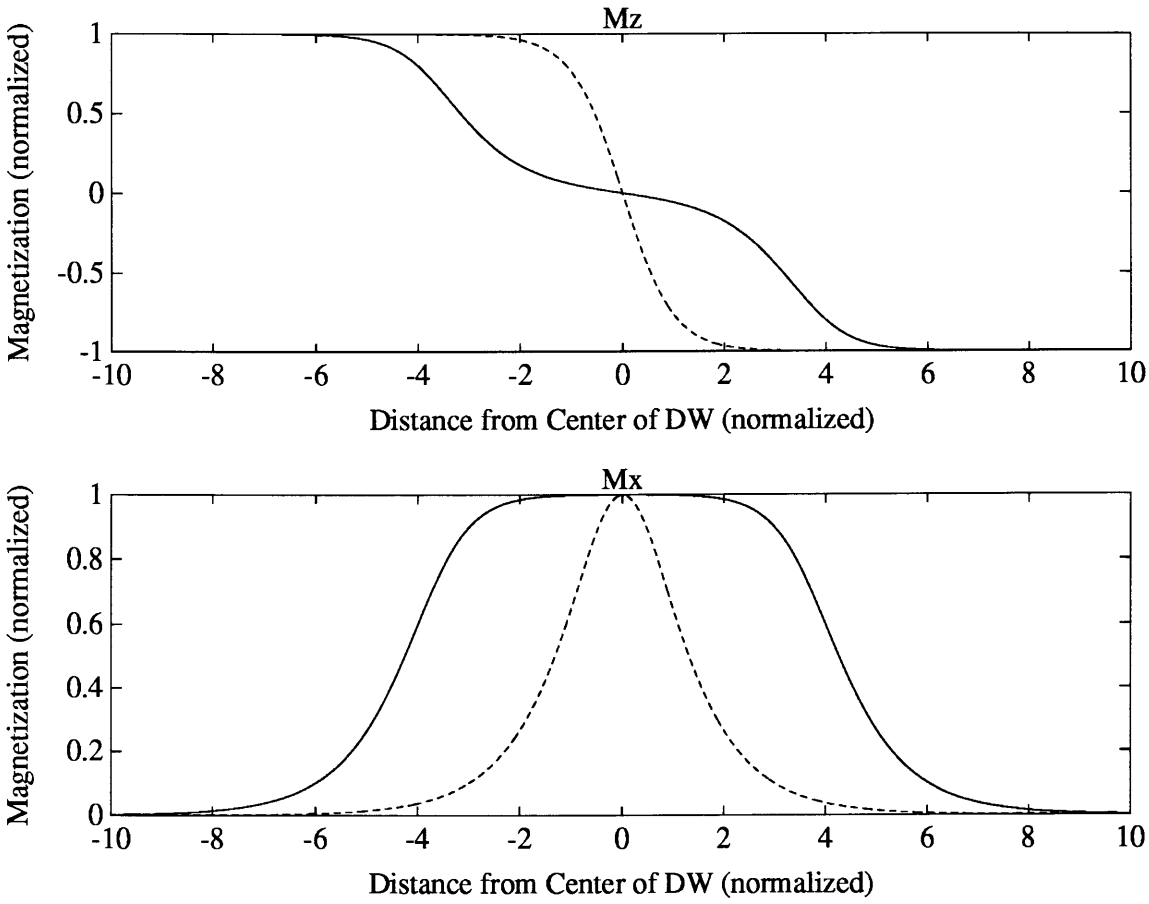

Figure II.4 Magnetization as a function of position relative to the center of the domain wall. a) The z-component of the magnetization. b) The x-component of magnetization. The solid lines are calculated for a cubic material including a uniaxial "magnetoelastic anisotropy" with $P = 2.4 \times 10^{-3}$. The dashed lines are calculated for a pure uniaxial material with the same value for the domain wall width parameter, Δ, as that of the cubic case. The distance is normalized to Δ. The magnetization is normalized to the saturation magnetization, M_s. Note the elongation of the domain wall width for the cubic material.

Lifshitz has also assumed that the infinitesimal strain approximation is valid for this system. The finite strain of a material is given by,

$$e_{ij} = \frac{1}{2}\left(\frac{\partial u_i}{\partial x_j} + \frac{\partial u_j}{\partial x_i} + \frac{\partial u_k}{\partial x_i}\frac{\partial u_k}{\partial x_j}\right). \tag{II.29}$$

Infinitesimal strain is approximately valid for small deformation [Landau and Lifshitz 1970 and Segel 1977]. In the infinite system deformation will cumulate and, as shown in Appendix B, approach infinity under the infinitesimal strain approximation, invalidating the infinitesimal strain approximation. Any conclusion using the infinitesimal strain approximation is suspect.

Brown [1966, and 1967] has suggested that since the magnetoelastic energy density is a first order function of strain (this is for a cubic material where B_1 and B_2 are constants),

$$\begin{aligned} f_{mag} = B_1 &\left[e_{xx}\left(\alpha_1^2 - \tfrac{1}{3}\right) + e_{yy}\left(\alpha_2^2 - \tfrac{1}{3}\right) + e_{zz}\left(\alpha_3^2 - \tfrac{1}{3}\right)\right] \\ &+ 2\,B_2\left[\alpha_1\,\alpha_2\,e_{xy} + \alpha_2\,\alpha_3\,e_{yz} + \alpha_1\,\alpha_3\,e_{xz}\right], \end{aligned} \tag{II.30}$$

and elastic strain energy density is second order function of strain,

$$\begin{aligned} f_{el} = \frac{c_{11}}{2}&\left(e_{xx}^2 + e_{yy}^2 + e_{zz}^2\right) + 2\,c_{44}\left(e_{xy}^2 + e_{yz}^2 + e_{zx}^2\right) \\ &c_{12}\left(e_{xx}\,e_{yy} + e_{yy}\,e_{zz} + e_{zz}\,e_{xx}\right), \end{aligned} \tag{II.31}$$

the finite strain must be used. In the elastic energy (II.31), the lowest order terms are second order in the derivatives of the displacement vector. Thus the second order term of the finite strain in equation (II.30) is of the same order as the lowest order term in (II.31). It is important to keep terms of the same order in the derivative of the displacement vector. This would mean that any calculation of equilibrium between the magnetoelastic and the elastic strain energy must initially involve finite strain.

The final aspect of Lifshitz work which must be discussed is his assumption that the only magnetic energy dependent on the strain in the material which will significantly contribute to the magnetic equilibrium of the system is the standard magnetoelastic

energy, derived from the magnetocrystalline anisotropy energy. The exchange energy is also dependent on the strain [Callen and Callen 1963 and 1965, Brown 1966 and 1967, and Turov 1965]. A more complete magnetoelastic energy density can be written as

$$f_{t-mag} = b_{jklm}\, e_{jk}\left[\frac{\partial \alpha_i}{\partial x_l}\frac{\partial \alpha_i}{\partial x_m}\right] + f_{mag}, \qquad \text{(II.32)}$$

where the coefficient of the magnetoelastic exchange term, b_{jklm}, can be simplified using the symmetry of the magnetic system investigated [Brown 1966 and 1967, and Turov 1965]. In a uniformly magnetized material the exchange term, more descriptively called the non-uniform term by Landau and Lifshitz [1986], is zero. Thus as expected the behavior is described by the standard magnetostriction.

In a material containing domain walls, the volume of domain walls makes up a small percentage of the total volume. Thus the bulk magnetoelastic behavior is dominated by the properties of the domains, where the non-uniform energy term is zero. This would also suggest that in the unsaturated magnetic material the bulk magnetoelastic properties are accurately predicted by standard magnetoelastic energies.

Within the material, in the local region surrounding the domain wall, the magnetization is very non-uniform. This suggests that the exchange term could be important. Since in the domain wall the magnitude of the exchange energy is of the same order as that of the magnetocrystalline anisotropy energy, additional contributions caused by a local strain field modification of the exchange field could quite possibly be on the same order as the magnetocrystalline anisotropy based magnetoelastic energy. The inclusion of the exchange-elastic energy in investigation of domain walls is suggested by Brown [1966].

A qualitative description of the results derived by Lifshitz [1944] has been presented by Kittel [1949] and Kittel and Galt [1956]. Kittel's discussion, in which the assumption of a uniform strain throughout the material is not assumed a priori, attempts to present a description of the effects of magnetoelasticity on the formation of the 180°

domain wall. Kittel argues that if one requires that the magnetization be in opposite directions at negative and positive infinity (presupposing the existence of a change in magnetization direction of 180°), then minimization of the magnetic energy of the system, using only exchange and magnetocrystalline anisotropy energy, requires the existence of two tangential 90° domain walls separated by an infinite distance.

In Chapter II.4d of this chapter it is shown that the model of a domain wall using only exchange and magnetocrystalline anisotropy energies yields a single tangential 90° domain wall. A second wall at infinity is constructed to match the required antiparallel magnetization. Kittel asserts that the existence of this infinite domain with magnetization orthogonal to the two domains with opposite magnetization is impossible because this adds a large amount of magnetoelastic energy to the magnetic system. Thus the crystalline stresses will force the two infinitely separated tangential 90° domain walls to coalesce into a single 180° domain wall. This model does not require any assumptions about the strain field within the material, but does require boundary conditions at $y = \pm \infty$.

The assumption that the system, without the inclusion of magnetostatic self energy, has magnetization which is already antiparallel at $\pm \infty$, an assumption that immediately forces the existence of a single tangential 90° domain wall to be impossible, is not justified. This constraint means that the system is not resting in its lowest non-uniformly magnetized energy state, assuming only exchange and magnetocrystalline anisotropy energy, but is actually constrained to have magnetization in a particular direction somewhere in the system. The only way to require this is to have an external force or an additional internal magnetic force constraining the magnetization. This additional internal magnetic force could be the result of including the effects of magnetostatic self energy in the cubic material. This is discussed in the next section

II.6 Effects of Magnetostatic Energy on the Domain Wall in a Cubic Material

The models of the domain wall discussed so far have attempted to excluded the magnetostatic self energy. The uniaxial material model predicts a reasonable size domain wall for a uniaxial material. Modeling the domain wall in a cubic material by the addition of only the magnetoelastic energy is incorrect. Magnetoelastic energy is not the dominant energy term, rather the magnetostatic self energy is responsible for the formation of the 180° domain wall in the cubic material.

Scheinfein et al. [1989 and 1991] have pointed out that in any finite cubic material a 180° domain wall is stable because of magnetostatic self energy terms from the surfaces. In this case the 180° domain wall, although a distinct region of transition, does not have the same magnetization distribution as that of the 180° domain wall in a uniaxial material. Scheinfein et al. [1989 and 1991] have numerically modeled the domain structure using a discrete magnetization array. In addition, they model the infinite cubic material by minimizing the magnetic energy of the material, including only magnetocrystalline anisotropy and exchange energies, over a finite array subject to the constraint that the magnetization is antiparallel on the two edges of the grid, parallel to the domain wall [Scheinfein et al. 1991]. This model gives a pair of tangential 90° domain walls separated by as much distance as possible in the finite array. Such a conclusion is consistent with the description presented by Kittel [1949] and Kittel and Galt [1956]. In this later calculation Scheinfein et al. [1991] have assumed that the contribution from magnetostatic self energy is zero. Yet they have introduced a constraint on the magnetization at the edges of the array. This assumption presupposes the existence of either a 180° domain wall or two 90° domain walls just as Kittel has done. The presupposition that the magnetization is antiparallel at either side of the transition region is based on the desire to model 180° domain walls which are observed experimentally.

The magnetostatic self energy plays the critical role in the formation of the 180° domain wall in both the finite and infinite cubic material. The finite geometry is the best

choice to illustrate the role the magnetostatic self energy plays in the formation of the 180° domain wall. Landau and Lifshitz [1935] first pointed out that in order to minimize the total energy of a finite material with small, but finite, magnetocrystalline anisotropy, closure domains must be present at the surfaces of the material orthogonal to the direction of magnetization. These closure domains permit both div(**M**)=0 throughout the material and $\mathbf{M}_n$=0 at the surface. In the model, which is presented for a uniaxial material, but can be extended to the cubic material, they have ignored the surfaces orthogonal to the plane of their 180° domain wall. It is these surfaces, that contain the Néel walls identified by Krinchik and Benidze [1974] and Scheinfein et al. [1989 and 1991], which act as microclosures along the 180° domain wall to minimize the magnetostatic self energy.

The extension to finite cubic material requires a re-examination of all closure domains. For a cubical block of material containing a single tangential 90° domain wall it is no longer possible to form closure domains on any of the surfaces. Thus if the tangential 90° domain wall were to exist, the magnetization would arrange itself to minimize the magnetostatic self energy. But in this case both conditions, div(**M**)=0 and $\mathbf{M}_n$=0, cannot be satisfied. The energy contribution from the finite magnetostatic self energy would be significant. Scheinfein et al. [1989 and 1991] have determined, by including magnetostatic self energy, that the type of domain wall with the lowest energy state is the 180° domain wall, not the tangential 90° domain wall. In the finite cubic material the magnetization is arranged such that closure domains exist at two surfaces, and surface Néel walls exist at two other surfaces.

The extension of the model from a finite to an infinite material is done using the same conclusion made by Landau and Lifshitz [1935] for the uniaxial material. That conclusion, which can be applied to the cubic material, is that when the surfaces of the material are expanded to infinity, the closure domains are still required to minimize the magnetostatic self energy. In other word, the closure domains and surface Néel walls do

not cease to exist. Since it is not possible to form closure domains in a material with a tangential 90° domain wall, the tangential 90° domain wall configuration has a much higher energy than that of the 180° domain wall. Thus in the infinite cubic material the 180° domain wall exists because the magnetostatic self energy contribution to the total energy is minimized.

The final question is whether the 180° domain wall can break up into two tangential 90° domain walls within the bulk of a large cubic material far from either the closure domains or the surface Néel walls. The formation of the closure domain results in a magnetostatic self energy which is *approximately* zero. Likewise the formation of surface Néel walls result in a small magnetostatic self energy contribution. In a region far from the closure domains and surface Néel walls, the magnetostatic self field is *approximately* zero. In Chapter II.4d it is shown that if magnetostatic self field is not included in the model of the domain wall that a tangential 90° domain wall forms. To account for the constraints of antiparallel magnetization at the surfaces parallel to the plane of the domain wall a pair of 90° domain walls form [Scheinfein et al. 1989 and 1991]. Such a configuration could be envisioned as two large antiparallel domains inclosing a smaller domain magnetized orthogonally to the others. The triple domain configuration could be localized in a region far from the closure domains.

For this triple domain configuration to form it must be more energetically favorable than the 180° domain wall. This configuration is not energetically favorable because in the region where the domain wall begins to split $\mathrm{div}(\mathbf{M}) \neq 0$. This then contributes to the magnetostatic self energy of the material increasing the total magnetic energy of the material. The actual 180° domain wall must be formed to balance the increase in magnetostatic self energy with the other constraints on the magnetization distribution. This balance is achieved by a 180° domain wall of a character distinct from that of the uniaxial material. This type of 180° domain wall configuration is the most energetically favorable domain wall in the infinite cubic material.

II.7 The Static Domain Wall: Cubic Material with Magnetostatic Self Energy

It is established in section II.6 that the magnetostatic self energy is required to calculate a realistic model for a 180° domain wall in an infinite cubic material. An analytic expression for the magnetization configuration of the 180° domain wall is still needed. But an exact analytic expression is impossible because of the non-local nature of the magnetostatic self field needed in the model.

Scheinfein et al. [1989 and 1991] have determined the magnetization distribution for a thin (0.5 μm.) cubic material numerically. The 180° domain wall in this model is slightly thicker than that of the uniaxial material, with the same domain wall thickness parameter Δ. Aharoni and Jakubovics [1991] have verified this numerical calculation to films greater than 1 μm. The magnetization also exhibits a distinct region at the center of the wall where there is an elongation of the domain wall width in the y-direction (Figure II.4). Such a configuration is very similar to the domain wall calculated in a cubic material when a uniaxial "magnetoelastic anisotropy" is introduced (Figure II.4), except that the size of the elongated region is much less here. A second disparity from that of the uniaxial material in the calculation by Scheinfein et al. is a slight negative magnetization, relative to the center of the domain wall, attributed to flux looping back along the edges of the domain wall. This effect is small and will not be dealt with in this thesis.

Although it is not possible to obtain an analytic expression for the 180° domain wall in a cubic material, an approximate expression can be found for which the magnetization distribution appears to be similar to that calculated by Scheinfein et al. [1991]. The 180° domain wall is modeled to be two tangential 90° domain walls trying to split but held together very closely by magnetostatic self energy. The contribution from the magnetostatic self field is approximated by an induced effective uniaxial anisotropy called the "magnetostatic anisotropy". The addition of this effective anisotropy to the

cubic material results in a magnetization distribution identical to that found by Lifshitz [1944]

$$M_z = M_s \left[\frac{-\left(\frac{P}{1+P}\right)^{1/2} \sinh\left(\frac{y(1+P)^{1/2}}{\Delta}\right)}{\left(1+\left(\frac{P}{1+P}\right)\sinh^2\left(\frac{y(1+P)^{1/2}}{\Delta}\right)\right)^{1/2}} \right], \tag{II.27}$$

and

$$M_x = \pm M_s \left(1+\left(\frac{P}{1+P}\right)\sinh^2\left(\frac{y(1+P)^{1/2}}{\Delta}\right)\right)^{-1/2}. \tag{II.28}$$

with a different value of P. Figure II.5a nd 5b is an example of the magnetization within the domain wall assuming P = 0.1. This configuration does not differ significantly from that calculated by Scheinfein et al. [1991], again ignoring the flux looping effect.
It is apparent from Figure II.5 that this 180° domain wall is very similar to that of the uniaxial material. There is a slight broadening of the domain wall at the central region. If the domain wall width parameter, Δ, is doubled for the uniaxial case, it is possible to achieve a better approximation to the cubic material 180° domain wall using the magnetization distribution (Figures II.6a and 6b).

For the remainder of this thesis this approximation for the 180° domain wall in a cubic material is used. This is done because of the desire to determine an analytic expression for the interaction of the moving 180° domain wall with the elastic strain field within an infinite cubic material. The analytic expressions for the 180° domain wall in the uniaxial material are easier to use than are the approximate analytic expressions for the 180° domain wall in the cubic material (equations II.27 and II.28).

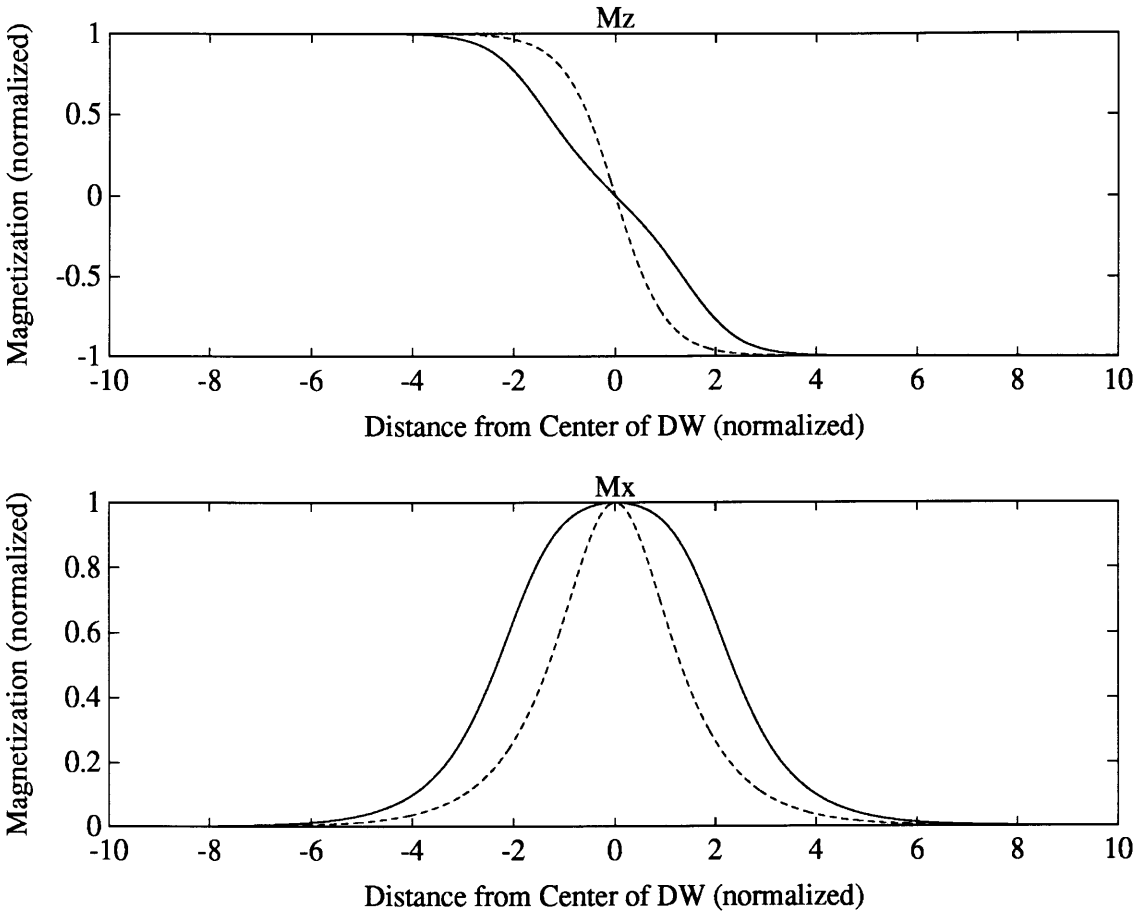

Figure II.5 Magnetization as a function of position relative to the center of the domain wall. a) The z-component of the magnetization. b) The x-component of magnetization. The solid lines are calculated for a cubic material including a uniaxial "magnetostatic anisotropy" with P = 0.1. The dashed lines are calculated for a pure uniaxial material. The distance is normalized to the domain wall width parameter, Δ. The magnetization is normalized to the saturation magnetization, M_S.

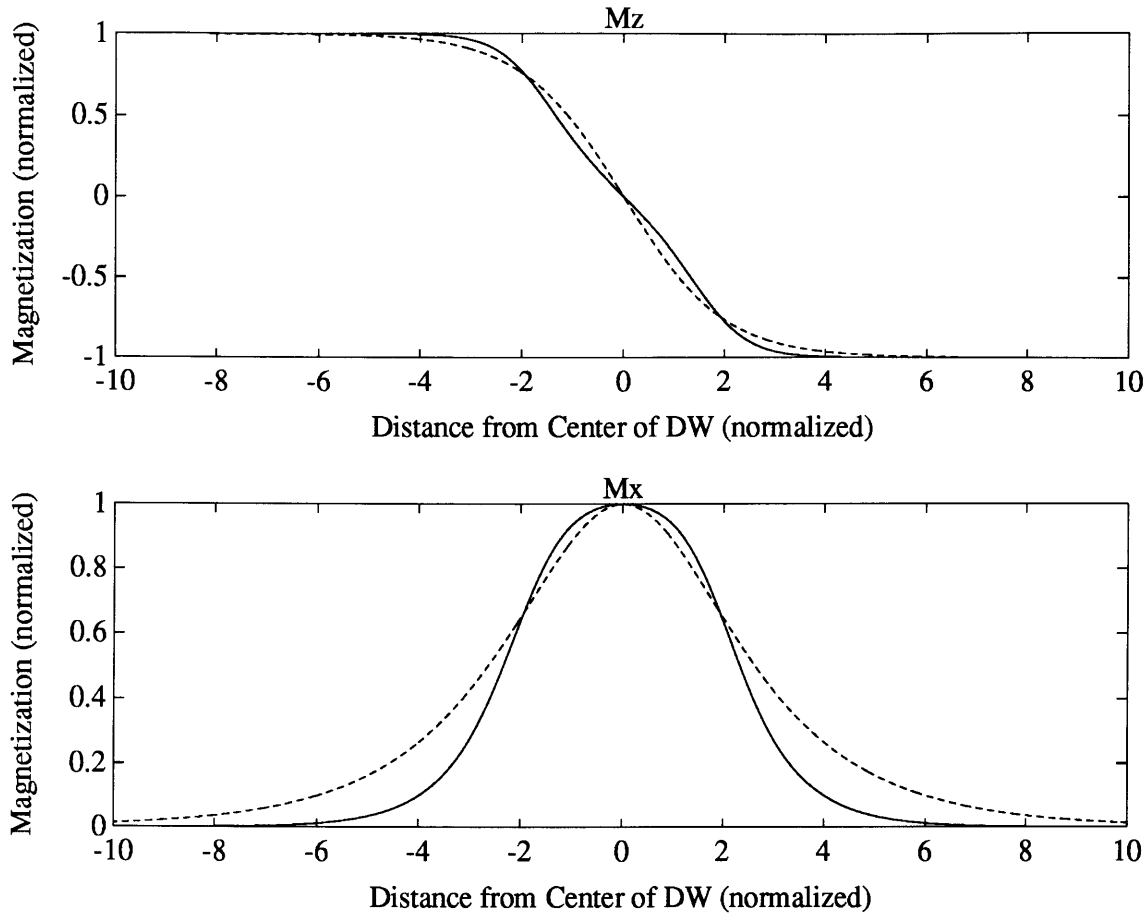

Figure II.6 Magnetization as a function of position relative to the center of the domain wall. a) The z-component of the magnetization. b) The x-component of magnetization. The solid lines are calculated for a cubic material including a uniaxial "magnetostatic anisotropy" with P = 0.1 The dashed lines are calculated for a pure uniaxial material using a domain wall width parameter, $\Delta_1 = 2\,\Delta$. The distance is normalized to the domain wall width parameter, Δ, of the cubic material. The magnetization is normalized to the saturation magnetization, M_s.

Chapter III: Elastic Radiation during Magnetization: A Review

III.1 Introduction

Magnetoacoustic emission has been attributed by most authors to the net change in the static strain field of a magnetic material due to the magnetization process [Kusanagi et al. 1979a, Ono 1986, Jiles 1988 and 1991]. This conclusion is made using a macroscopic model of the magnetization process where the net difference in the strain is determined before and after a Barkhausen jump. In using such a model it is asserted that only non-180° domain walls can be sources of magnetoacoustic emission [Kusanagi et al. 1979a]. This is a result of the assumption that only the static net change of magnetostriction can produce magnetoacoustic emission; dynamic processes are ignored. By this reasoning translation of a 180° domain wall does not result in a static net change in the magnetostriction of the material and thus cannot be an emission source. It is concluded that a non-180° domain wall can be a source of magnetoacoustic emission, since the movement of a non-180° domain wall causes a static net change in the magnetostrictive state of the magnetic material.

More recently, a number of authors have suggested other possible mechanisms for magnetoacoustic emission. Both groups [Guyot et al. 1987, 1988, 1990a, 1990, 1991, and 1993 and Kim and Kim 1989] present mechanisms which emphasize creation/annihilation of domain walls as the source of magnetoacoustic emission. These mechanisms are based on the assumption that the local strain field in the vicinity of the domain wall is the source of magnetoacoustic emission. The models suggest that creation/annihilation of a domain wall couples to the magnetic crystal elastically, resulting in a magnetoacoustic emission. Guyot et al. do not explicitly specify how the coupling takes place. But they contend that their data eliminates magnetostriction as a candidate. Kim and Kim attempt to construct a magnetostrictive model of the strain field in the vicinity of the domain wall. But their method contains several invalid assumptions.

It was postulated by Lord [1967] that a 180° domain wall oscillating at high frequency can emit elastic radiation, or a magnetoacoustic emission. This model is based on the equations of motion within an elastic medium [Lord 1967, and Landau and Lifshitz 1970]. Lord assumed that the domain wall is spatially stationary with only an amplitude modulation, thus approximating a creation/annihilation mechanism of a Curie point transition. Kuleev et al. [1986], using the similar approach as Lord, have suggested that any moving 180° domain wall should be a source of magnetoacoustic emission. In their presentation [Kuleev et al.] the equations of motion are set up but not solved. Both Lord and Kuleev et al. have made a symmetry assumption about the elastic nature of the cubic crystal. They have stated that the displacement vector is a spatial function of only the normal component to the plane of the domain wall. In order to be consistent with the required relationship between the displacement vector and the strain tensor [Brown 1966 and Love 1944], the strain tensor must have two diagonal terms that are equal to zero. In addition, they have assumed that the only magnetoelastic contribution to the energy comes from the first order correction, for infinitesimal strain, of the magnetocrystalline anisotropy energy. This assumes a symmetric stress tensor and that the rotation tensor plays no role in the elastic magnetic material.

The possibility of a non-symmetric stress tensor and the effects of the rotation tensor is discussed by Brown [1965] and Auld [1968]. Auld suggests that in the case of ferrimagnetic materials, when dealing with electron spin resonance phenomena, such assumptions are invalid. Although Auld does not directly mention ferromagnetic domain walls, similar inaccuracies in a simple magnetoelastic model exist at the domain wall. This is the case because within the domain wall the magnetization is rapidly varying spatially.

A review of the models mentioned above is presented in this chapter, concentrating on the model proposed by Kusanagi et al. [1979a] to permit an assessment of the validity of the conclusion that 180° domain walls cannot be emission sources. This

concept pervades the literature [Ono 1986, Jiles 1988 and 1991], and the Kusanagi et al. model serves as the basis.

III.2 Previous Emission Models

The four major models for magnetoacoustic emission that have been presented in the literature are discussed below. The strengths and weakness of each of the models are identified.

III.2a Previous Emission Models: Magnetoelastic Energy Model

The basic model used as a starting point for most interpretations of magnetoacoustic emission is that proposed by Kusanagi et al. [1979a]. This model looks at the difference in static elastic energies associated with a net change in the position of a single domain wall. The model does not deal directly with the motion, instead looking at the static system before and after motion. Kusanagi et al. deal with the general case where the magnetic material can be under an externally applied stress, have residual stress, or contain no residual or externally applied stress at all. The model developed by Kusanagi et al. is discussed below for the case where no externally applied or residual stresses are present.

Calculation of the net change in the total elastic energy of a magnetic material resulting from a positional change of the magnetic domain wall requires an energy expression that accurately reflects the microscopic strain field within the material. Kusanagi et al. [1979a] attempt to do this by modeling the strain field as the sum of two strain terms. The first term, which accounts for the spontaneous strain associated with magnetization and is determined by an energy minimum condition, is valid only for a uniformly magnetized region of the material, the magnetic domain. This term does not accurately represent the local strain field in the domain wall. The second term is

postulated as a local strain field, i.e. at pinning sites, which permits the domain wall to move reversibly by local flexing in an externally applied magnetic field. The local strain field is involved in the pinning of the domain wall.

Kusanagi et al. [1979a] derive the spontaneous strain field caused by magnetostriction by determining the energy contributions from the standard magnetoelastic and elastic strain energies. In most treatments, including the one presented below, the contribution of exchange elastic energy is ignored because within the domain the magnetization is essentially uniform. This is a flaw in any model that looks at elastic effects within a domain wall, where the magnetization is non-uniform. This fundamentally flawed approach is continued below to permit analysis of the models in the literature. But the validity of the computed strain field in the vicinity of the domain wall is questionable.

In a ferromagnetic material which has cubic symmetry, the standard magnetoelastic energy density is given by

$$f_{mag} = B_1\left[e_{xx}\left(\alpha_1^2 - \tfrac{1}{3}\right) + e_{yy}\left(\alpha_2^2 - \tfrac{1}{3}\right) + e_{zz}\left(\alpha_3^2 - \tfrac{1}{3}\right)\right] + 2\,B_2\left[\alpha_1\,\alpha_2\,e_{xy} + \alpha_2\,\alpha_3\,e_{yz} + \alpha_1\,\alpha_3\,e_{xz}\right], \tag{III.1}$$

where e_{ij}'s are the components of the strain tensor, and α_i's are the direction cosines of the magnetization relative to the easy axes [Chikazumi 1986]. The elastic strain energy density is give by

$$f_{el} = \frac{c_{11}}{2}\left(e_{xx}^2 + e_{yy}^2 + e_{zz}^2\right) + 2\,c_{44}\left(e_{xy}^2 + e_{yz}^2 + e_{zx}^2\right) c_{12}\left(e_{xx}\,e_{yy} + e_{yy}\,e_{zz} + e_{zz}\,e_{xx}\right), \tag{III.2}$$

where c_{11}, c_{12} and c_{44} are the elastic moduli. The total elastic energy for a volume is the volume integral of the two energy density terms,

$$E = \int_v \left(f_{el} + f_{mag}\right) dV. \tag{III.3}$$

The exchange elastic term is ignored at this time.

In the case where the magnetization is uniform, i.e. the energy density is not an explicit function of the spatial variable, which is approximately true within the domain far from any domain wall, minimization of energy with respect to strain is the same a minimizing energy density with respect to strain [Brown 1966, Weinstock 1974, and Amazigo and Rubenfeld 1980]. Thus by simply minimizing the two energy densities with respect to the strain tensor, the strain tensor can be determined:

$$\begin{aligned} e_{xx}^{s} &= \frac{3}{2}\lambda_{100}\left(\alpha_1^2 - \frac{1}{3}\right), \\ e_{yy}^{s} &= \frac{3}{2}\lambda_{100}\left(\alpha_2^2 - \frac{1}{3}\right), \\ e_{zz}^{s} &= \frac{3}{2}\lambda_{100}\left(\alpha_3^2 - \frac{1}{3}\right), \end{aligned} \tag{III.4a}$$

$$\begin{aligned} e_{xy}^{s} &= 3\,\lambda_{111}\,\alpha_1\,\alpha_2, \\ e_{yz}^{s} &= 3\,\lambda_{111}\,\alpha_2\,\alpha_3, \\ e_{xz}^{s} &= 3\,\lambda_{111}\,\alpha_1\,\alpha_3, \end{aligned} \tag{III.4b}$$

where λ_{100} and λ_{111} are the magnetostriction coefficients. This implies that $\sigma_{ij} = 0$ throughout the material since

$$\sigma_{ij} = \frac{\partial\left(f_{el} + f_{mag}\right)}{\partial e_{ij}}. \tag{III.5}$$

Kusanagi et al. [1979a] assumes that the total spontaneous strain caused by magnetostriction within the material, including within the domain walls, is given by equations (III.4). These expressions are calculated assuming uniform magnetization. If the magnetization is not uniform, as in the domain wall, the energy minimization conditions result incorrectly in the conclusion that $\sigma_{ij} = 0$, not the correct requirement that

the div(σ) = 0 [Brown 1966, and Weinstock 1974]. Thus the strain tensor calculated by Kusanagi et al. is incorrect in the vicinity of the domain wall.

A correction to the model for the uniformly magnetized material can be made by adding the effects of the local strain field in the vicinity of the domain wall. As the domain wall moves, this local strain field moves with the wall. If the magnetization within the domain wall is unchanged during motion, the local domain wall strain field is unchanged and cannot be a source of magnetoacoustic emission. Kusanagi et al.[1979a] fail to include this local domain wall strain field.

The omission of the local strain field from the calculation present by Kusanagi et al. [1979a] is a result of the incorrect use of the methods of variational calculus to determine the strain field from the total magnetic energy of the material. In order to evaluate the validity of the model presented by Kusanagi et al., it will be assumed (as is done by Kusanagi et al.) that the effects of the local domain wall strain field are very small and because the volume of the domain wall is much less than the volume swept out when the wall is moving, the relative contribution of this local strain field is also small. The approximation that the effect of the local domain wall strain field is small is in general not valid. It is shown in this thesis that it is this contribution that accounts for magnetoacoustic emission from 180° domain walls.

In the approach used by Kusanagi et al. [1979a], the total strain is then the sum of the strain field determined above (III.4), and a second contribution, e^{i}_{ij}, which accounts for an internal strain responsible for the reversible motion of the domain wall in an applied magnetic field, i.e. the domain wall pinning. Although irreversible domain wall motion is not discussed directly in this model, Kusanagi et al. imply that the model is applicable for the Barkhausen effect also. It is implicitly assumed by Kusanagi et al. that this internal strain is small compared to the spontaneous strain, i.e. that the magnitude

and volume over which this strain exists is small. The assumption that the internal strain is a perturbation permits one to add e^i_{ij} as a correction to e^s_{ij}. This gives a total strain of

$$e^t_{ij} = e^s_{ij} + e^i_{ij}. \tag{III.6}$$

In reality, if one postulates the existence of an internal strain, then the assumption that the material is a perfect crystal is no longer valid. If the internal strain is large, then the method for determining the spontaneous strain by minimizing the energy *density* with respect to spontaneous strain only is incorrect.

Kusanagi et al. [1979a] substitute the total strain fields, e^t_{ij}, into the elastic strain energy density alone (equation (III.2)). They should substitute e^t_{ij} into the total energy density, both elastic strain and standard magnetoelastic. Thus their energy expression is incorrect. Upon substitution of total strain field into the energy density it can be shown that the energy density is given by

$$\begin{aligned} f_t = {} & A_1 + A_2\left(\alpha_1^4 + \alpha_2^4 + \alpha_3^4\right) + A_3\left(\alpha_1^2\alpha_2^2 + \alpha_2^2\alpha_3^2 + \alpha_1^2\alpha_3^2\right) \\ & + \frac{c_{11}}{2}\left(e^{i}_{xx}{}^2 + e^{i}_{yy}{}^2 + e^{i}_{zz}{}^2\right) + 2\,c_{44}\left(e^{i}_{xy}{}^2 + e^{i}_{yz}{}^2 + e^{i}_{xz}{}^2\right) \\ & + c_{12}\left(e^i_{xx}\,e^i_{yy} + e^i_{yy}\,e^i_{zz} + e^i_{xx}\,e^i_{zz}\right), \end{aligned} \tag{III.7}$$

where A_1, A_2 and A_3 are constants which are related to the c_i's and λ_i's. This expression is very different from that derived by Kusanagi et al., who have a first order term in internal strain. In addition they have incorrectly assumed that the second order terms in both λ_{100} and λ_{111} are small compared to their first order terms in internal strain. In the case where a small perturbational strain is added, the energy density $f(e^t_{ij})$ can be expanded about the spontaneous strain:

$$f_t(\mathbf{e}^t) = f_t(\mathbf{e}^s) + \mathbf{e}^i \cdot \left[\frac{\partial f_t(\mathbf{e}^t)}{\partial\, \mathbf{e}^t}\right]_{\mathbf{e}^s} + \mathbf{e}^{i2} \cdot \left[\frac{\partial^2 f_t(\mathbf{e}^t)}{\partial\, \mathbf{e}^{t2}}\right]_{\mathbf{e}^s}. \tag{III.8}$$

The first order term in e^i_{ij} must be zero because of the zero stress condition used to find equations (III.4). As stated earlier, if the internal strain is not considered a small perturbation, then the whole approach of minimizing the energy density with respect to spontaneous strain only is invalid.

The availability of energy to be converted to a magnetoacoustic emission from a positional change of the domain wall can now be examined using the corrected energy density expression (III.7). The magnetization on either side of the domain wall is considered to be uniform and given by $\mathbf{M}_1$ with direction cosines (α_1, α_2, α_3), and $\mathbf{M}_2$ with direction cosines (β_1, β_2, β_3), where the magnitude on each side of the domain wall is identical. Once again ignoring the microscopic effects within the domain wall, if the domain wall is displaced such as to sweep out a volume ΔV, then the net effect of this motion is to change the magnetization from $\mathbf{M}_1$ to $\mathbf{M}_2$ in a volume ΔV of material. Since the magnetization is uniform over this volume and the strains are constant, the total change in elastic energy density is given by the difference of energy densities multiplied by the volume change, ΔV. The second order term in internal strain has no effect because it is assumed to be unchanged by the motion of the domain wall. Thus the total energy change per volume is given by

$$\begin{aligned}\frac{\Delta E}{\Delta V} = {} & A_2\left((\beta_1{}^4 - \alpha_1{}^4) + (\beta_2{}^4 - \alpha_2{}^4) + (\beta_3{}^4 - \alpha_3{}^4)\right) \\ & + A_3\left((\beta_1{}^2\beta_2{}^2 - \alpha_1{}^2\alpha_2{}^2) + (\beta_2{}^2\beta_3{}^2 - \alpha_2{}^2\alpha_3{}^2)\right) \\ & + A_3\left(\beta_1{}^2\beta_3{}^2 - \alpha_1{}^2\alpha_3{}^2\right).\end{aligned} \tag{III.9}$$

The expression for the total change in elastic energy is an even function of direction cosines. The rotation of magnetization by 180° results in (β_1, β_2, β_3) = (-α_1, -α_2, -α_3). The net change in total elastic energy for the case where a 180° domain wall is displaced is zero. In this model the 180° domain wall cannot be a source of magnetoacoustic

emission. If a non-180° domain wall is displaced, then the net change in total elastic energy is non-zero and the possibility of a magnetoacoustic emission exists.

This expression (III.9) differs from that of Kusanagi et al. [1979a] because it has leading terms that are second order in λ_{100} and λ_{111} and contains no first order term in internal strain. One criticism of the model by Kusanagi et al. is that it predicts that magnetoacoustic emission is zero if the internal strain becomes very small [Ono and Shibata 1981, Kwan 1983]. As a material is annealed, the amount of magnetoacoustic emission is observed to increase and become quite large. The model proposed by Kusanagi et al. apparently predicts the opposite effect. The energy expression given in equation (III.9) can account for this if the volume swept out by the domain wall increases with annealing. Thus this model permits the existence of magnetoacoustic emission even in well annealed materials.

The model for magnetoacoustic emission presented in equation (III.9) does have a number of shortcomings. It does not include any direct dependence on the dynamics of the domain wall, or the local strain field around the domain wall. Attempts to deal more directly with these omissions have been proposed by Ono and Shibata [1981] and Kim and Kim [1989] respectively. Ono and Shibata also predicts that the magnetoacoustic emission is dependent on the square of the magnetostriction constants, λ_{100} and λ_{111}, which suggest a stronger coupling to magnetostriction than even Kusanagi et al. [1979a] proposed. This is not observed and is a key argument for the creation/annihilation model suggested by Guyot et al. [1990a,1990b, 1991].

III.2b Previous Emission Models: Dynamic Inelastic Strain Model

The weaknesses in the original model described above led to the development of a dynamic model [Ono and Shibata 1981]. In this model the abrupt motion of a domain wall results in a change in inelastic strain Δe^*_{ij}. If one is given Δe^*_{ij}, then by using a

dynamic Green's function method [Malén and Bolin 1974 and Ono 1979], it is possible to estimate the size of the stress wave emitted. Malén and Bolin assume that the velocity change in inelastic strain occurs as a step function. They do not give any specifics about Δe^*_{ij}. They approximate the temporal step function as a Gaussian error function of magnitude Δe^*_{ij}. The Δe^*_{ij} is assumed to be spatially uniform over the volume of interest.

Ono and Shibata [1981] assume that the cause of the change in inelastic strain is exactly that concluded by Kusanagi et al. [1979a] and employ the model developed by Malén and Bolin [1974] and Ono [1979]. Now as the domain wall moves the strain function is a function of time. Thus this dynamic model is really an attempt to describe how some of the energy calculated by Kusanagi et al. is converted to magnetoacoustic emission by including its dynamic aspects. Δe^*_{ij} is not quantified but rather used as an unknown. Ono and Shibata do assume that the change in inelastic strain must be a net change before and after the domain wall moves. The inclusion of a Gaussian error function time dependence is used only to permit a dynamic approach. If one assumes that $e^*_{ij} = e^*_{ij}(\mathbf{r},t)$, then acoustic emission occurs if instantaneously

$$\frac{D\, e^*_{ij}(\mathbf{r}, t)}{D\, t} \neq 0, \tag{III.10}$$

at any point during the motion of the domain wall, even if the net $\Delta e^*_{ij} = 0$. Equation (III.10) uses the convective derivative which represents the rate of change of the inelastic strain from the point of view of an observer moving with the domain wall [Lin and Segel 1974 and Melcher 1981], where the convective derivative is defined as

$$\frac{D\, e^*_{ij}(\mathbf{r}, t)}{D\, t} = \frac{\partial\, e^*_{ij}(\mathbf{r}, t)}{\partial\, t} + \left(\frac{\partial\, \mathbf{r}}{\partial\, t} \cdot \nabla\right) e^*_{kj}(\mathbf{r}, t). \tag{III.11}$$

The use of the convective derivative simplifies the evaluation of the total strain field within the magnetic material because it allows for the assessment of the local effects in the

vicinity of the domain wall as the domain wall moves. It is the requirement of a non-vanishing convective derivative of inelastic strain which permits one to evaluate what types of domain walls are possible sources of magnetoacoustic emission.

Ono and Shibata [1981] conclude that 180° domain wall cannot be a source of magnetoacoustic emission because there is no net change in the strain field before and after the domain wall moves. Although this assumption does not explicitly include the local strain field associated with the domain wall, it does not ignore the local strain field as is done by Kusanagi et al. [1979a]. This is discussed by Kwan [1983], who suggests that the strain field around the domain wall could contribute to the change in Δe^*_{ij}. She indicates that the 180° domain wall could be a source of magnetoacoustic emission. But her conclusion is made without suggesting how the local strain field at the domain wall can contribute to Δe^*_{ij}, and is later discounted in her thesis.

III.2c Previous Emission Models: Creation/Annihilation Models

Two domain wall creation/annihilation models have been proposed to describe magnetoacoustic emission. Kim and Kim [1989] have attempted to determine the net change in inelastic strain associated with the annihilation of a 180° domain wall. Their calculation is invalid because they have mistakenly used the strain fields given by equations (III.4). These strain fields are invalid in the vicinity of the domain wall because, as discussed in chapter III.2a, their derivation is predicated upon the assumption of uniform magnetization. This is not the case in the vicinity of the domain wall.

Guyot et al. [1987, 1988, 1990a, 1990b,1991 and 1993] have proposed that a creation/annihilation mechanism is consistent with their observations of a relationship between hysteresis loss and magnetoacoustic emission. They claim that magnetoacoustic emission could contribute to the conversion of magnetic energy into heat and thus hysteresis loss in magnetic materials. Their model does not explicitly describe how the coupling between the creation/annihilation of a domain wall and magnetoacoustic

emission occurs. The model is based on experimental evidence that suggests that magnetoacoustic emission occurs at the knee of the hysteresis loop where creation/annihilation of domain walls exists. They draw support for their argument from reports that acoustic emission is caused exclusively by creation/annihilation of domain walls in ferroelectric materials [Mohamad et al. 1982 and Zammit-Mangion 1984]. Although there are some analogous behaviors between ferroelectric and ferromagnetic materials, one area where there is a significant difference is at the domain wall. The domain wall of the ferroelectric material is much narrower than that of the ferromagnetic material [Känzig 1957]. For a model based on the local strain field in the vicinity of the domain wall, the magnitude of the local strain is important, as is the volume affected. The results of Mohamad et al. and Zammit-Mangion only prove that no acoustic emission is associated with ferroelectric domain wall motion at a level detectable by their experimental equipment.

Guyot et al. [1987, 1988, 1990a, 1990b, 1991 and 1993] have measured both magnetoacoustic emission and the Barkhausen effect in polycrystalline ferromagnetic and ferrimagnetic materials. Their results, for different materials with a small shape demagnetizing effect, suggest that there is little magnetoacoustic emission in the vicinity of the coercive field, the region where most 180° domain wall activity exists. They do observe magnetoacoustic emission throughout during the entire magnetization process in single crystal ferrimagnetic disks [Guyot et al. 1987], but this is explained as an artifact of the large shape demagnetizing effect associated with this geometry. Their results do not eliminate 180° domain wall motion as a possible source, but suggest that in their polycrystalline samples a 180° domain wall mechanism is not dominant.

The dependence of magnetoacoustic emission on magnetostriction within ferromagnetic materials is also disputed by Guyot et al. [1990a, 1990b, 1991, and 1993]. They show that for a ferrimagnetic material, $Y_3Fe_{4.92}Mn_{0.08}O_{12}$, which has zero

saturation magnetostriction but non-zero λ_{100} and λ_{111} [Dionne and Goodenough 1972], magnetoacoustic emission is non-zero. They conclude that for ferromagnetic materials with zero saturation magnetostriction the same results are true, except for the material discussed by Kwan et al. [1984]. According to the model presented by Ono and Shibata [1981], the magnetoacoustic emission should be linearly related to the saturation magnetostriction. Since Kwan [1983] and Kwan et al. [1984] observe inconsistencies in the dependence of magnetoacoustic emission with saturation magnetostriction, they suggest the dependence could be on the individual magnetostriction coefficients, which are not zero for the ferrimagnet investigated by Guyot et al. If the model is based on the dynamics of the individual domain wall, the local strain field is critical and there should be some dependence on either λ_{100} and λ_{111}.

Guyot et al. [1990a, 1990b, 1991, and 1993] do point out a number of inconsistencies with their model. They predict that magnetoacoustic emission should decrease as grain size increases. The opposite relation is observed. The hysteresis loss and the magnetoacoustic emission do not track each other as a function of temperature. The biggest difficulty with the creation/annihilation model presented by Guyot et al. is that it does not give a mechanism to transfer the energy from the creation/annihilation of a domain wall directly to elastic waves within the material, especially if the dependence on magnetostriction is neglected.

III.2d Previous Emission Models: 180° Domain Wall Model

Lord [1967] theoretically predicted the existence of magnetoacoustic emission prior to any experimental measurement of the effect. His model investigates the elastic interaction of a planar 180° domain wall within a magnetic crystal. By presupposing the shape of the domain wall and modulating the amplitude of that domain wall Lord is able to show that a 180° domain wall can be a source of elastic radiation.

The approach used by Lord solves the equations of motion for the displacement vector, **U**, in the magnetic material. The equations of motion for an elastic medium are given by

$$\rho \frac{\partial^2 \mathbf{U}}{\partial t^2} = \nabla \cdot \boldsymbol{\sigma} + \mathbf{F}_b, \qquad \text{(III.12)}$$

where ρ is the density of the material, **U** is the displacement vector, $\mathbf{F}_b$ are all external body forces, and σ is the stress field tensor [Landau and Lifshitz 1970, Segel 1977, and Auld 1968, 1971 and 1990]. Lord, assuming that there are no external body forces, determines that through magnetoelastic coupling the domain wall acts as a radiation source term in the equations of motion. He postulates that **U** is a function spatially in only the normal direction to the domain wall. By modulating the domain wall by sinusoidal function $e^{i\omega t}$, he determines the magnitude of the emitted elastic radiation using a Green's function solution to the wave equation.

The approximation that **U** is a function of only one variable leads to a striking inconsistency in the model. The strain tensor which is assumed to be given by the spatial derivative of the displacement vector, equation (II.23) or (II.29), is non-zero for only the three components e_{ii}, and e_{ij}, where i is the variable for the normal direction, and j is either of the other two spatial variable. The symmetry approximation is made to simplify the equations of motion, but by invoking it the strain configuration at the domain wall can no longer match that of the domain.

Lord's model [1967] contains a number of other approximations which result from a failure to correctly include elastic effects in a deformable material. Lord has used the infinitesimal strain approximation when determining the contribution from magnetoelastic and elastic strain energy densities. The finite strains should be used to more accurately determine the energy of the magnetic system [Brown 1965 and 1966 and

Auld 1968]. In addition, Brown [1965] and Auld [1968] suggests that two other errors are typically made in most models of magnetoelastic effects. These errors are: the emission of magnetic body forces caused by nonuniform magnetization; the assumption that the stress tensor is symmetric, or that the strain tensor can be used without inclusion of the rotation tensor. Although Auld points out that in many cases, especially in a uniformly magnetized material, these errors are not significant, he does suggest that the errors can be quite large in other cases. One such instance is that of the domain wall where body forces and body torques may be present since the magnetization is highly non-uniform [Brown 1965].

Although the model proposed by Lord [1967] does predict magnetoacoustic emission from a 180° domain wall that modulated in amplitude, it does not deal with the moving domain wall. It is immediately apparent, when looking only at the region local to the domain wall how such a configuration can be the source of elastic radiation. When the modulation function of the domain wall, $e^{i\omega t}$, is zero, there is no magnetoelastic coupling at all. As the amplitude of the modulation function changes the magnetoelastic coupling changes. This is equivalent to modulating M_s. It should be note that this model does not accurately reflect the magnetization within the domains. In order to have the magnetization consistent across the domain wall, M_s within the domain must also modulate. Thus the picture present by Lord more accurately reflects the magnetoacoustic emission from a magnetic material oscillating about the Curie point.

Kuleev et al. [1986] look directly at the motion of the domain wall. In their model they assume the same symmetry as that of Lord [1967]. But they assume that the domain wall is moving at a constant velocity. The specific work deals with the motion of 90° domain walls, but comments are also presented about 180° domain walls. Kuleev et al. note that if there is displacement of the magnetization vector within the domain wall from the plain of the domain wall there should be magnetoacoustic emission. Since the

magnetic moments within a moving 180° domain wall do have a component normal to the plane of the domain wall this requirement is satisfied. But this is not the sufficient requirement to have magnetoacoustic emission from a moving domain wall. As is shown in this thesis, magnetoacoustic emission can exist only when there is a change in the inelastic strain within the magnetic material (equation III.10)

$$\frac{D\, e_{ij}^{*}(\mathbf{r}, t)}{D\, t} \neq 0, \qquad \text{(III.10)}$$

This does not occur when the 180° domain wall moves at a constant velocity. But, it does occur when the domain wall accelerates, or decelerates. Kuleev et al. do not actually calculate the emission from the moving 180° domain wall and so they do not predict this. It is shown in this thesis that the 180° domain wall can be a source of a magnetoacoustic emission only during acceleration or deceleration.

Chapter IV: Elastic Radiation Emitted by a Moving 180° Domain Wall

IV.1 Introduction

A model for the emission of a moving 180° domain wall in a perfect crystalline magnetic material with cubic symmetry is presented in this chapter, along with discussion of the models previously proposed. The model assumes an infinite, planar 180° domain wall similar to that derived by Lifshitz [1944]. In order to avoid complication in this model, the region being investigated is assumed to be far from any closure domains. The surface Néel walls are ignored because their volume is quite small relative to the volume of a domain wall for a material with thickness much larger than the thickness of the domain wall itself. Thus it is assumed that the elastic radiation from the strain fields associated with the surface Néel walls makes only a small contribution to the magnetoacoustic emission from the entire wall.

If a microscopic picture is now considered, the effects of the actual dynamics of the domain wall, which can couple into the strain field, must be included in a model for magnetoacoustic emission. When the domain wall is moving, the strain field within the crystal is also moving. In addition, as the domain wall accelerates, or decelerates, the magnetic distribution within the domain wall changes, as does the local strain field. In the case of the 180° domain wall, this change in local strain field can be a source of magnetoacoustic emission. Within a real material, which has both non-180° and 180° domain walls, both types of domain walls are sources of magnetoacoustic emission. The creation/annihilation of domain walls can also be an emission source. The relative contribution of each mechanism is thus far unknown.

The model for magnetoacoustic emission from a moving 180° domain wall presented in this chapter has a major short coming: It is based on the pre-existing models in the literature for 180° domain wall and magnetoelastic interactions in ferromagnets, and thus shares all the problematic assumptions that are previously described for each model. The model uses the same symmetry previously presented by Lord [1967] and Kuleev et

al. [1986]. The use of this symmetry results in a model that should predict only the approximate size and the shape of the magnetoacoustic emission from a single planar 180° domain wall. Also the model does not include corrections for the errors pointed out by Brown [1965] or Auld [1968] for which no one has yet published corrections of the underlying domain wall models. Still, the model presented in this thesis does suggest a mechanism by which a 180° domain wall can be an emission source. A more accurate representation requires a re-examination of the nature of magnetoelastic effects within the domain wall. This is beyond the scope of this thesis.

IV.2 Dynamic Emission Source

The original magnetoacoustic emission model presented by Lord [1967] and the later suggestions by Kuleev et al. [1986] include the elastic coupling of the domain wall to the crystal lattice. This domain wall effect is important to consider when modeling magnetoacoustic emission in a material. Microscopically, the local strain field of the domain wall, produced by an equilibrium between elastic strain and magnetoelastic energies, does move relative to the crystal. In addition, it is shown below using a simplified model that the strain field within the domain wall changes as the wall accelerates. This local changing strain field can be a source of magnetoacoustic emission.

For the domain wall calculation, it is assumed that external body forces, $\mathbf{F}_b$, are zero. The stress tensor can be written as a function of free energy density of the system (equation (III.4)). This gives, from equation (III.12), a general equation of the motion for an elastic medium of

$$\rho \frac{\partial^2 \mathbf{U}}{\partial t^2} = \nabla \cdot \frac{\partial f_t}{\partial \mathbf{e}} . \qquad \text{(IV.1)}$$

The general energy density expression, f_t, is given by the sum of the equations (III.1) and (III.2). All terms in the free energy density which are independent of the strain can be ignored for these calculations. Also any contribution from the exchange elastic energy density (equation (II.32)) is ignored for the present calculation. The general equations of motion for the three components of the displacement vector can then be determined:

$$\rho \frac{\partial^2 U_x}{\partial t^2} = \frac{\partial \left[B_1 \left({\alpha_1}^2 - \frac{1}{3} \right) + c_{11} e_{xx} + c_{12} \left(e_{yy} + e_{zz} \right) \right]}{\partial x} + \frac{\partial \left[B_2 \alpha_1 \alpha_2 + c_{44} e_{xy} \right]}{\partial y} + \frac{\partial \left[B_2 \alpha_1 \alpha_3 + c_{44} e_{xz} \right]}{\partial z}, \tag{IV.2a}$$

$$\rho \frac{\partial^2 U_y}{\partial t^2} = \frac{\partial \left[B_1 \left({\alpha_2}^2 - \frac{1}{3} \right) + c_{11} e_{yy} + c_{12} \left(e_{xx} + e_{zz} \right) \right]}{\partial y} + \frac{\partial \left[B_2 \alpha_2 \alpha_1 + c_{44} e_{xy} \right]}{\partial x} + \frac{\partial \left[B_2 \alpha_2 \alpha_3 + c_{44} e_{yz} \right]}{\partial z}, \tag{IV.2b}$$

$$\rho \frac{\partial^2 U_z}{\partial t^2} = \frac{\partial \left[B_1 \left({\alpha_3}^2 - \frac{1}{3} \right) + c_{11} e_{zz} + c_{12} \left(e_{xx} + e_{yy} \right) \right]}{\partial z} + \frac{\partial \left[B_2 \alpha_3 \alpha_1 + c_{44} e_{xz} \right]}{\partial x} + \frac{\partial \left[B_2 \alpha_3 \alpha_2 + c_{44} e_{yz} \right]}{\partial y}. \tag{IV.2c}$$

In each of the three equations there are terms involving c_{11}, c_{44} and c_{12} and the components of the strain tensor which result form the elastic strain energy density expression (III.2). If the magnetoelastic coupling is zero, i.e. $B_1 = 0$ and $B_2 = 0$, then only these terms remain. This results in the homogeneous wave equation [Auld 1971].

The derivative terms from the magnetoelastic energy are the source terms making the wave equation inhomogeneous. Whenever their contribution to the equations of motion is non-zero, the magnetic contribution to the system can be a source of elastic waves. In order to determine the characteristics of the elastic radiation from a domain wall or even verify the existence of elastic radiation a specific model for the domain wall

is needed. The model used here is that developed in Chapter II. As stated earlier the magnetic domain configuration is two regions, infinite in extent in both the x- and z-directions, with magnetization $|M_s|$, the left being positive and the right being negative, with a domain wall x-z planar separating the regions (see Figure II.2). If the wall is moving, it travels normal to the wall, the y-direction. The model looks at two situations: a static wall; a wall moving with either constant velocity or undergoing a step change in velocity.

IV.3 The Static 180° Domain Wall

The static domain wall does not radiate elastic waves according to the dynamic model. This is because there is no change in the inelastic strain (equation (III.10)). The spatial dependence of the direction cosines (α_1, α_2, α_3) in equations (IV.2) can be determined by looking at the magnetization throughout space. The symmetry used in this model requires that the direction cosines be independent of the spatial variables x and z and dependent only on y. It is assumed, as shown in Figure II.2, that the magnetization is initially in the positive z-direction for large negative values of y. This vector rotates through 180° for increasing values of y.

For a domain wall centered at y = 0 the magnetization vector components are

$$\begin{aligned} M_x &= \pm M_s \operatorname{sech}\left(\frac{y}{\Delta}\right), \\ M_y &= 0, \\ M_x &= -M_s \tanh\left(\frac{y}{\Delta}\right), \end{aligned} \tag{IV.3}$$

where M_s is the saturation magnetization and Δ is the domain wall width parameter. As discussed in Chapter II, the equilibrium configuration of the static 180° domain wall in a perfect cubic material is a non-trivial calculation. Using the approximation of an effective "magnetostatic anisotropy" permits the spatial dependence of the magnetization within the

domain wall to be determined (equations (II.27) and (II.28)). These expressions are quite complicated. Thus in this thesis the domain wall in a cubic material is approximated by the expression for the 180° domain wall in the uniaxial material (equations IV.3), where the cubic domain wall width parameter is assumed to be larger than that determined using the standard relationship $\Delta = (A/K_1)^{1/2}$, (see Figure II.5 and Figure II.6).

Since the magnetization (equations (IV.3)) can also be written as a function of the direction cosine, the direction cosines can be written as a function of y,

$$\begin{aligned} \alpha_x &= \pm \operatorname{sech}\left(\frac{y}{\Delta}\right), \\ \alpha_y &= 0, \\ \alpha_x &= -\tanh\left(\frac{y}{\Delta}\right). \end{aligned} \tag{IV.4}$$

These expression can be used to determine the contribution from the magnetoelastic terms in the elastic equations of motion (IV.2). First the direction cosines are only functions of y. Thus all derivatives with respect to x and z are zero. This leaves only magnetoelastic contributions from terms including a derivative with respect to y. These terms are (by component of the displacement vector),

$$\begin{aligned} &\frac{\partial [B_2 \alpha_1 \alpha_2]}{\partial y}, && \text{(x-component)}, \\ &\frac{\partial \left[B_1 \left(\alpha_2^2 - \frac{1}{3}\right)\right]}{\partial y}, && \text{(y-component)}, \\ &\frac{\partial [B_2 \alpha_2 \alpha_3]}{\partial y}, && \text{(z-component)}. \end{aligned} \tag{IV.5}$$

Since α_2 is always zero for the static domain wall model, the magnetoelastic contribution is always zero. This yields the homogeneous wave equations for (IV.2). Thus, as expected, there is no emission of elastic radiation from a stationary domain wall.

Upon further examination of the elastic equations of motion for a planar domain wall, it is apparent that there will be no source terms for elastic radiation unless the

domain wall develops a component of magnetization in the direction of motion [Kuleev et al. 1986]. This concept is consistent with the theoretical description of Landau and Lifshitz [1935], Dillon [1963], Schryer and Walker [1974], and O'Dell [1981], where a component of magnetization normal to the 180° domain wall is required in a moving planar domain wall. It should be noted that a component of magnetization normal to the plane of the domain wall is a necessary, but not a sufficient condition for magnetoacoustic emission. As is shown in this chapter, within the domain wall the relative component of magnetization normal to the plane of the domain wall must be changing with time in order to produce magnetoacoustic emission. For the 180° case this occurs only when the domain wall is accelerating.

IV.4 Magnetization Distribution for the Moving 180° Domain Wall

So far the static 180° domain wall has been dealt with in depth. The investigation of the dynamic aspects of the 180° domain wall as a source of magnetoacoustic emission requires a description of that moving domain wall. The simplest approach is to transform the static domain wall into a moving domain wall by introducing a spatial translation in equations (IV.3) such that the spatial variable y is given by

$$y(t) = y_o - \int v(t)\, dt. \qquad \text{(IV.6)}$$

If it is assumed that the wall maintains its stationary configuration (equations (IV.3)), i.e. that there is no magnetization in the direction of motion, the wall will not radiate elastically under any condition. In addition Landau and Lifshitz [1935], Dillon [1963], Schryer and Walker [1974], and O'Dell [1981] point out that the wall cannot remain in the stationary configuration during motion. This argument is briefly presented below.

A dynamic description of magnetization was first developed by Landau and Lifshitz [1935]. In order to have a time rate of change in magnetization there must be a net torque on the magnetic moments caused by the magnetic field. Thus the equilibrium

condition used for micromagnetic calculations (equation (II.1)) is no longer valid. Instead the Landau and Lifshitz equations of motion [Landau and Lifshitz 1935, O'Dell 1981, and Chen 1986] give the dynamic description of the magnetization. The general form of the Landau and Lifshitz equation is

$$\left(-\frac{1}{|\gamma|}\right)\frac{\partial \mathbf{M}}{\partial t} = (\mathbf{M}\times\mathbf{H}) - \alpha\left[\mathbf{H} - \frac{(\mathbf{H}\cdot\mathbf{M})\,\mathbf{M}}{M_s^{\,2}}\right], \qquad \text{(IV.7)}$$

where γ is the magneto-mechanical ratio, α is a damping coefficient and $\mathbf{H}$ is the total magnetic field. The cross product term in this expression is the torque on a magnetic moment by the magnetic field. The damping term is introduced to account for *viscous* loss in real materials. It drives the magnetization such that it spirals towards $\mathbf{H}$, eventually becoming parallel to $\mathbf{H}$. The damping term has been written in a slightly different manner to better represent the *viscous* nature of the damping [Gilbert 1955]. The resulting equation of motion is referred to as the Landau-Lifshitz-Gilbert equation,

$$\left(-\frac{1}{|\gamma|}\right)\frac{\partial \mathbf{M}}{\partial t} = (\mathbf{M}\times\mathbf{H}) - \frac{\lambda}{|\gamma|}\,\frac{\mathbf{M}\times\frac{\partial \mathbf{M}}{\partial t}}{|\mathbf{M}|}, \qquad \text{(IV.7a)}$$

where λ is the Gilbert damping parameter [Eschenfelder 1980]. This can be used in both insulating magnetic materials where the loss mechanism is a relativistic spin-orbit effect, and conducting magnetic materials where eddy current loss dominates.

Motion of the domain wall results from an effective 'applied' magnetic field in the vicinity of the domain wall. The source of this additional effective 'applied' magnetic field, $\mathbf{H}_A$, is not specified in this problem, but is assumed to be independent of the magnetization. $\mathbf{H}_A$ contributes additional terms to the magnetic field equations (II.11) and (II.12) used in Chapter II.4c and II.4d to determine the magnetization distribution

within the domain wall. For a total effective magnetic field in the z-direction only, the magnetic field can be written:

$$\begin{aligned} H^e_x &= H^s_x \,, \\ H^e_z &= H^s_z + H_o, \end{aligned} \tag{IV.8}$$

where H^s_i's are the static field given in equations (II.11) and (II.12). No magnetic field is introduced in the y-direction.

This total magnetic field results in the Landau and Lifshitz equation (IV.7) with a y-component of magnetization given by

$$\frac{1}{|\gamma|}\frac{\partial M_y}{\partial t} = M_x H^e_z. \tag{IV.9}$$

Here damping is ignored. Since the magnetization distribution is assumed unchanged from that of the static case the static field terms cancel and (IV.9) gives

$$\frac{1}{|\gamma|}\frac{\partial M_y}{\partial t} = M_z H_o. \tag{IV.10}$$

This equation is inconsistent with the prior assumption that $M_y = 0$, since the right hand side is non-zero. Thus in order to have motion of the domain wall, the wall cannot remain in the same configuration it has when stationary. The wall must develop a magnetization component in the direction of motion in order to move under the influence of an applied magnetic field.

IV.4a The 180° Domain Wall with Constant Velocity

O'Dell [1981] models the magnetization distribution within a 180° domain wall that is moving at a constant velocity using a coordinate system in which the y-axis is the polar axis. Using this coordinate system the components of the magnetization vector can be written

$$M_x = M_s \cos\phi \sin\theta,$$
$$M_y = M_s \sin\phi, \qquad \text{(IV.11)}$$
$$M_z = M_s \cos\phi \cos\theta,$$

where θ is the angle of the projection of the magnetization vector in the x-z plane from the z-axis, the same definition used in Chapter II, and ϕ is the angle of the magnetization vector out of the x-z plane, see Figure IV.1. The calculation is restricted to the case where ϕ is small. This is the case when the domain wall moves much more slowly than the Walker limiting velocity (typically $O(10^3$ m/sec), which is an estimate of the maximum velocity of a domain wall using a model with approximation similar to those used in the model presented in this thesis [Dillon 1963, Schryer and Walker 1974, Eschenfelder 1980, and O'Dell 1981].

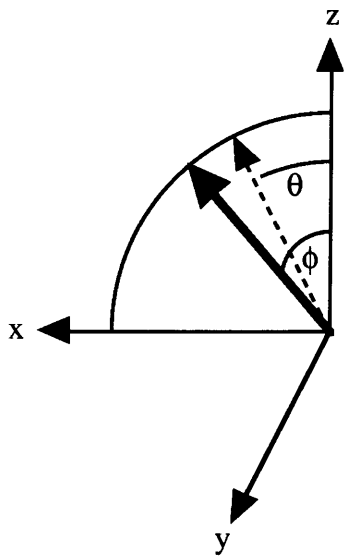

Figure IV.1 Coordinate system used for the moving domain wall. The polar axis is the y-axis. θ is the angle of the projection of the magnetization vector in the x-z plane from the z-axis. ϕ is the cant angle of the magnetization vector out of the x-z plane

The total magnetic field within the domain wall, ignoring damping is given by

$$H_x = -\frac{2K_1}{M_s}\sin\theta + \frac{2A}{M_s}\frac{\partial^2 \sin\theta}{\partial y^2}, \qquad \text{(IV.12a)}$$

$$H_y = -\left(\frac{2K_1}{M_s} - \frac{M_s}{\mu_o}\right)\phi + \frac{2A}{M_s}\frac{\partial^2 \phi}{\partial y^2}, \qquad \text{(IV.12b)}$$

$$H_z = \frac{2A}{M_s}\frac{\partial^2 \cos\theta}{\partial y^2} + H_o. \qquad \text{(IV.12c)}$$

A demagnetizing field is added to H_y to account for the non-zero magnetostatic self field now present. It is important to note these expressions are made using the approximation that the even in the cubic material the anisotropy can be expressed as if the material is uniaxial, where K_1 is a modified cubic magnetocrystalline anisotropy constant. O'Dell [1981] assumes that if the domain wall is moving at a constant velocity, then the effective applied magnetic field, $\mathbf{H_A}$, exactly cancels out the damping term in the Landau and Lifshitz equation. This assumption is made because once a normal component of magnetization is introduced, the domain wall will continue to move even without an applied magnetic field, if damping is ignored [Chikazumi 1986]. Once moving, in the absence of an applied magnetic field and damping, the domain wall moves at a constant velocity.

The Landau and Lifshitz equation can be reduced to two differential equations for the θ, and ϕ;

$$\frac{\partial \theta}{\partial t} = \frac{2A|\gamma|}{M_s}\left(\frac{\partial^2 \phi}{\partial y^2} - \phi\left(\frac{\partial \theta}{\partial y}\right)^2\right) - \left(\frac{2K_1}{M_s} - \frac{M_s}{\mu_o}\right)|\gamma|\,\phi\cos^2\theta, \qquad \text{(IV.13)}$$

and

$$\frac{\partial \phi}{\partial t} = -\frac{2A|\gamma|}{M_s}\frac{\partial^2 \theta}{\partial y^2} + \frac{2K_1|\gamma|}{M_s}\cos\theta\sin\theta. \qquad \text{(IV.14)}$$

If ϕ is independent of time, then the second equation is just (II.13), the equation for the static domain wall. Such a time independent solution is postulated by Walker [Dillon 1963 and Schryer and Walker 1974]. His solution also requires ϕ to be spatially constant. Although this is not a good solution at $y = \pm \infty$, there $\phi = 0$, the Walker solution does give insight into the dependence of the domain wall velocity on the applied magnetic field. This solution is discussed in Appendix C.

The main goal of this calculation is to obtain an expression for ϕ. Thus a solution is postulated that matches the boundary conditions. This is the approach used by O'Dell [1981]. It is assumed that at the center of the domain wall ϕ, the cant angle of magnetization, is a maximum, ϕ_{max}. This angle must be zero far away from the domain wall. In addition, the spatial derivative must have a maximum on one side of the domain wall and a minimum on the other. To satisfy this, a solution for the spatial derivative of ϕ is postulated to be

$$\frac{\partial \phi}{\partial y} = C \cos\theta \sin\theta. \tag{IV.15}$$

Equation (IV.15) can then be used to find the time derivative of ϕ by employing the fact that the convective derivative of ϕ is zero;

$$\frac{\partial \phi}{\partial t} = - v_y \frac{\partial \phi}{\partial y}, \tag{IV.16}$$

where the velocity v_y is assumed to be constant. This can then be used with equations (IV.15) and (IV.14) to find a simple equation for θ

$$\Delta^2 \frac{\partial^2 \theta}{\partial y^2} - \left(1 + \frac{v_y C M_s}{2 K_1 |\gamma|}\right) \cos\theta \sin\theta = 0. \tag{IV.17}$$

Equation (IV.17) is identical to equation (II.13), the equilibrium equation for the static uniaxial domain wall, with a new domain wall width parameter Δ' which can be written as

$$\Delta' = \Delta\left(1 + \frac{v_y C M_s}{2 K_1 |\gamma|}\right)^{-1/2}. \qquad \text{(IV.18)}$$

Equation (IV.17) can be solved yielding $\theta(y)$ identical to that of the uniaxial static case except for the modified domain wall width parameter, Δ'.

Although O'Dell [1981] does postulate the solution (IV.15), he does not solve for ϕ and text the consequences of his postulate. An expression for ϕ can be determined and the constant C can be found by assuming that the maximum angular displacement in the y-direction, ϕ_{max}, occurs at the center of the domain wall. From the solution of equation (IV.17) $\cos\theta(y)$ and $\sin\theta(y)$ can be substituted into expression (IV.15), using equations (IV.4). Thus ϕ can be written as

$$\phi = \int C \tanh\left(\frac{y}{\Delta'}\right) \operatorname{sech}\left(\frac{y}{\Delta'}\right) dy. \qquad \text{(IV.19)}$$

This can be integrated yielding

$$\phi = C\,\Delta' \operatorname{sech}\left(\frac{y}{\Delta'}\right) + D, \qquad \text{(IV.20)}$$

where the constant D is found to be zero by requiring the cant angle, ϕ, to be zero at $y = \pm\infty$. At the center of the domain wall, $y = 0$, using the assumption that the cant angle has a maximum value, ϕ_{max}, equation (IV.20) reduces to a quadratic equation in C. Assuming that the velocity of the domain wall is small compared to the Walker velocity,

and that the domain wall width parameter for the moving wall is approximately that of the stationary domain wall, C is shown to be

$$C = \frac{\phi_{max}}{\Delta}. \qquad \text{(IV.20a)}$$

The constant C calculated here differs by a factor of 1/2 from that found by O'Dell [1981] who using a general argument about the overall shape of the magnetization distribution to approximate the spatial derivative of the cant angle. ϕ can be used to determine the velocity versus applied magnetic field for the 180° domain wall. For small cant angle, small velocity, the results are identical to that of the Walker solution (where the cant angle is assumed to be a constant) [Dillon 1963, Schryer and Walker 1974 and How et al. 1989]. This is shown in Appendix C. In addition, it is shown in Appendix C that the energy density is less for the solution determined in this thesis than that of the Walker solution. Thus the solution derived in this thesis is an improved solution to the Walker solution.

The maximum cant angle is can be expressed in terms of the Walker velocity, v_w, where $2v_w = M_s|\gamma|\,\Delta'/\mu_o$ [O'Dell 1981]:

$$\phi_{max} = \frac{v_y}{2\,v_w}. \qquad \text{(IV.21)}$$

The resultant equations for the magnetization distribution can be written as

$$\begin{aligned} M_x &= \pm M_s \,\mathrm{sech}\left(\frac{y - v_y t}{\Delta'}\right), \\ M_y &= M_s \frac{v_y}{2\,v_w} \,\mathrm{sech}\left(\frac{y - v_y t}{\Delta'}\right), \\ M_z &= - M_s \tanh\left(\frac{y - v_y t}{\Delta'}\right). \end{aligned} \qquad \text{(IV.22)}$$

The magnetization distribution in the x- and z-direction are identical for both the moving domain wall and the static domain wall, with the exception of the translation of the y

variable. On the other hand M_y is now non-zero with the same general shape as M_x, except that the magnitude is now directly proportional to the velocity of translation of the 180° domain wall. For this first order approximation $M_x^2 + M_y^2 + M_z^2 \neq M_s^2$. This can be easily fixed by scaling each component of **M**.

IV.4b The Accelerating 180° Domain Wall

If the domain wall is accelerating the modeling used in section 4a is no longer accurate. A number of different assumptions must be used to model the magnetization distribution in within the accelerating 180° domain wall. It is still possible to use equation (IV.6) to express the translation of the spatial variable y. But the requirement that the convective derivative is zero (equation (IV.16)) is not valid. The convective derivative is now written

$$\frac{D\phi}{Dt} = \frac{\partial \phi}{\partial t} + \frac{dy}{dt}\frac{\partial \phi}{\partial y}. \tag{IV.23}$$

The case presented here is that in which the velocity function is a Heaviside function, u(t). Thus the convective derivative is written

$$\frac{D\phi}{Dt} = \frac{\partial \phi}{\partial t} + v_y\, u(t)\frac{\partial \phi}{\partial y}. \tag{IV.24}$$

Although it maybe more realistic to model the acceleration of the domain wall by using a continuous smooth function, the use of the Heaviside function does approximate the effect of the Barkhausen effect. In the Barkhausen effect the magnetization of the material changes in a discontinuous and irreversible manner. One source of this effect is the depinning of a 180° domain wall from a pinning site. Since modeling the effect by attempting to accurately determine the magnetic fields involved local to the pinning site is very difficult, for the purpose of magnetoacoustic emission calculation, it is sufficient to

ignore how the motion of the domain wall is produced. Instead it is assumed that the 180° domain wall moves and the consequence of that motion is determined.

As is presented in section 4a the magnetic field within the domain wall is given by equations (IV.12). For the 180° domain wall moving with constant velocity it is assumed that the steady state contribution of the Gilbert damping terms in the Landau and Lifshitz equation of motion cancel those of the effective applied magnetic field. This is no longer the case for the accelerating domain wall, which for the step change in velocity occurs at t = 0 in this model. In this case, the damping term in the Landau and Lifshitz equation of motion only cancels the effective applied magnetic field contribution when $t \gg 0$, since the step occurs at t = 0. In addition, when $t < 0$, the domain wall is stationary and the effective applied magnetic field is assumed to be zero.

The magnetization distribution is assumed to be the same as in equations (IV.11), where ϕ is small;

$$\begin{aligned} M_x &= M_s \sin\theta, \\ M_y &= M_s \phi, \\ M_z &= M_s \cos\theta, \end{aligned} \tag{IV.25}$$

The total magnetic field is also the same as that in equations (IV.12). If the spatial function of ϕ is assumed to be the similar to the constant velocity case, then equation (IV.15) is still valid

$$\frac{\partial \phi}{\partial y} = C \cos\theta \sin\theta. \tag{IV.15}$$

The M_y component of the Landau and Lifshitz equation becomes

$$\begin{aligned} \frac{D\phi}{Dt} = &-\frac{2A|\gamma|}{M_s}\frac{\partial^2\theta}{\partial y^2} + \left(\frac{2K_1|\gamma|}{M_s} + v_y\, u(t)\, C\right)\cos\theta\sin\theta \\ &+|\gamma|(H_{Az}\sin\theta - H_{Ax}\cos\theta) + D(\mathbf{M}, \mathbf{H}), \end{aligned} \tag{IV.26}$$

where D(**M**, **H**) represents the damping terms. It is assumed here that the during the acceleration of the 180° domain wall that the contribution of the convective derivative of ϕ approximately cancels out the net contribution of the effective applied magnetic field and the magnetic damping. In the case of a continuous acceleration such an assumption results in a smooth transition of the domain wall from the static configuration to the constant velocity configuration. Such a model cannot predict how the domain wall moves for an applied field. It instead determines the magnetization distribution for a change in the domain wall velocity.

In the case of the step in velocity the result is a differential equation which is similar to equation (IV.17),

$$\Delta^2 \frac{\partial^2 \theta}{\partial y^2} - \left(1 + \frac{v_y\, u(t)\, C\, M_s}{2\, K_1 |\gamma|}\right) \cos\theta \sin\theta. \qquad \text{(IV.27)}$$

Again if the velocity is considered to be small the constant C is related to the maximum cant angle. Thus ϕ can be written in terms of the Walker velocity;

$$\phi = \frac{v_y\, u(t)}{2\, v_w} \operatorname{sech}\left(\frac{y - v_y\, u(t)\, t}{\Delta'}\right), \qquad \text{(IV.28)}$$

where Δ' is given by equation (IV.18) with the velocity equal to $v_y u(t)$. M_x and M_z are identical to the expressions in equation (IV.22) with the velocity equal to $v_y u(t)$.

IV.5 Magnetoacoustic Emission from the Moving 180° Domain Wall

The expression for the magnetization can now be used to determine whether elastic radiation is emitted from a moving planar 180° domain wall. In section IV.3 it is shown that the possibility of magnetoacoustic emission only exists, for a planar 180° domain wall, if there is a component of magnetization normal to the plane of the domain wall. This is the case for both the 180° domain wall moving with constant velocity and the 180° domain wall undergoing acceleration. Kuleev et al. [1986] state that in the case

for constant velocity there *is* emission of elastic radiation. It is shown in the next section that this is not true. Instead the necessary condition is that the domain wall must be accelerating. This results from the requirement that the convective derivative of the inelastic strain tensor must be non-zero (equation III.10) for magnetoacoustic emission to be produced. When the 180° domain wall is moving at constant velocity the convective derivative of the inelastic strain tensor is zero. On the other hand when the 180° domain wall is undergoing acceleration the condition given in equation (III.10) is satisfied and elastic radiation results. All calculations are done assuming a *cubic* ferromagnetic material as discussed in section IV.4a.

IV.5a Green's Function Solution to the Inhomogeneous Wave Equation

The motion of the displacement vector in the ferromagnetic material is given by equations (IV.2). As is shown in this chapter these equations can be reduced to three inhomogeneous wave equations. By making a number of approximations to the magnetoelastic interaction in the ferromagnet, symmetry reduces the equations to three one-dimensional inhomogeneous wave equations. The solution to these equations can be found by using the Green's function approach [Morse and Feshbach 1953 and Jacobsen 1960].

The Green's function approach is based on the fact that the inhomogeneous wave equation having a source function given by a delta function has a solution called a Green's function. This Green's function has the property that its convolution with any source function results in the solution to a inhomogeneous wave equation for that source function. For the one-dimensional case the inhomogeneous wave equation for the Green's function is

$$\frac{\partial^2 g}{\partial y^2} - \frac{1}{c^2}\frac{\partial^2 g}{\partial t^2} = -4\pi\,\delta(y - y_o)\,\delta(t - t_o), \qquad \text{(IV.29)}$$

[Morse and Feshbach 1953], where c is the velocity and the Green's function g is defined as

$$g(y, t \mid y_o, t_o) = 2\,\pi\,c\,u\left[(t - t_o) - \frac{|y - y_o|}{c}\right]. \tag{IV.30}$$

The function u(y,t) is the Heaviside function.

A one-dimensional scalar wave equation with a source function q(y, t),

$$\frac{\partial^2 U(y, t)}{\partial y^2} - \frac{1}{c^2}\frac{\partial^2 U(y, t)}{\partial t^2} = -4\,\pi\,q(y, t), \tag{IV.31}$$

has a solution [Morse and Feshbach 1953] given by

$$U(y, t) = \int_0^{t+\varepsilon} d\,t_o \int d\,y_o\, g(y, t \mid y_o, t_o)\, q(y_o, t_o)$$
$$- \frac{1}{4\,\pi c^2}\int d\,y_o \left[\left(\frac{\partial\, g}{\partial\, t_o}\right)_{t_o = 0} U_o(y_o) - \left(g\,\frac{\partial\, U(y_o, t_o)}{\partial\, t_o}\right)_{t_o = 0}\right]; \quad \varepsilon \to 0^+. \tag{IV.32}$$

The second term on the right hand side of the solution represents the initial conditions of the system being investigated. The contribution of the initial conditions is often taken to be zero by defining both $U_o(y_o)$ and the time derivative of $U_o(y_o)$ to be zero. Thus if the first integral can be solved in closed form, an analytic solution to the inhomogeneous wave equation (IV.31) can be found.

IV.5b The Wave Equation for the Moving 180° Domain Wall

The inhomogeneous wave equations for the displacement vector in a ferromagnet used in this thesis are given by equations (IV.2). These equations are written in terms of the magnetization direction cosines, α_i, and the strain tensor, **e**. It is assumed that both the direction cosines and the displacement vectors are purely functions of the spatial variable normal to the plane of the domain wall [Lord 1967 and Kuleev et al. 1986]. The

result is that all derivatives with respect to x and z vanish. It is apparent that for the finite strain approximation (equation (II.23)) that two of the three diagonal components of the strain tensor must be zero in this case. Thus equations (IV.2) can be reduced to the following:

$$\rho \frac{\partial^2 U_x}{\partial t^2} = \frac{\partial \left| B_2 \alpha_1 \alpha_2 + c_{44} e_{xy} \right|}{\partial y}, \tag{IV.33a}$$

$$\rho \frac{\partial^2 U_y}{\partial t^2} = \frac{\partial \left[B_1 \left(\alpha_2{}^2 - \frac{1}{3} \right) + c_{11} e_{yy} \right]}{\partial y}, \tag{IV.33b}$$

$$\rho \frac{\partial^2 U_z}{\partial t^2} = \frac{\partial \left[B_2 \alpha_3 \alpha_2 + c_{44} e_{yz} \right]}{\partial y}. \tag{IV.33c}$$

Since the strain tensor can be written as the symmetrized gradient of the displacement vector, assuming infinitesimal strain, equations (IV.2) can be rewritten as:

$$\rho \frac{\partial^2 U_x}{\partial t^2} = c_{44} \left[\frac{\partial^2 U_x}{\partial y^2} + \frac{\partial^2 U_y}{\partial x \partial y} \right] + \frac{\partial \left[B_2 \alpha_1 \alpha_2 \right]}{\partial y}, \tag{IV.34a}$$

$$\rho \frac{\partial^2 U_y}{\partial t^2} = c_{11} \frac{\partial^2 U_y}{\partial y^2} + \frac{\partial \left| B_1 \left(\alpha_2{}^2 - \frac{1}{3} \right) \right|}{\partial y}, \tag{IV.34b}$$

$$\rho \frac{\partial^2 U_z}{\partial t^2} = c_{44} \left[\frac{\partial^2 U_z}{\partial y^2} + \frac{\partial^2 U_y}{\partial z \partial y} \right] + \frac{\partial \left[B_2 \alpha_3 \alpha_2 \right]}{\partial y}. \tag{IV.34c}$$

Both equations (IV.34a) and (IV.34c) have a derivative term in U_y. Reversing the order of differentiation results in this term being equal to zero, again it is assumed that there is only y dependence.

The requirement that all α's and U's be functions of y only appears to have the same difficulties that are discussed in Chapter II and Appendix B. The strict relationship between the displacement vector and the strain tensor severely limits the possible

functionality of the displacement vector. In order have both the strain and displacement vector be functions of y only, e_{xx}, e_{zz} and e_{xz} must be zero throughout the ferromagnetic material. This appears to violate the fact that there is magnetostrictive strain within the domains and these components of the strain tensor are non-zero there. The major difference between the strains here and those discussed in Chapter II and Appendix B are that these are a dynamic contribution to the static strain field. Thus the static strain field remains the same but the components of the dynamic strain field listed above are zero.

Upon substitution for the direction cosines (IV.25) assuming a small cant angle the resulting one-dimensional wave equations are

$$\begin{aligned}
\rho \frac{\partial^2 U_x}{\partial t^2} - c_{44} \frac{\partial^2 U_x}{\partial y^2} &= B_2 \frac{\partial \phi \sin\theta}{\partial y}, \\
\rho \frac{\partial^2 U_y}{\partial t^2} - c_{11} \frac{\partial^2 U_y}{\partial y^2} &= B_1 \frac{\partial \left(\phi^2 - \frac{1}{3}\right)}{\partial y}, \\
\rho \frac{\partial^2 U_z}{\partial t^2} - c_{44} \frac{\partial^2 U_z}{\partial y^2} &= B_2 \frac{\partial \phi \cos\theta}{\partial y}.
\end{aligned} \tag{IV.35}$$

The magnetization distribution calculated for the 180° domain wall moving with constant velocity after a step from zero velocity at t=0 results in expression for $\theta(y, t)$ and $\phi(y, t)$;

$$\begin{aligned}
\sin\theta &= \pm \operatorname{sech}\left(\frac{y - v_y\, u(t)\, t}{\Delta}\right), \\
\phi &= \frac{v_y\, u(t)}{2\, v_w} \operatorname{sech}\left(\frac{y - v_y\, u(t)\, t}{\Delta}\right), \\
\cos\theta &= -\tanh\left(\frac{y - v_y\, u(t)\, t}{\Delta}\right),
\end{aligned} \tag{IV.36}$$

where the contracted domain wall width parameter Δ' is approximated by the static domain wall width parameter, Δ since the v_y is small.

Upon substitution into equation (IV.35) the equations of motion can be written

$$\frac{\partial^2 U_x}{\partial y^2} - \frac{1}{c_t^2}\frac{\partial^2 U_x}{\partial t^2} = \pm \frac{B_2 v_y u(t)}{c_{44} v_w \Delta} \operatorname{sech}^2\left(\frac{y - v_y u(t) t}{\Delta}\right) \tanh\left(\frac{y - v_y u(t) t}{\Delta}\right), \qquad \text{(IV.37a)}$$

$$\frac{\partial^2 U_y}{\partial y^2} - \frac{1}{c_l^2}\frac{\partial^2 U_y}{\partial t^2} = \frac{B_1}{2 c_{11} \Delta}\left(\frac{v_y u(t)}{v_w}\right)^2 \operatorname{sech}^2\left(\frac{y - v_y u(t) t}{\Delta}\right) \tanh\left(\frac{y - v_y u(t) t}{\Delta}\right), \qquad \text{(IV.37b)}$$

$$\frac{\partial^2 U_z}{\partial y^2} - \frac{1}{c_t^2}\frac{\partial^2 U_z}{\partial t^2} =$$
$$\frac{B_2 v_y u(t)}{2 c_{44} v_w \Delta}\left(\operatorname{sech}\left(\frac{y - v_y u(t) t}{\Delta}\right) \tanh^2\left(\frac{y - v_y u(t) t}{\Delta}\right) - \operatorname{sech}^3\left(\frac{y - v_y u(t) t}{\Delta}\right)\right), \qquad \text{(IV.37c)}$$

where c_t and c_l are the transverse and longitudinal velocities of sound in the ferromagnetic material. In this calculation the $+\sin\theta$ is used. The three inhomogeneous wave equations given in equations (IV.37) are solved using the Green's function approach discussed in the last section. The terms on the right hand side are the source functions, $4\pi q(y,t)$ used in equation (IV.32) to find $U_i(y,t)$.

IV.5c Solution to the Wave Equation for a Moving 180° Domain Wall

The method of solution for the inhomogeneous wave equations (IV.37) for the three components of displacement vector is presented below. Using equation (IV.30) and (IV.32) and the general source vector function $\mathbf{q}(y,t)$, the general solution for the displacement vector is

$$\mathbf{U}(y, t) = 2\pi c_i \int_0^{t+\varepsilon} d t_o \int d y_o \, u\left[c_i (t - t_o) - |y - y_o|\right] \mathbf{q}(y_o, t_o), \qquad \text{(IV.38)}$$

where c_i is the appropriate velocity of sound. The limits of integration have been shifted from $t_o = 0$ to $t_o = -\alpha$ to simplify the evaluation of the initial conditions. The initial

conditions at - α, where α is a positive definite time, are that all $\mathbf{U}_o$ and $\partial \mathbf{U}_o/\partial t_o$ are zero. This results in no contribution to $\mathbf{U}$ from the second integral term in the equation (IV.32).

The Heaviside function in the spatial part of equation (IV.38) can be used to restrict the spatial limits of integration. This step function defines a sound cone within which the integrand is non-zero. These limits of integration are given by

$$y_o = y \pm c_i (t - t_o). \tag{IV.39}$$

Substituting this into equation (IV.38) results in the following general expression for the solution to the inhomogeneous wave equations

$$\mathbf{U}(y, t) = 2 \pi c_i \int_{-\alpha}^{t+\varepsilon} d t_o \int_{y - c_i (t - t_o)}^{y + c_i (t - t_o)} d y_o \, \mathbf{q}(y_o, t_o). \tag{IV.40}$$

First looking at the two transverse waves U_x and U_z the source terms are given by

$$q_x (y_o, t_o) = \mp \frac{B_2 v_y u(t)}{4 \pi c_{44} v_w \Delta} \operatorname{sech}^2\left(\frac{y - v_y u(t) t}{\Delta}\right) \tanh\left(\frac{y - v_y u(t) t}{\Delta}\right), \tag{IV.41a}$$

$$q_z (y_o, t_o) = - \frac{B_2 v_y u(t)}{8 \pi c_{44} v_w \Delta} \times \left(\operatorname{sech}\left(\frac{y - v_y u(t) t}{\Delta}\right) \tanh^2\left(\frac{y - v_y u(t) t}{\Delta}\right) - \operatorname{sech}^3\left(\frac{y - v_y u(t) t}{\Delta}\right)\right). \tag{IV.41b}$$

Using (IV.41a) U_x can be written as

$$U_x = \mp \frac{B_2 v_y c_t}{2 c_{44} v_w \Delta} \int_0^{t + \varepsilon} d t_o \int_{y - (t - t_o) c_t}^{y + (t - t_o) c_t} d y_o \left(\operatorname{sech}^2\left(\frac{y_o - v_y t_o}{\Delta}\right) \tanh\left(\frac{y_o - v_y t_o}{\Delta}\right)\right), \tag{IV.42}$$

where the step functions in the integrand have been incorporated into the limits of integration of the time function. The spatial integration results in

$$U_x = \pm \frac{B_2 v_y c_t}{4 c_{44} v_w} \times$$
$$\int_0^{t+\varepsilon} d t_o \left(\operatorname{sech}^2 \left(\frac{y + t c_t - (c_t + v_y) t_o}{\Delta} \right) - \operatorname{sech}^2 \left(\frac{y - t c_t + (c_t - v_y) t_o}{\Delta} \right) \right). \quad \text{(IV.43)}$$

The time integration can also be done resulting in

$$U_x = \mp \frac{B_2 v_y c_t \Delta}{4 c_{44} v_w} \times \left\{ \begin{array}{l} \frac{1}{c_t + v_y} \left[\tanh \left(\frac{y - v_y t}{\Delta} \right) - \tanh \left(\frac{y + c_t t}{\Delta} \right) \right] \\ + \frac{1}{c_t - v_y} \left[\tanh \left(\frac{y - v_y t}{\Delta} \right) - \tanh \left(\frac{y - c_t t}{\Delta} \right) \right] \end{array} \right\}, \quad \text{(IV.44)}$$

.

Assuming that the speed of sound is much greater than the velocity of the domain wall, a condition satisfied since $v_y << v_w$ and $v_w \approx c_i$ (IV.44) can be rewritten as

$$U_x = \pm \frac{B_2 v_y \Delta}{4 c_{44} v_w} \left[\tanh \left(\frac{y - c_t t}{\Delta} \right) + \tanh \left(\frac{y + c_t t}{\Delta} \right) \right] \quad \text{(IV.45)}$$
$$\mp \frac{B_2 v_y \Delta}{2 c_{44} v_w} \tanh \left(\frac{y - v_y t}{\Delta} \right).$$

Using the same procedure the second transverse component of the displacement vector can be solved;

$$U_z = - \frac{B_2 v_y \Delta}{4 c_{44} v_w} \left[\operatorname{sech} \left(\frac{y - c_t t}{\Delta} \right) + \operatorname{sech} \left(\frac{y + c_t t}{\Delta} \right) \right] \quad \text{(IV.46)}$$
$$+ \frac{B_2 v_y \Delta}{2 c_{44} v_w} \operatorname{sech} \left(\frac{y - v_y t}{\Delta} \right).$$

Each of the transverse waves have three wave components: One moving in the positive y-direction with velocity c_t, one moving in the negative y-direction with velocity c_t and a third moving in the positive y-direction with a velocity v_y. The first two waves

are elastic plane radiation emitted from the domain wall as the wall steps from zero velocity to v_y. The last wave is the elastic disturbance localized with the domain wall resulting from the local strain field at the domain wall when the wall develops a component of magnetization normal to the plane of the wall.

The solution to the longitudinal component of the displacement vector is of the same form as the x-component of the displacement vector. This is because their spatial functionality of the longitudinal source function are identical (see equations (IV.37a) and (IV.37b)). The amplitude and the velocity of the elastic radiation does differ in the longitudinal and transverse case. Solving equation (IV.37b) in the same manner as is done above yields

$$U_y = \frac{B_1 v_y^2 \Delta}{4 c_{11} v_w^2}\left[\tanh\left(\frac{y - c_l t}{\Delta}\right) + \tanh\left(\frac{y + c_l t}{\Delta}\right)\right] - \frac{B_1 v_y^2 \Delta}{2 c_{11} v_w^2}\tanh\left(\frac{y - v_y t}{\Delta}\right). \qquad \text{(IV.47)}$$

IV.5d Strain Waves Radiated from a Moving 180° Domain Wall

The results given in equations (IV.45), (IV.46) and (IV.47) each contain elastic radiation terms and thus demonstrate that 180° domain walls can produce magnetoacoustic emission. The displacement vectors can be used to determine the strain waves associated with the motion of the domain wall. These equations can be used to estimate the amplitude of elastic radiation from a planar 180° domain wall. Since each U_i is only a function of y there are only three components to the strain wave emitted; e_{yy}, e_{xy}, and e_{yz}:

$$e_{xy} = \pm \frac{B_2 v_y}{4 c_{44} v_w}\left[\operatorname{sech}^2\left(\frac{y - c_t t}{\Delta}\right) + \operatorname{sech}^2\left(\frac{y + c_t t}{\Delta}\right)\right] \mp \frac{B_2 v_y}{2 c_{44} v_w} \operatorname{sech}^2\left(\frac{y - v_y t}{\Delta}\right), \tag{IV.48a}$$

$$e_{yy} = \frac{B_1 v_y^2}{4 c_{11} v_w^2}\left[\operatorname{sech}^2\left(\frac{y - c_l t}{\Delta}\right) + \operatorname{sech}^2\left(\frac{y + c_l t}{\Delta}\right)\right] - \frac{B_1 v_y^2}{2 c_{11} v_w^2} \operatorname{sech}^2\left(\frac{y - v_y t}{\Delta}\right), \tag{IV.48b}$$

$$e_{yz} = + \frac{B_2 v_y}{4 c_{44} v_w}\left[\operatorname{sech}\left(\frac{y - c_t t}{\Delta}\right)\tanh\left(\frac{y - c_t t}{\Delta}\right) + \operatorname{sech}\left(\frac{y + c_t t}{\Delta}\right)\tanh\left(\frac{y + c_t t}{\Delta}\right)\right] - \frac{B_2 v_y}{2 c_{44} v_w} \operatorname{sech}\left(\frac{y - v_y t}{\Delta}\right)\tanh\left(\frac{y - v_y t}{\Delta}\right). \tag{IV.48c}$$

Each of these expressions (IV.48a - IV.48c) contains a strain term (the last in each) that is the dynamic disturbance that moves with the domain wall. This term is not considered radiation. The strain field associated with a moving 180° domain wall has been modeled by How et al. [1989]. In this calculation the shear strain waves traveling with the domain wall are determined for a general velocity. The results of How et al. reduce to the last terms in equations IV.48a and IV.48c in the case of small velocity. This suggests that the approximation for the magnetization distribution in the direction normal to the domain wall is valid.

For an observation point far from the domain wall on the positive y side only the positive moving elastic strain wave passes through that point. Figures IV.2a and IV.2b show the shape of the normalized elastic strain wave passing through an observation point as a function of time. The amplitude of the transverse components, called a shear wave, and the longitudinal component, called a compressional wave, are different. Also

since the shear wave and compressional wave travel at different velocities, the shear velocity of sound and longitudinal velocity of sound respectively, the two types of elastic waves reach the observation point at different times.

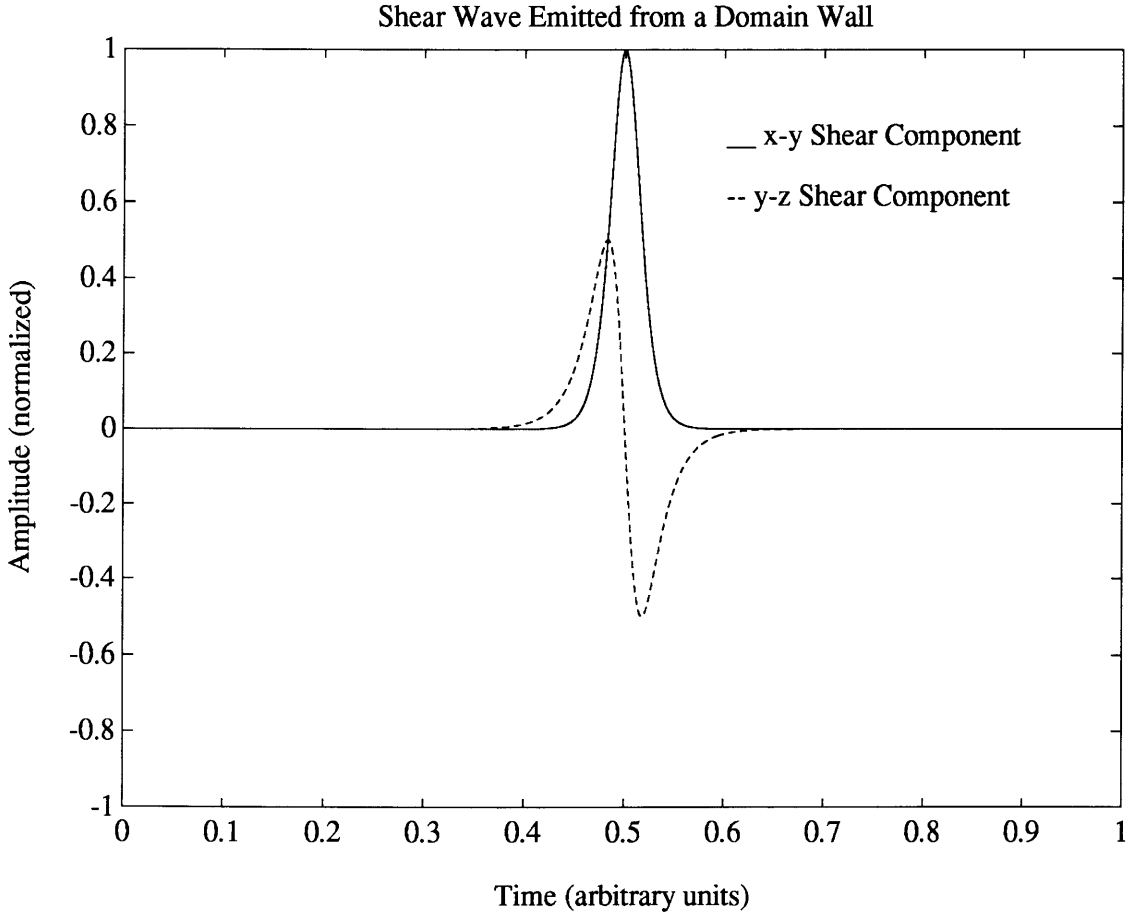

Figure IV.2a The shear components of elastic radiation emitted from a 180° domain wall undergoing a step change in velocity at t = 0. The amplitude of the elastic waves are normalized. The time is in arbitrary units.

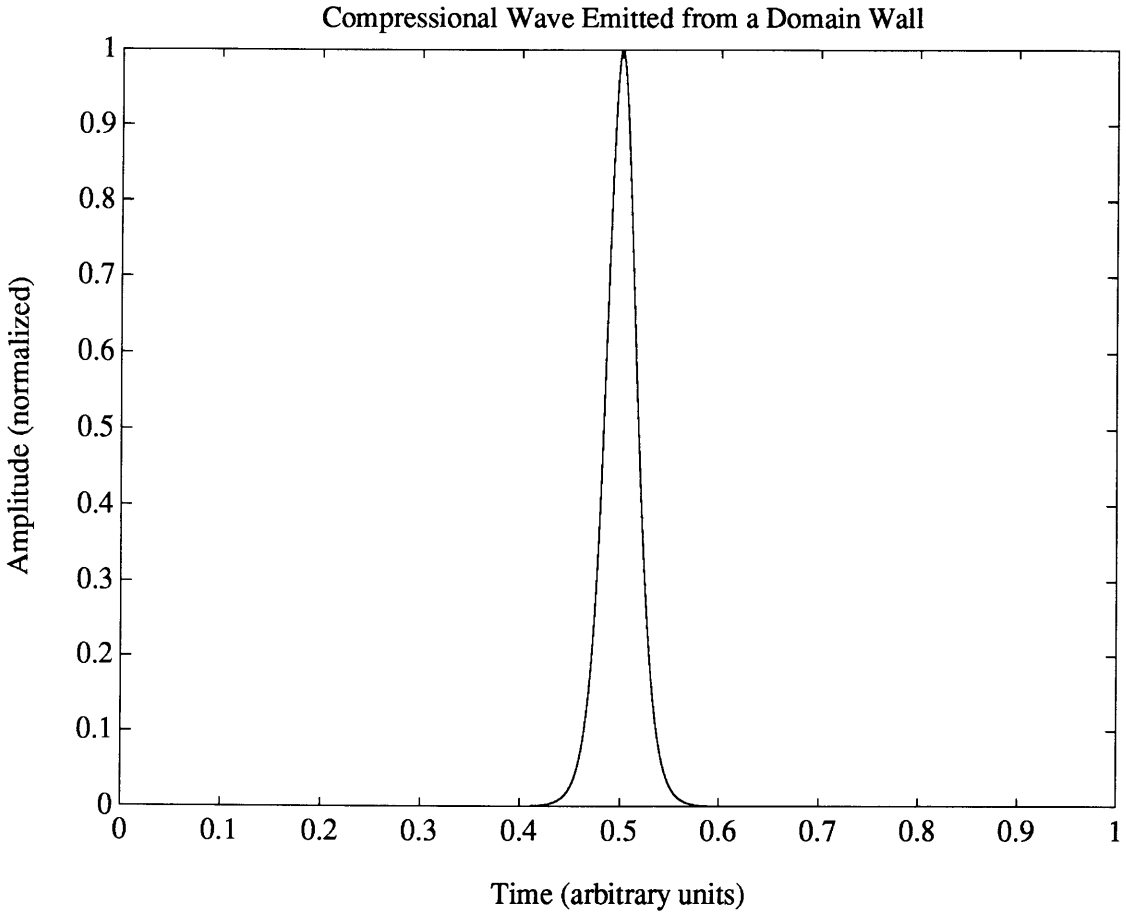

Figure IV.2b The compressional component of elastic radiation emitted from a 180° domain wall undergoing a step change in velocity at t = 0. The amplitude of the elastic wave is normalized. The time is in arbitrary units.

The elastic radiation emitted from the moving domain wall has the following properties:

At any observation point the center of the elastic disturbance arrives exactly at the time required for radiation from the center of the domain wall to travel that distance if the radiation is emitted at the time the step in velocity occurs, when the domain wall's acceleration can be expressed as a delta function. At all other times the acceleration of the domain wall is zero.

The width of the elastic radiation field at any time is exactly that of the domain wall. The arguments of the radiation functions in equations (IV.48) are similar to the

arguments in the function for the domain wall, equations (IV.22), with a differing only by the spatial translation.

At a time much greater than the time taken for the peak elastic radiation field to reach the observation point there is no additional radiation observed. At this point if radiation were being emitted, it would be emitted from a domain wall moving at a constant velocity. There is no observed radiation because there is no convective change in the inelastic strain field at the 180° domain wall. The elastic radiation's displacement vectors appear to be the convolution of the acceleration function, here a delta function, with the domain wall strain field. Thus only an accelerating 180° domain wall can be a source of elastic radiation.

IV.6 Estimates of the Size of Elastic Radiation from a Moving Domain Wall

The size of the elastic radiation from an accelerating 180° domain wall is dependent on the Walker velocity, the magnetoelastic and elastic coefficients, and in the case of the step in velocity the final velocity of the domain wall. Table IV.1 lists the appropriate values for these constants. Iron has a [100] easy direction, thus the model present above is consistent. Nickel and most ferrite materials have and easy axis in the [111] direction. This means that the magnetization vector must be rotated relative to the crystal axes and the model must be slightly modified. The general form of the elastic radiation does not change significantly. Thus the estimate of the size of the elastic radiation for materials with a [111] easy direction is calculated using equation (IV.48).

The values of the elastic strain waves emitted from metals are quite small compared to that of the ferrite materials. This is because of the velocity of the domain wall is limited by eddy current loss and thus is very small for fields on the order of 1 Oe. For larger field the domain wall does not remain planar [Williams et al. 1950]. This will be discussed in Chapter VI. It would appear as if 180° domain walls should not contribute significantly to magnetoacoustic emission in metals. In a real metal where

domain wall motion is much more complicated than this simple planar wall model additional effects must be added to the model if 180° domain wall motion is to be considered a significant contributor to magnetoacoustic emission.

The ferrite materials should exhibit very large elastic radiation from a step in domain wall velocity in an applied field of 1 Oe. Thus in ferrites acceleration of 180° domain walls could be a significant source of magnetoacoustic emission.

	Iron	Nickel	Nickel Ferrite	YIG
V_w (cm/sec)	4.1×10^{5}	3.6×10^{5}	1.8×10^{5} [B]	1.3×10^{5} [B]
V_y (cm/(sec Oe))	4 [C]	4 [D]	2.0×10^{4} [A]	2.0×10^{4} [D]
e_{xy} (Oe^{-1})	3.6×10^{-10}	4.0×10^{-12}	3.3×10^{-7}	3.2×10^{-7}
e_{yz} (Oe^{-1})	1.3×10^{-10}	2.0×10^{-12}	1.7×10^{-7}	1.6×10^{-7}
e_{yy} (Oe^{-1})	5.8×10^{-16}	1.5×10^{-15}	$O(10^{-8})$ [D]	$O(10^{-8})$ [D]

Table IV.1 Amplitude of emission associated with a step change in the velocity of the domain wall in a 1 Oe applied magnetic field. The values come form the following sources: [A] Chikazumi [1986], [B] O'Dell [1981], [C] Williams et al. [1950], [D] approximate values based on iron and nickel ferrite.

Chapter V: Technique for Measurement of Magnetoacoustic Emission

V.1 Introduction

The measurement of magnetoacoustic emission from a single moving 180° domain wall requires instrumentation that is sensitive to the level of strain determined in Chapter IV. In addition, because the elastic radiation emitted by an accelerating domain wall can be a transient phenomenon, high bandwidth detection is desirable. For a typical 180° domain wall undergoing a step in velocity the elastic radiation pulse width is less than 0.1 nanosecond. A more realistic pulse width, taking into account the finite acceleration of a 180° domain wall, is on the order of 1 microsecond, for a velocity risetime of approximately 1 microsecond. Thus the strain sensor should be capable of detecting elastic disturbances at a surface in the frequency range of 100kHz to 10MHz.

The standard technique used to measure magnetoacoustic emission employs a piezoelectric transducer as the primary sensing device. Most commercially available piezoelectric transducers have bandwidths of 10's to 100's of kilohertz in the frequency range of 10 kHz to order 1MHz. A highly sensitive piezoelectric transducer has maximum sensitivity on the order of 1μV/μbar for longitudinal stress waves [Williams 1980]. For a wideband measurement this translates to a strain sensitivity of $O(10^{-11})$, depending on the noise level of the high impedance wideband amplification system used. The sensitivity is diminished for shear components of emission [Spanner 1974].

There are additional limitations to the capabilities of a piezoelectric transducer. Most transducers are used to count acoustic emission pulses and measure the size of emission, not determine the pulse shape. This is because the transducer either integrates or averages the acoustic signal for most types of elastic waves, further limiting the sensitivity to transient emission. The method of operation is determined by the orientation of the piezoelectric poling, and the geometry and size of the transducer. The piezoelectric transducer may be adequate for detection of acoustic emission from a

moving 180° domain wall in the ferrite type material (see Table IV.1), but cannot be used for metallic ferromagnets. In order to gain sensitivity and measure the actual shape of the acoustic wave a modified type of sensor is needed.

One type of acoustic wave transducer which is highly sensitive to transient emission is the capacitive transducer. This type of transducer senses absolute movement of the surface of the material under test, or in some setups the acoustic wave transfer block. The capacitive transducer has been employed successfully to investigate step changes in the stress field at a point, a non-plane wave analogy to the step motion in the planar 180° domain wall [Breckenridge et al. 1975]. Because of its wideband nature and absolute motion detection, this type transducer facilitates the deconvolution of the absolute surface motion to determine the change in the stress field which acts as the source of the acoustic emission for longitudinal waves [Breckenridge et al. 1975 and Lord 1981]. The transducer is constructed from two parallel conducting plates, separated by a distance O(1μm), which cover a small area of the surface of the material, or transfer block. It is possible to use the surface of the material or transfer block as one of the electrodes of the capacitor. The design of the capacitive transducer makes it highly sensitive to normal surface displacement, but highly insensitive to transverse displacement of the surface. In addition any local surface movement will be averaged over the area of the capacitive plates.

In order to employ the best features of the capacitive transducer as well as sensitivity to local surface motion and shear acoustic emission, an electron tunneling transducer has been developed for this thesis. Such a transducer is based on the Scanning Tunneling Microscope (STM) [Binnig and Rohrer 1982 and 1986]. The transducer utilizes the high sensitivity to topography [Binnig and Rohrer, Chen 1993], and to surface displacement [Brizzolara and Colton 1990 and 1992].

Electron tunneling has been used by Brizzolara and Colton [1990 and 1992] to measure surface displacement caused by magnetostrictive magnetic materials. But this

was done at low frequency. The detection of the surface motion caused by elastic radiation from a moving 180° domain wall requires a higher bandwidth than is typically available on an STM. Thus a wideband modification has been built for a commercially available STM that will permit operation to 5MHz. Recently an STM, modified in a similar manner to that used in this thesis, has been used to measure periodic surface displacement by ultrasonic waves launched into a quartz crystal [Moreau and Ketterson 1992].

V.2 The Electron Tunneling Transducer

The electron tunneling transducer, called the tunneling transducer in this thesis, is built with a standard Scanning Tunneling Microscope (STM) with modification to permit measurement of high frequency changes in the tunneling current. The first STM was built by Binnig and Rohrer [1982 and 1986]. The instrument utilizes the quantum mechanical phenomenon of tunneling to permit surface imaging of either conducting, semiconducting, or superconducting materials.

V.2a Tunneling Background for the Tunneling Transducer

The STM uses the tunneling configuration consisting of a metal-insulator-(surface material) electrode-counterelectrode structure. The metal electrode is the tunneling tip, which is built into the STM itself. The insulator can be vacuum, a gas, or a liquid. In this thesis the insulating material is air. The metal counterelectrode is the sample surface under test. Although the STM can be used for tunneling into semiconducting and superconducting surfaces, in addition to conducting surfaces, [Chen 1993], the work in this thesis is limited to metallic counterelectrodes and thus the STM is discussed in that light.

In the original publications by Binnig and Rohrer [1982 and 1986], the phenomenon of tunneling is discussed using a (tunneling tip)-insulator-(sample surface)

in a simple planar heterostructure. Some effects of a more accurate geometry are presented, but the basic equation for the relationship between tunneling current density, voltage and (tunneling-tip)-surface separation is based on the planar model. The insulating layer in their work is vacuum. Binnig and Rohrer model the tunneling current-voltage characteristics using the small biasing potential approximation presented by Simmons [1963]. Simmons work is based on the "transfer Hamiltonian approach" [Duke 1969] in which tunneling takes place from an *initial* eigenstate of one Hamiltonian through a rectangular barrier to a *final* eigenstate of a different Hamiltonian. The resulting current density-voltage relationship is given by

$$j = \left(\frac{e^2}{\hbar}\right)\left(\frac{\kappa_o}{4\,\pi^2\,s}\right) V \exp\left[-2\,\kappa_o\,s\right], \tag{V.1}$$

where κ_o is the inverse decay length of the wavefunction outside the surface, s is the sample surface to tunneling tip distance, and V is the biasing voltage [Simmons 1963, Binnig and Rohrer 1982 and 1986]. The inverse decay length, κ_o, can be written in terms of the average work function of the tunneling tip and the sample being investigated. Assuming tunneling through a vacuum barrier the inverse decay length is written as

$$2\,\kappa_o\,(\text{angstoms}) \approx 1.025\,\sqrt{\frac{\varphi_1 + \varphi_2}{2}}, \tag{V.2}$$

where φ_i's are the work functions of the tunneling tip and surface.

The model presented assumes a planar tunnel junction. The (tunneling tip)-surface is far from planar and some measure of the lateral current distribution is needed. Assuming equation (V.1) is reasonable for the height dependence of the tunneling current, if the radius of curvature of the tunneling tip is much greater than the (tunneling tip)-surface separation it can be shown [Chen 1993] that the tunneling current density is localized around the apex of the tunneling tip. With this highly local tunneling current

routine measurements with spatial resolution as small as 2Å have been made [Chen]. Additional limitations to the model of Simmons [1963] exist because the model does not account for the effect of image potential, and ignores the actual local density of states at the Fermi surface at the finite temperature of both the tunneling tip and the sample surface. Even with these omissions the predicted current density versus (tunneling tip)-surface separation in equation (V.1) is very close to the almost purely exponential dependence observed experimentally [Chen 1993].

The change in tunneling current associated with a change in the (tunneling tip)-surface distance can be found from equation (V.1). If it is assumed that the lateral dependence of the tunneling current density does not change for small relative displacements, the ratio of tunneling currents is given by

$$\frac{I_2}{I_1} = \frac{s_1}{s_2} \exp\left[-2\,\kappa_o\,(s_2 - s_1)\right]. \qquad (V.3)$$

Evaluating this for an average work function of about 5 eV, the tunneling current changes by approximately one decade for a change in (tunneling tip)-surface separation of 1Å. This assumes that the (tunneling tip)-surface separation is on the order of 10Å. Such an exponential response is observed [Binnig and Rohrer 1982 and 1986, and Chen 1993], where the tunneling current changes by the about one decade per angstrom. It should be noted that the decade per 1Å current response is for vacuum.

In air the tunneling barrier is a dielectric material and the effective barrier is reduced. This leads to a reduction in sensitivity [Chen 1993, and Moreau and Ketterson 1992]. Digital Instruments, Inc., the manufacturer of the base STM for the experiments performed in this thesis, claims that the response is reduced to a level where the tunneling current changes by a factor of two for every 2Å change in (tunneling tip)-sample separation. Similar numbers are given by Moreau and Ketterson. Thus in air the inverse

decay length can be found to be $2\kappa_o$ (Å) ≈ 0.35. Assuming a purely exponential tunneling current dependence on distance [Chen],

$$I_t = C\ V \exp[-0.35\ s], \tag{V.4}$$

where C is a constant and s is in angstroms.

V.2b The Standard STM Instrumentation

The STM is constructed to permit one tunneling electrode, the tunneling tip, to be brought controllably to within 1nm of the surface being scanned, which acts as the counterelectrode. The surface being scanned cannot be insulating. The tunneling tip is made of a fine metallic wire, typically platinum with 20% iridium, which has been mechanically cut or electrochemically etched to a very sharp point. A radius of curvature on the order of 10 nm is attainable [Chen 1993]. This tunneling tip is mounted on a piezoelectric material, typically a tube, which can be deformed in all three orthogonal directions (see Figure V.1) permitting the tip to be moved over the surface following the surface topography.

The piezoelectric tube used in the STM can be deformed in the x- and y-direction to permit displacement of more than 100μm. The z-direction deformation is much less, on the order of 5μm . Thus in order to initiate tunneling, engaging the tunneling tip, the tip must be brought close to the sample using a different mechanical system.

As the STM scans the tunneling tip in the x-y plane it must respond to the surface topography to prevent the tip to surface distance from becoming quite large, and causing the tunneling current to go to zero, or touching the surface (a tip crash), causing continuous electrical contact with the surface. This is prevented by an electronic feedback system shown in Figure V.2. This system consists of a preamplifier, with a 15kHz low pass filter, which in one type of design monitors the current through a resistor, or in other designs acts as a current to voltage converter directly. The frequency cutoff of

15kHz is chosen so that the STM operates below the natural frequencies of the piezoelectric tube, typically above 30kHz. The preamplifier is connected to the piezoelectric controller by a feedback loop to keep the tunneling current at a predetermined constant level by adjusting the voltage applied to the piezoelectric tube, controlling the (tunneling tip)-surface separation.

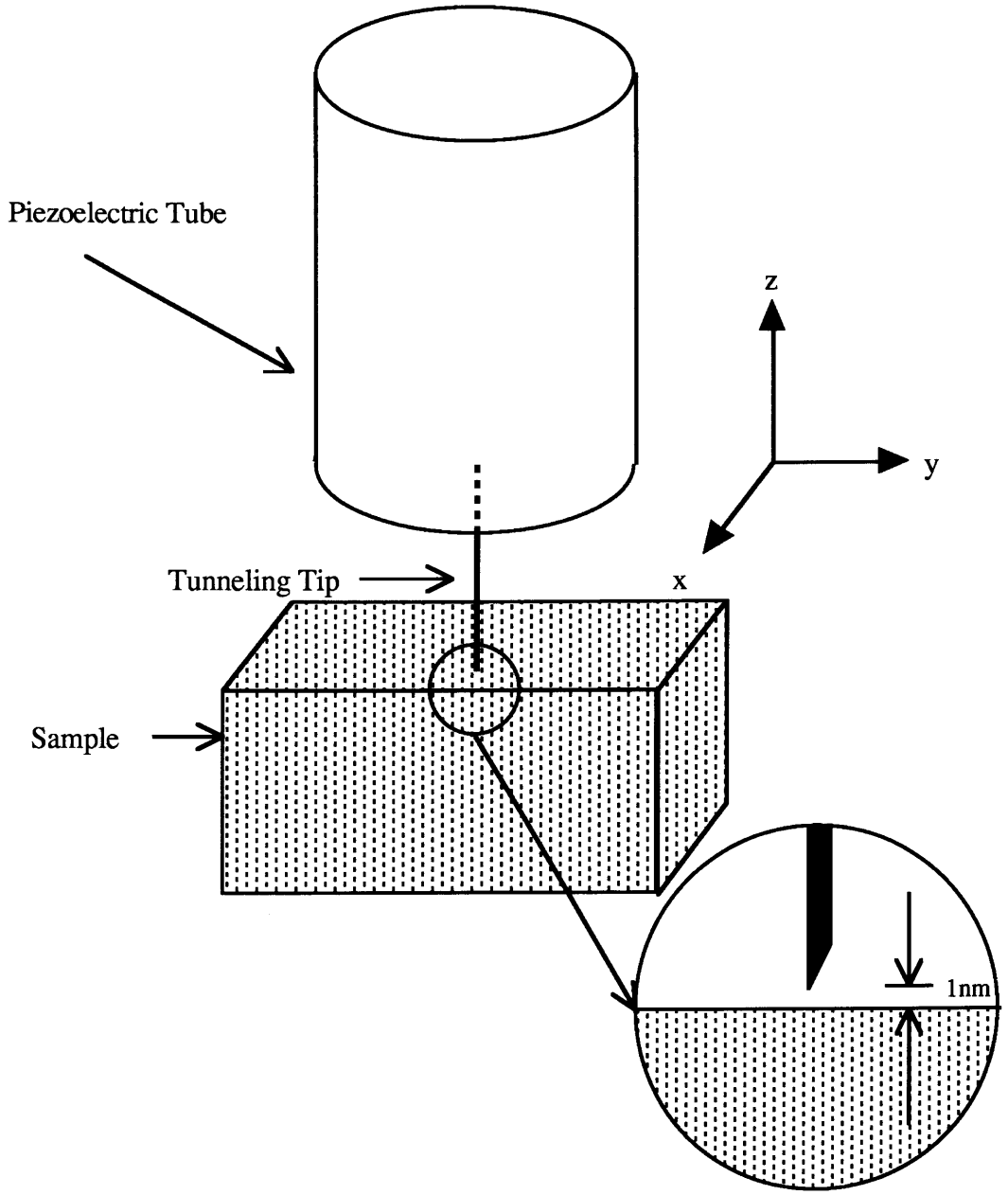

Figure V.1 Piezoelectric tube and tunneling tip relative to sample being scanned. The tunneling tip height off the surface is on the order of 1nm.

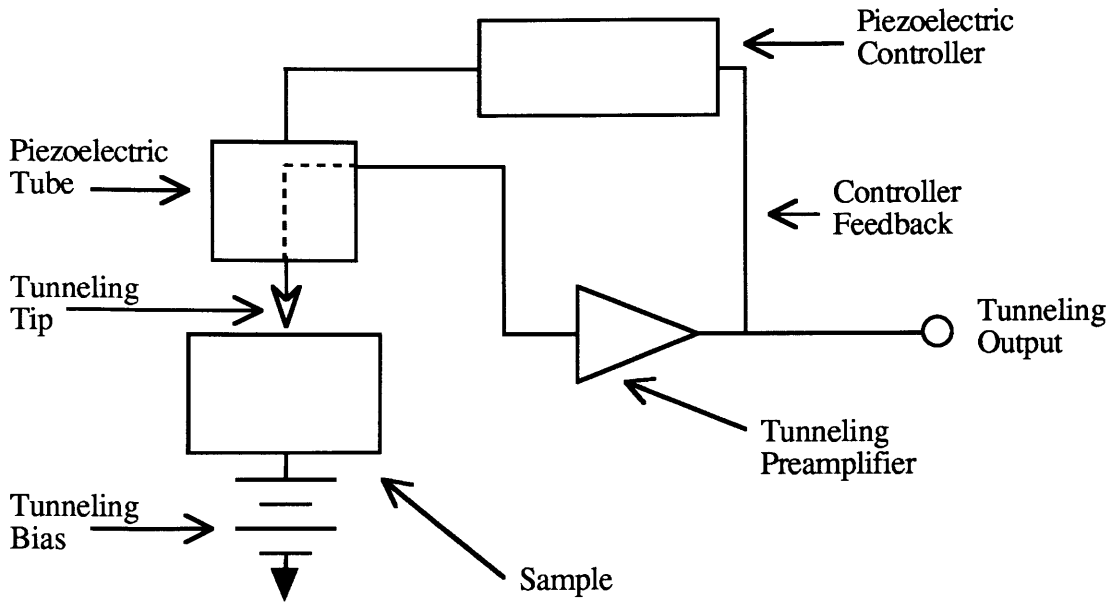

Figure V.2 Block diagram of standard Scanning Tunneling Microscope. The preamplifier can either measure the voltage drop across a resistor to ground produced by the tunneling current, or can be a current to voltage converter. The preamplifier is FET input to limit the required biasing current since the typical tunneling currents are on the order of 1nAmp.

The voltages applied to the piezoelectric tube are a direct measure of the surface topography if is the average work function of the tunneling tip and sample remains constant. For most simple imaging applications the average work function is assumed to be constant. Deviation from this can cause spurious imaging results.

V.2c The Tunneling Transducer Design

The standard STM has a number of limitations that require modification in order for it to be used as a transducer to measure acoustic emission. The 15kHz low pass filter on the preamplifier, though critical for piezoelectric control purposes, is almost three orders of magnitude too low for meaningful measurement of acoustic emission from domain wall motion. Thus a second tunneling current amplification system is needed to measure the high frequency components to the tunneling current (see Figure V.3).

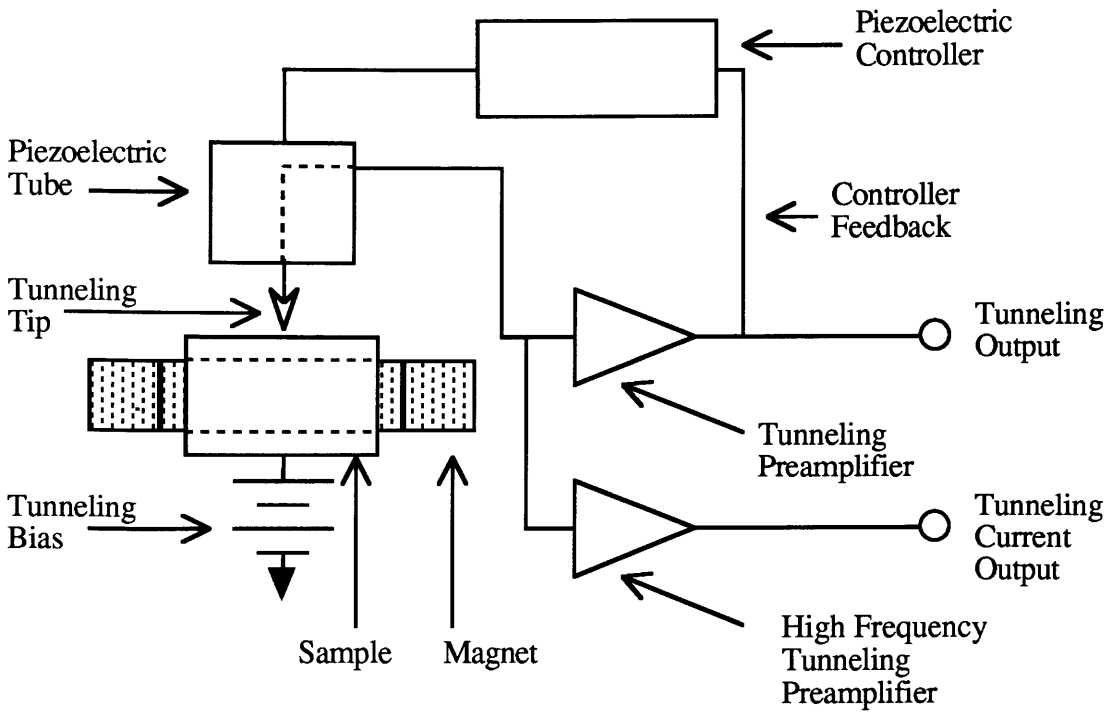

Figure V.3 Modification of a standard Scanning Tunneling Microscope to measure high frequency magnetoacoustic emission. A second high frequency tunneling preamplifier is added to the circuit. Also the sample is shown surrounded by an electromagnet to permit magnetization of the sample.

The tunneling transducer uses the low frequency feedback system to keep the DC and low frequency tunneling current constant by adjusting the absolute position of the tunneling tip. The high frequency amplifier is able to measure the high speed absolute deflection of the tunneling surface as long as that surface does not move enough to cause the tip to disengage or crash into the surface. Thus the surface deflection should be less that the separation between the tunneling tip and the surface. The resulting transducer is highly sensitive to small motion of the surface but does not have a large dynamic range.

The design of the tunneling transducer to be used for measurement of acoustic emission continues to use the feedback loop to control the tunneling tip to surface distance at low frequencies. But to measure high frequency surface motion the x-y scanning capability is not needed and is not used. Instead the tunneling tip remains fixed

in the x-y direction and responds only to z-direction motion. Assuming no low frequency drift of the surface in the x-y plane and small amplitude high frequency motion in the x-y plane, the average work function remains approximately constant and the measured change in tunneling current is directly related only to the surface deflection.

The systems used for the experiments in this thesis were built using the Digital Instruments, Inc. (Santa Barbara, California); Nanoscope I and Nanoscope III STM and control system. The preamplifier provided with the STM is a FET input 100X non-inverting amplifier which measures the voltage produced across a 1MΩ resistor by the tunneling current (see Figure V.4a). The low frequency preamplifier has a 15kHz low pass filter. The high frequency amplifier creates a virtual ground at its input and is an inverting current to voltage converter with gain of 10^7volts/amp (see Figure V.4b).

The circuit diagram for the current to voltage converter is shown in Figure V.5. It uses a bipolar input AD5539 operational amplifier, buffered by a first stage MOSFET input to restrict the tunneling biasing current needed to drive the circuit. The circuit has a gain of 10^7volts/amp, and a frequency response of at least 10^7volts/amp up to almost 5MHz, with some peaking above 100kHz (Figure V.6). The limitation to the frequency is determined by the 1MΩ sensing resistor in the original Digital Instruments, Inc. circuitry and the parasitic capacitance at the inputs of the current to voltage converter. Ferrite beads are added to the circuit to minimize high frequency transient pickup above 50MHz. These beads are #73 material made by Amidon Associates (North Hollywood, California).

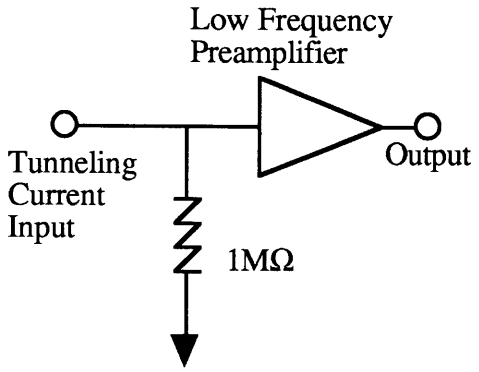

Figure V.4a

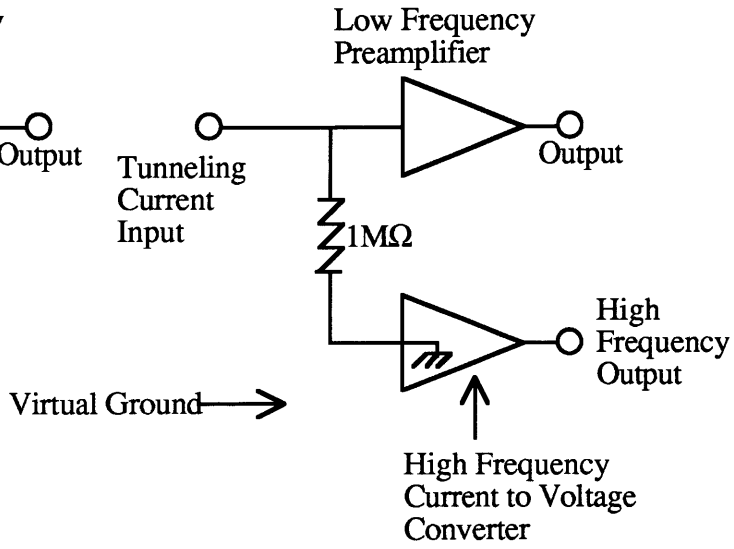

Figure V.4b

Figure V.4 a) The block circuit diagram of the Digital Instruments Inc. tunneling head. The preamplifier is built with a AD711 FET input operational amplifier. The preamplifier measures the tunneling current by monitoring the voltage across a 1MΩ sensing resistor that is connected between the tunneling tip and ground. b) The modified amplification system. A high speed MOSFET input current to voltage converter is added to the setup by tieing the 1MΩ sensing resistor to a virtual ground and measuring the current into that virtual ground.

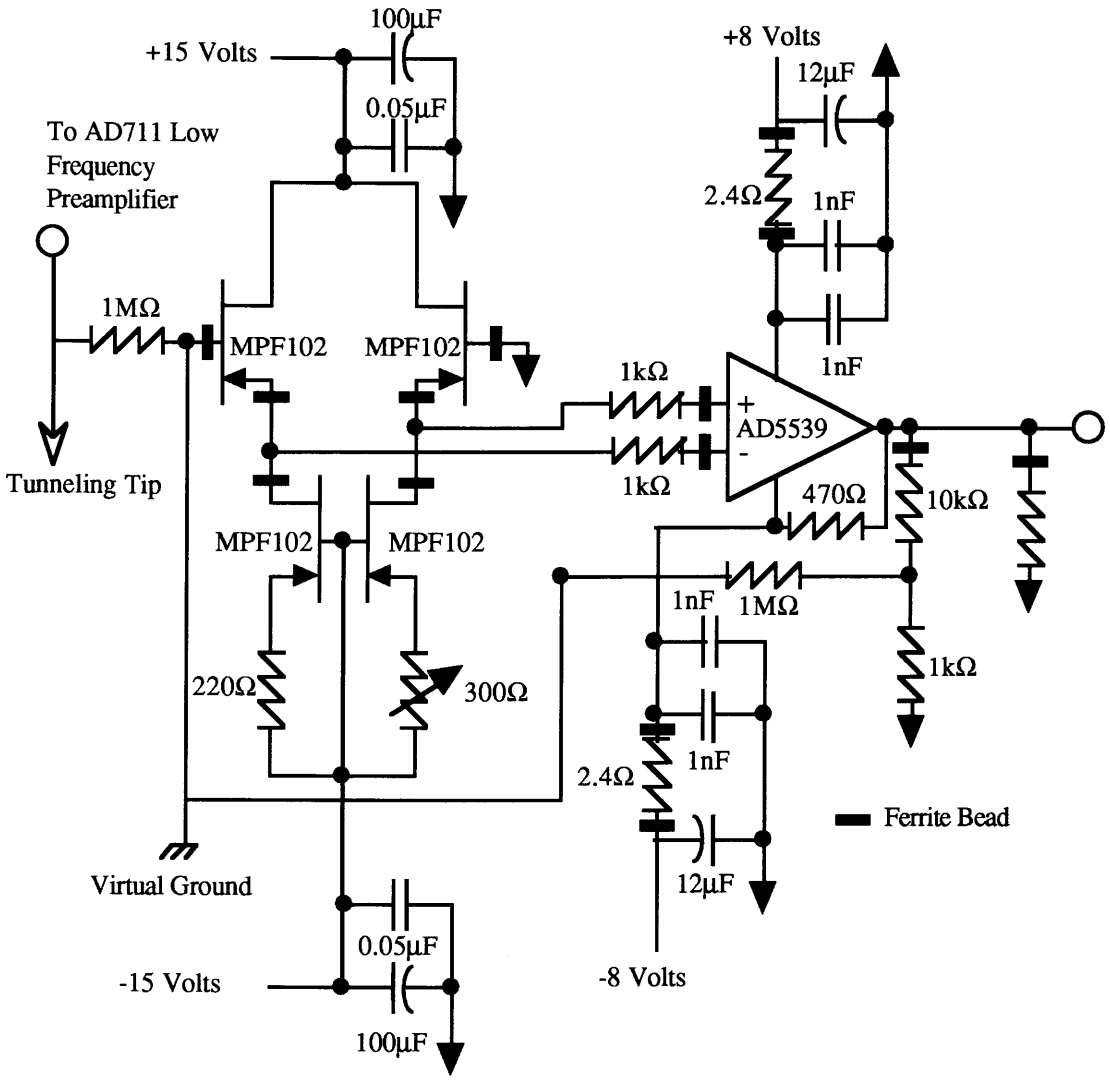

Figure V.5 High frequency inverting current to voltage converting amplifier. Amplifier has individual MOSFET's as a front end. The input of the tunneling current is the virtual ground point shown in Figure V.4b. Ferrite beads limits high frequency, greater than 50MHz, transients. LM7808 and LM7908 voltage regulators provide ± 8 volts for the AD5539. The circuit is built backed by a ground plane to cut down electromagnetic transient pickup.

The design of the current to voltage converter permits the STM to operate consistent with the original design of Digital Instruments, Inc. Normal operation of the STM is achieved by adjusting the potentiometer in the current to voltage converter to null

out any offset. It was found that during normal operation there is some drift in the circuit. Thus it is necessary to readjust the null occasionally during experimentation.

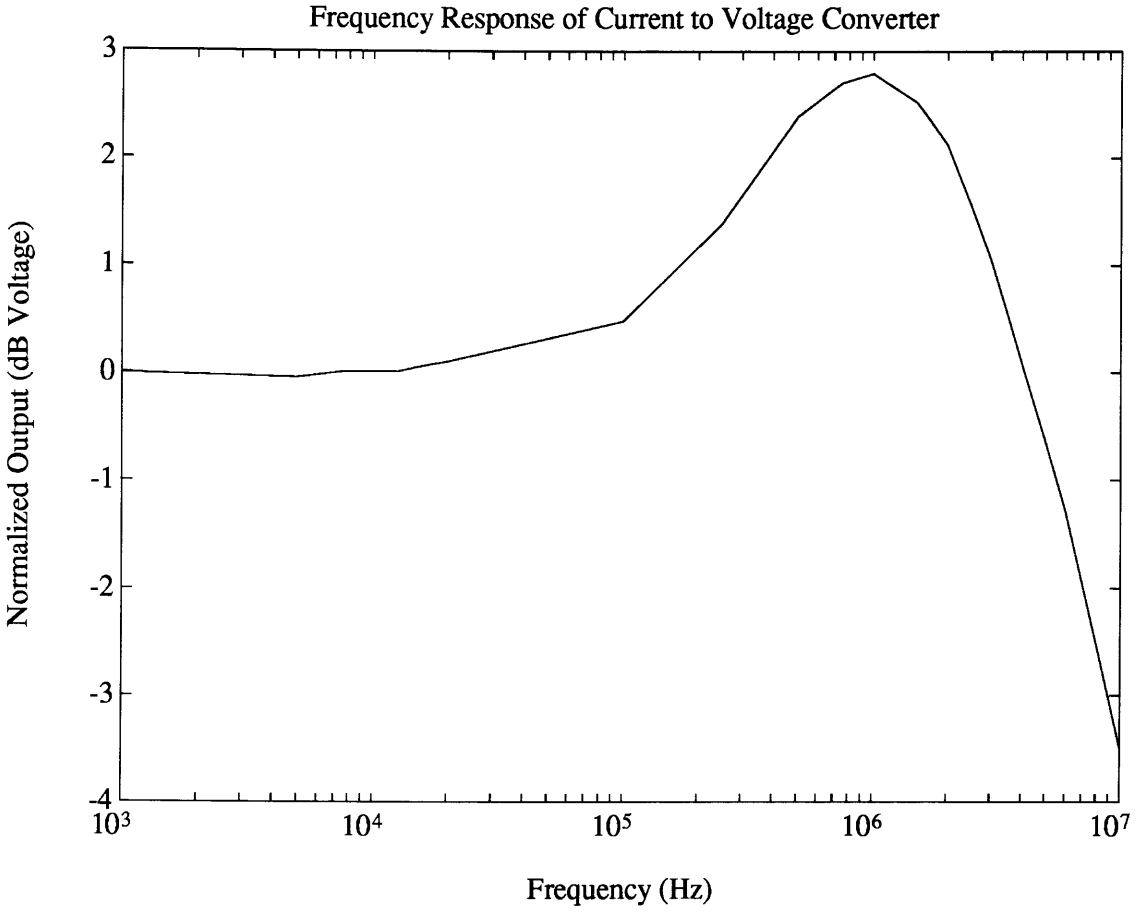

Figure V.6 The frequency response of the current to voltage converting amplifier shown in Figure V.5. The output is normalized to 10^7volts/amp, and is given in dB. The frequency response peaks at about 1MHz. But the gain does not drop below 10^7volts/amp until between 4 and 5MHz; 3dB bandwidth is almost 9MHz. The response is measured using an AC signal at the converter input.

V.2d Noise Performance of the Tunneling Transducer

The high frequency tunneling transducer has a much wider bandwidth than the STM and as a result, it experiences a much higher electrical noise level. The two main sources of noise are the shot noise caused by the tunneling process, and the amplifier

noise produced by the current to voltage converter. The root mean square shot noise is given in terms of the tunneling current I_t:

$$I_{sh} = \sqrt{2\, q\, I_t\, B}, \qquad (V.5)$$

where q is the electron charge, 1.6×10^{-19} coulombs, and B is the bandwidth [Ott 1976]. For a bandwidth of 5MHz $I_{sh} = 1.27 \times 10^{-6}(I_t^{1/2})$ in amps.

The peak to peak noise of the current to voltage converter is measured at its output with either a grounded or open front end. The measured peak to peak noise voltage can be used to determine the equivalent current noise at the input of the current to voltage converter. Figure V.7 is plot of the equivalent current noise introduced by the amplifier.

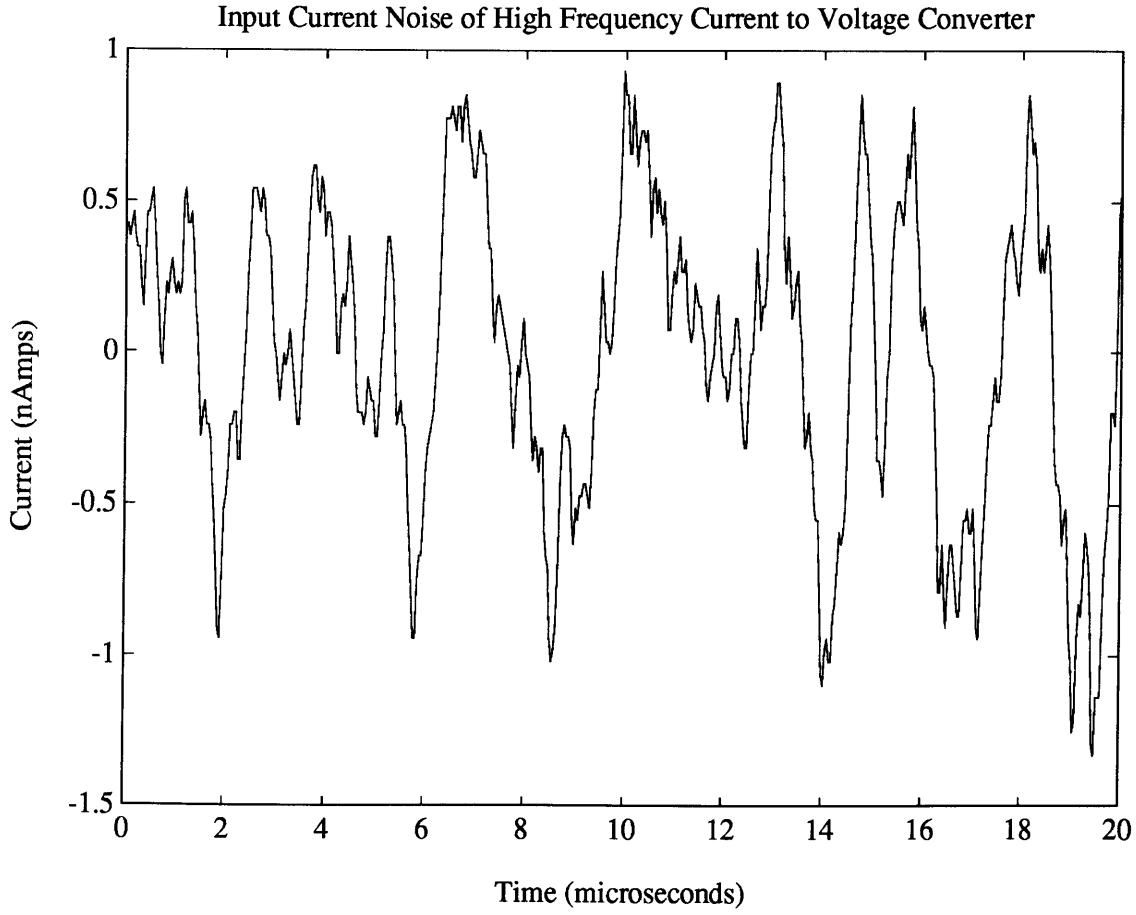

Figure V.7 Input current noise of current to voltage converter. Peak to peak noise level is approximately 2 nAmps.

The peak to peak current to voltage converter noise level is between 2 .0 and 2.5 nAmps. For shot noise to reach this level the tunneling current would have to be approximately 1μAmp. Thus in the current regime used in typical tunneling measurements (< 100nAmps) the dominant noise contribution is from the current to voltage converter.

The conversion of this noise level to equivalent surface deflection can be estimated using the relation that the tunneling current changes by a factor of two for each 2Å of change in (tunneling tip)-surface separation in air. Using equation (V.4) the change in the tunneling for small changes in the (tunneling tip)-surface separation is approximately given by

$$|\Delta s| = \frac{|\Delta I_t|}{0.35\, I_t}. \tag{V.6}$$

For a tunneling current of 10nA, the input noise of the current to voltage converter has an equivalent surface motion of approximately 0.6Å. Increase in the tunneling current will decrease the equivalent surface motion noise floor. In addition, a number of signal averaging techniques can be employed to further reduce the equivalent surface motion noise floor.

V.3 Measurement of Surface Motion Using a Tunneling Transducer

The tunneling transducer can be used in a number of configurations to permit measurement of surface deflection caused by acoustic emission. For a plane longitudinal elastic wave reflecting off a free surface, the tunneling transducer is mounted normal to the surface (see Figure V.8). As the surface moves towards the tunneling tip the tunneling current is increased. As the surface moves away from the tunneling tip, the tunneling current decreases. The sensitivity of the tunneling current to surface displacement is exponential. Using the in air approximation for the tunneling exponential function, the tunneling current changes by a factor of two for every 2Å of displacement of the surface.

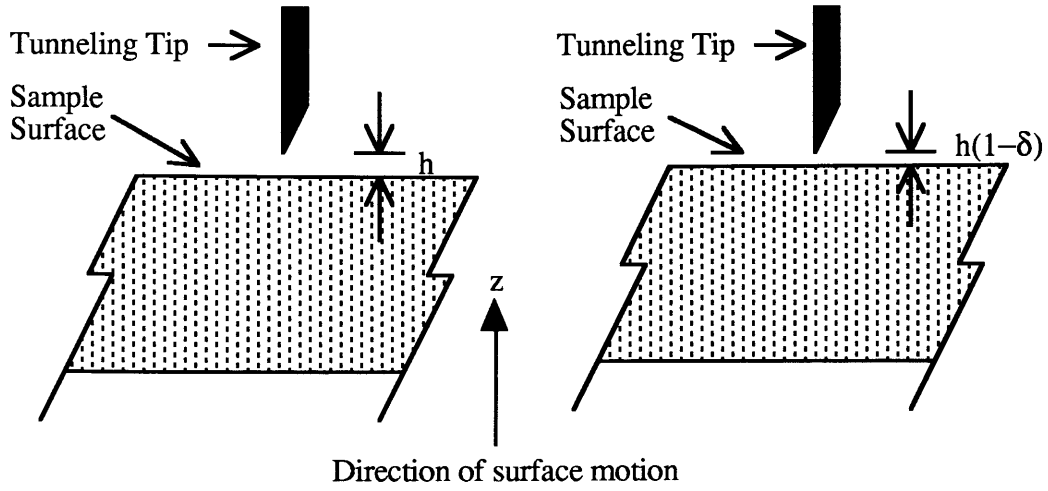

Figure V.8 Surface deflection relative to a stationary tunneling tip for a longitudinal plane elastic wave traveling in the z-direction. If the surface moves δh in the positive z-direction the tunneling tip to surface distance decreases by δh, causing an increase in the tunneling current.

The tunneling transducer is insensitive to a shear wave that are incident normal to a perfectly flat surface because the distance between the surface and the tunneling tip remains constant. If the surface is not smooth then the normal incident shear wave will cause topographical features to move under the tunneling tip and cause changes in the tunneling current (see Figure V.9). The tunneling transducer can detect large tangential surface motion in this manner. But quantification of the motion is very difficult because the tunneling transducer is only measuring the distance between the tunneling tip and the surface. To determine the extent of tangential surface motion the surface topography must be known.

For small tangential surface motion 1Å or less, the surface topography does not change enough to permit detection of the shear elastic wave. For small shear waves the tunneling transducer has the same disadvantage as the capacitive transducer, the direct

motional change due to the shear wave is smaller than the area of interaction between the tunneling tip and the surface. Thus, for small shear waves, a different setup is needed.

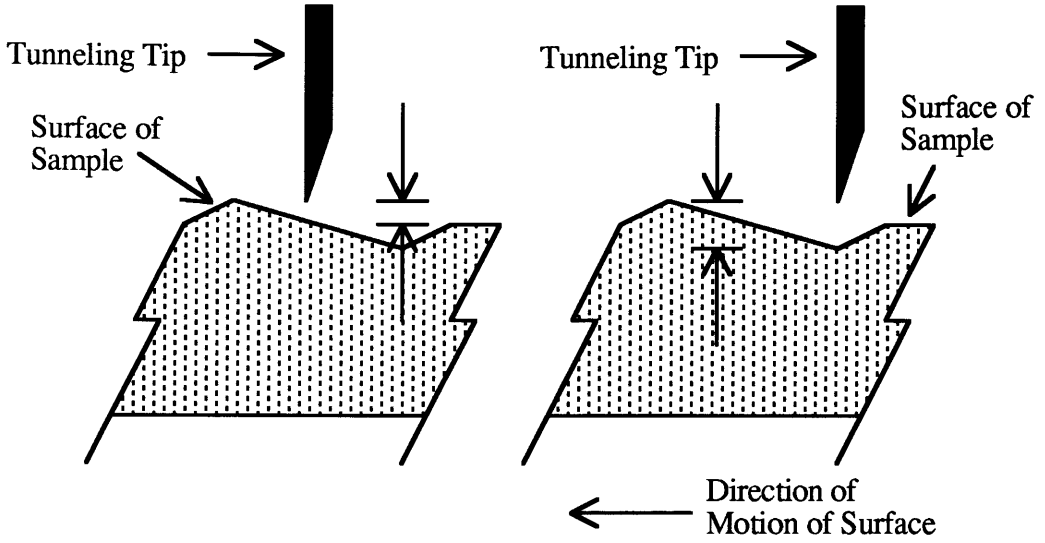

Figure V.9 Deflection of the surface caused by a shear elastic wave incident in the z-direction. The surface topography causes the tunneling tip to surface distance to change during tangential surface motion.

One method of measuring very small planar shear waves is to measure on a surface parallel to the direction of propagation of the shear wave. In this configuration the surface of the sample is once again moving either away from or towards the tunneling tip causing a change in the tunneling current (Figure V.10). Large shear as that shown in Figure V.10 as well as small traveling shear waves (Figure V.11) can be detected in this configuration. Such motion cannot be easily differentiated from Rayleigh waves [Kolsky 1963], suggesting that the tunneling transducer can also be used to detect small surface waves.

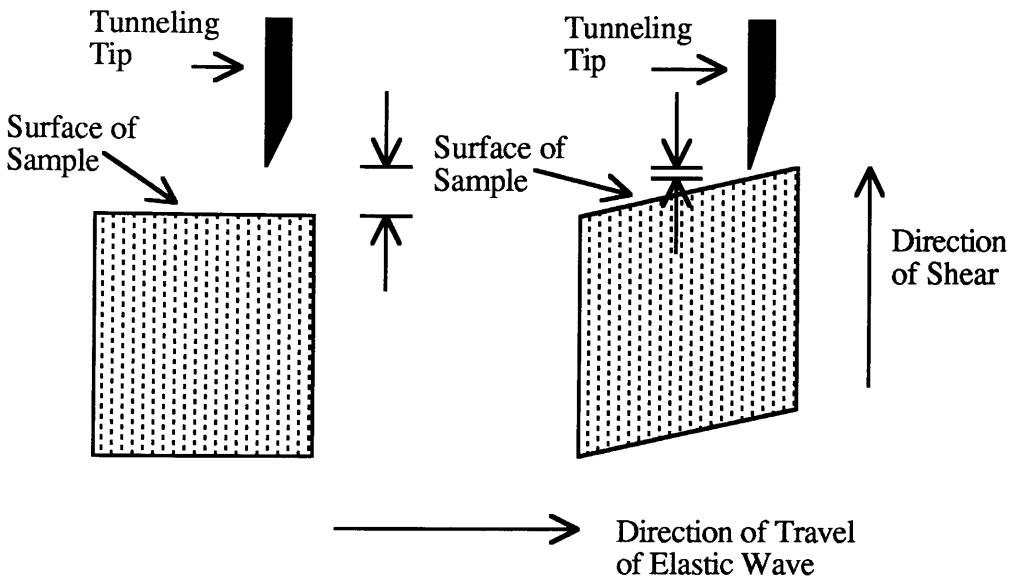

Figure V.10 Measurement of a shear wave on a surface parallel to the direction of propagation of the wave and orthogonal to the shear direction. In this configuration the surface moves in such a manner that the distance between the tunneling tip and the surface changes causing a change in tunneling current.

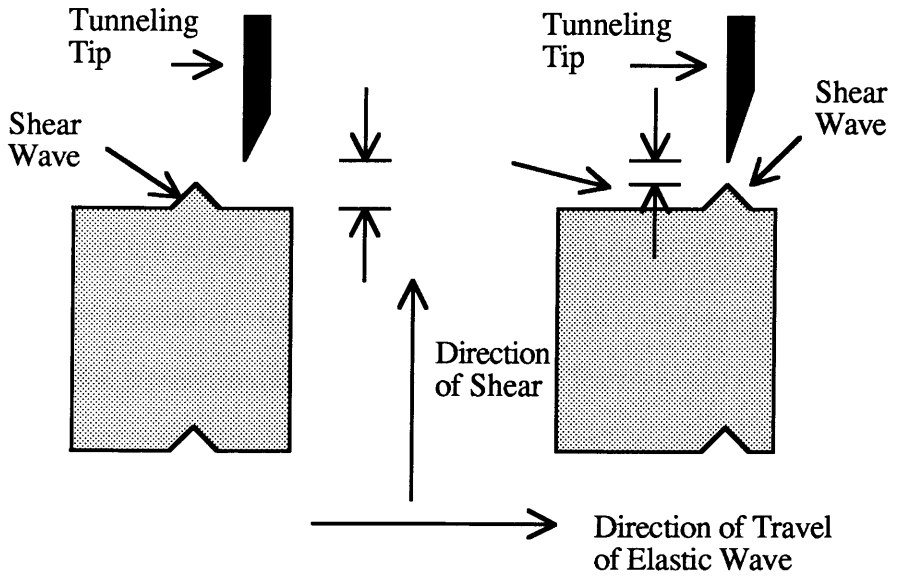

Figure V.11 Small shear wave traveling in a direction parallel to the surface being monitored. Here the stationary tunneling transducer is sensitive to surface features moving under the tunneling tip.

Chapter VI: Experimentation on a 3% SiFe Picture Frame Single Crystal

VI.1 Introduction

The verification of the existence of magnetoacoustic emission from an accelerating 180° domain wall requires an experiment method to isolate a moving 180° domain wall from all other moving domain walls. In most single crystal and polycrystalline materials the domain configuration is complicated enough to obfuscate the source of magnetoacoustic emission. Lord [1967] suggests that to isolate magnetoacoustic emission for a single domain wall a single crystal of picture frame geometry can be used. Although a picture frame single crystal made of a ferrite material is the ideal candidate to isolate large single source magnetoacoustic emission, such samples are not readily available, and very difficult to fabricate. On the other hand metallic picture frames are slightly easier to fabricate. Because of the availability of one sample for experimentation a metallic picture frame was chosen as the test sample for the thesis experimentation. The picture frame single crystal of 3% silicon iron was provided by Dr. Robert F. Krause of Magnetic International, Inc., Burns Harbor. Indiana.

VI.2 Picture Frame Single Crystal Background

The single crystal of picture frame geometry is ideal for experimentation which requires isolation of motion of 180° domain wall motion. In a single crystal of cubic magnetic material the picture frame geometry permits the formation of a very simple domain configuration. This simple domain configuration minimizes the magnetic energy of the material, while permitting magnetization entirely through 180° domain wall motion. There are non-180° domain walls in the picture frame. But these walls are immobile. Early experimentation on picture frame geometries exhibited high maximum permeability and low coercive field levels [Williams 1937, Williams and Shockley 1949 and Williams et al. 1949]. The high permeability and low coercive field make the geometry ideal for experimentation on single domain wall motion.

A number of picture frame geometries can be fabricated. The geometry is dependent on the type of 180° domain wall needed to be isolated, and whether the material has an easy axis in the [100] or [111] directions (see Appendix A). For a material with an easy axis in the [100] direction, a material with a positive cubic anisotropy constant, the picture frame geometry which isolates 180° domain wall in the (100) plane is shown in Figure VI.1. Here each surface side of the picture frame is a (100) plane.

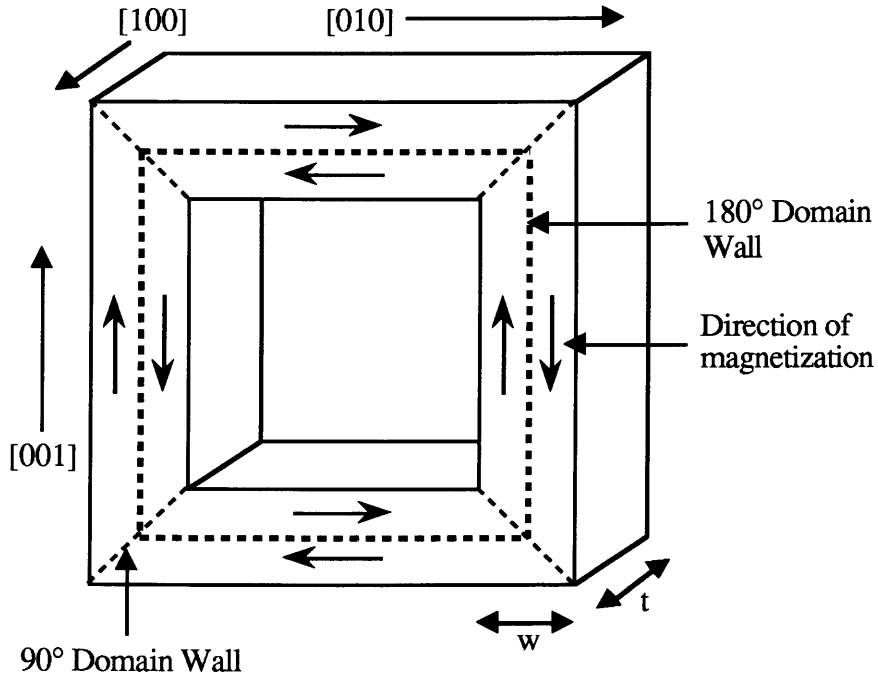

Figure VI.1 A single crystal picture frame with (100) plane 180° domain walls. If the width of a leg on the picture frame is greater than the thickness (w > t) the planes of the 180° domain wall are orthogonal to the largest faces of the crystal, as shown above. If t > w then the planes of the 180° domain walls are coplanar with the largest faces. The 90° domain walls are planes at the edge of the picture frame.

For a 180° domain wall in the (110) in a cubic material with positive anisotropy constant the shape of the picture frame is the same as that shown in Figure VI.1, except that the

sides of the picture frame are the (110) planes. Other 180° domain walls exist in this type of cubic material. But the two discussed above are the most common [Chen 1986].

If the material being investigated has an easy axis in the [111] direction, the picture frame has a diamond shape, see Figure VI.2. Typical materials that have the [111] easy axis are nickel and most ferrite materials. In this material the two most common 180°

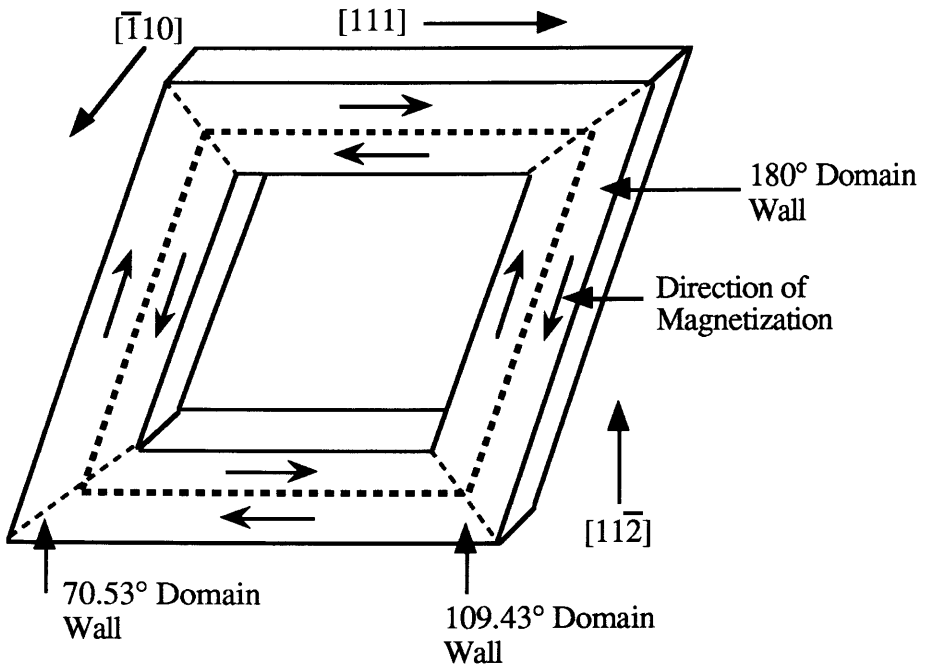

Figure VI.2 A single crystal picture frame with (110) plane 180° domain walls. Again depending on the size of the legs the 180° domain walls can either be (110) planar or (112) planar [Galt 1952, Chen 1986]. The edge domain walls, which are immobile are either 70.53° or 109.43°.

domain walls are referred to as 70.53° and 109.43° domain walls, or sometimes non-180° domain walls. In this geometry the non-180° domain walls are immobile, where as the 180° domain walls are mobile.

In order to drive the 180° domain walls in the picture frame single crystal a magnetic field is applied parallel to one the legs of the crystal [Stewart 1951]. When the field is applied all the 180° domain walls translate together around the crystal (see Figure

VI.3). If the 180° domain walls do not move in unison a large magnetostatic self field will form along the 90° domain walls. Motion in unison minimizes magnetostatic self field contributions. So far the description assumes that the domain wall remain planar.

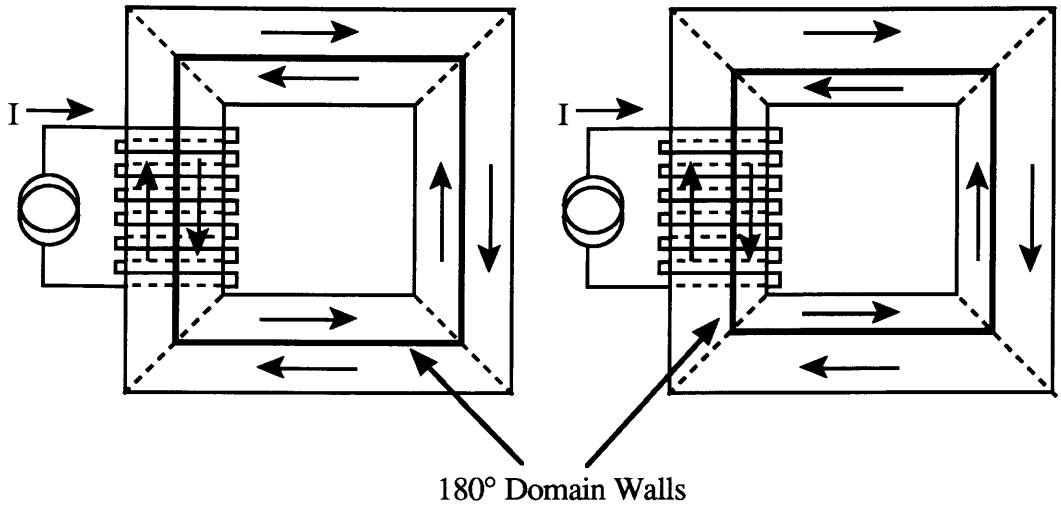

Figure VI.3 180° domain wall motion in a picture frame single crystal. As the magnetic field is applied in the up direction within the magnetic field source coil the domain wall moves toward the center of the single crystal. When the magnetic field is reversed the domain walls move toward the outer edges of the crystal.

The velocity of the 180° domain wall is determined in Appendix C to be a linear function of applied field. The micromagnetic calculation results in a velocity function which is inversely proportional to the Gilbert damping coefficient [Gilbert 1955, Schryer and Walker 1974]. This result has been experimentally verified by Williams et al. [1950], Stewart [1951] for SiFe and Galt [1952] and Dillon and Earl [1959] in ferrites. The velocity relation is slightly modified for a real crystal where a finite applied field is needed to initiate domain wall motion:

$$v_y = c\,(H_o - H_{cr}), \qquad \text{(VI.1)}$$

where H_{cr} is the critical field for domain wall displacement and c is a constant dependent on the material and geometry of the sample [Chikazumi 1986]. In a ferrite where the damping is caused by precessional loss the constant, c, is independent of geometry. In metallic magnetic materials where eddy current loss dominates, c is dependent on the sample geometry. In a high quality picture frame single crystal H_{cr} is very small, thus a 180° domain wall velocity is approximately $v_y = cH_o$.

So far the 180° domain wall model has assumed that the domain wall is planar. This is a good approximation for very small applied magnetic fields, i.e., low domain wall velocity. At larger fields the 180° domain wall no longer remains planar in metallic ferromagnets [Williams et al. 1950, Chikazumi 1986]. Instead the wall becomes curved and in some cases cylindrical in cross-section. This is caused by the difference in local eddy current damping, which is much larger in the center of the material than at the surface.

VI.3 Characterization of 3% SiFe Picture Frame

The 3% SiFe single crystal picture frame provided by Dr. Robert F. Krause of Magnetic International, Inc., Burns Harbor. Indiana, has dimensions 2cm x 2cm and a thickness of 0.017cm. The leg width is 0.5cm. The sample is (100)[001] cut from cube textured SiFe (See Chen [1986] for information on the metallurgy of transformer steels). The orientation was determined by Laue x-ray diffraction and alignment of the crystal is quoted to be better than 0.5° [Krause 1992]. The crystal was cut and mechanically polished. Finally the crystal was electrolytically polished and annealed to remove strain at the surfaces. The fabrication of the picture frame single crystal was done by Dr. Krause.

VI.3a Domain Structure

Measurements of the domain structure of the picture frame were made to determine the quality. The domain structure of one leg of the picture frame was found using Bitter patterning [Chikazumi 1986]. The Bitter patterning was done using a ferrofluid provided by Ferrofluidics Corporation, Nashua, New Hampshire. The ferrofluid is a suspension of fine ferromagnetic particles (approximately 80Å) in mineral oil.

Figures VI.4 is a photomicrograph of the Bitter pattern on one leg of the picture frame. The domain structure does not exhibit the simple structure shown in Figure VI.1. Instead there are complex "tree" pattern domains [William et al. 1949 and William and Shockley 1949]. The "tree" pattern is shown at higher magnification in Figure VI.5a.

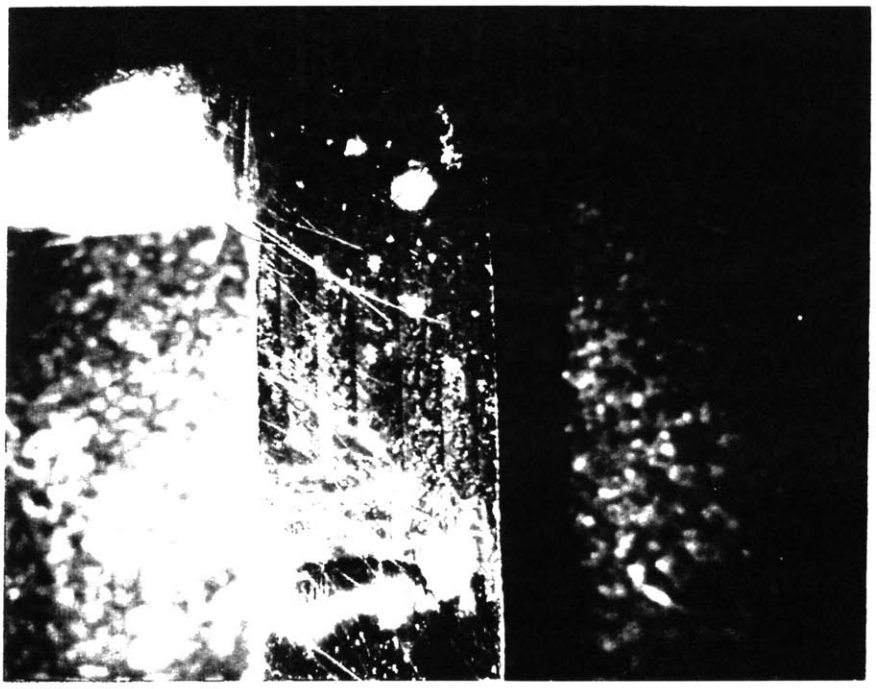

Figure VI.4 A photomicrograph of the domain configuration of the SiFe picture frame single crystal used for magnetoacoustic emission experiments. The leg contains six vertical 180° domain walls. Magnetization is 6.3X.

The "tree" domain pattern forms on a smooth strain relieved surface that is slightly misaligned with the plane containing an easy direction. Since the surface is slightly out of perfect alignment, there is magnetic poling on the surface (a finite magnetostatic self energy). The "tree" domains permit redistribution of the surface poles thus lowing the magnetostatic self energy of the crystal, Figure VI.5 [Chikazumi 1986]. William et al. determined experimentally that if the surface of a ferromagnet is between 0.5° and 1.3° out of alignment the "tree" pattern forms similar to that shown in Figure VI.5a. Since the "tree branches" have not filled the entire space along the domain wall in Figure VI.5a, alignment of the crystal is better than 1°.

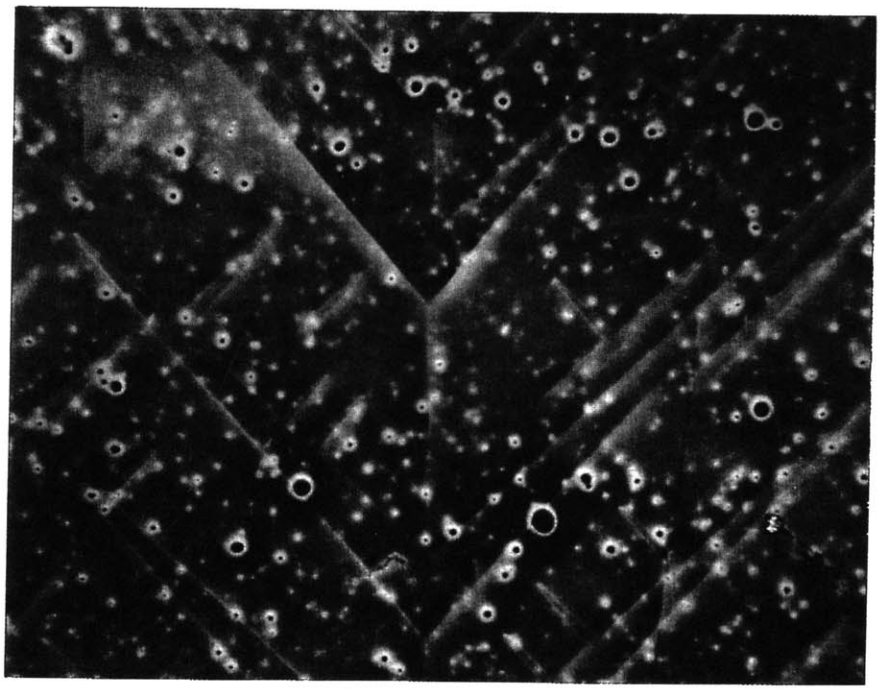

Figure VI.5a Shows a photomicrograph "tree" domains on the surface of SiFe picture frame. Magnification is 200X.

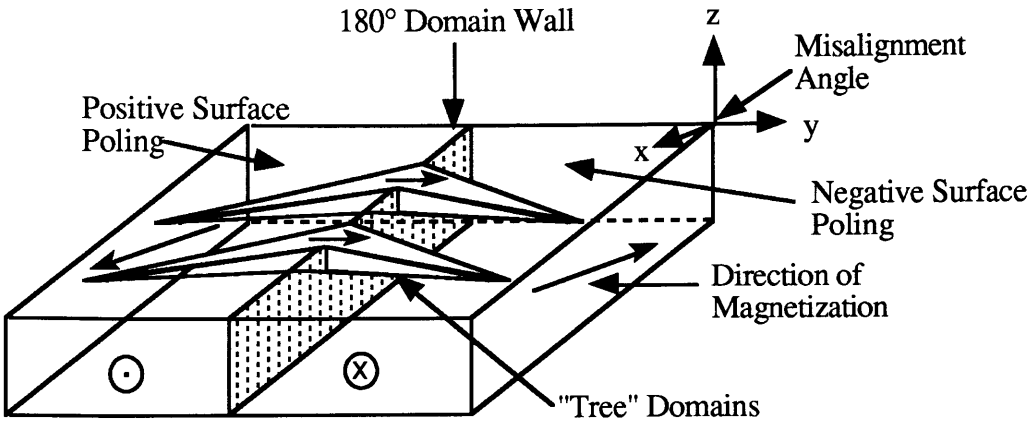

Figures VI.5b "Tree" domain pattern on a surface slightly misaligned relative to an easy axis. Poling and magnetization in the vicinity of the "tree" domain is depicted. Here the branches of the "tree" pattern are separated along the 180° domain wall. This type of pattern exists for misalignment from 0.5° to 1.3° [William and Shockley 1949]. The separation of individual branches along the 180° domain wall disappears as the misalignment approaches 1.3°.

The existence of "tree" domains on the surface of the picture frame results in a non-ideal domain configuration for absolute isolation of 180° domain wall motion. When the 180° domain wall moves the "tree" domains move resulting in motion of the 90° domain walls surrounding the "tree" domains. In addition in an applied magnetic field Williams et al. [1949] observe shrinking of the "tree" structure in domains that are oriented antiparallel to the applied magnetic field, and growth in domains parallel to the applied magnetic field. Still measurements made on SiFe picture frames containing "tree" domains indicate the magnetization process is dominated by the motion of the 180° domain walls [Williams and Shockley 1949]. This is because the "tree" domains penetrate only approximately 10% of their width [Williams et al.].

A second feature of the domain structure shown in Figure VI.4 is the multiple 180° domain walls on a single leg. Multiple domain walls are again a consequence of misalignment. The formation of two antiparallel domains and large "tree" domains is less energetically favorable than the formation of multiple antiparallel domains with small

"tree" domains. The reason for this is that the magnetostatic self energy caused by poling at the surface is proportional to the size of the domains [Chikazumi 1986]. The size of the domains is limited by the relative increase in domain wall energy for smaller domains. Thus even ignoring the "tree" domains, isolation of a single 180° domain is impossible in the picture frame. Instead the measurements must include six 180° domain walls at once.

V.3b Domain Wall Velocity Measurements

The velocity of the domain wall in the picture frame can be determined directly from magnetization measurements. The electromotive force produced in a sense coil is given by

$$V = -N\frac{\partial \Phi}{\partial t}, \tag{VI.2}$$

where Φ is the flux through the sense coil. Assuming the simple domain configuration of Figure VI.1 in a picture frame the velocity of the domain wall can be written in terms of the time derivative of the flux, see Figure VI.6

$$v_y = -\frac{V}{2 N M_s d}, \tag{VI.3}$$

where d is the thickness of the picture frame. The calculation assumes that $\partial H/\partial t$ is small compared to $\partial M/\partial t$. This is valid for fields levels required to move the domain walls in a soft magnetic material. In the case of multiple 180° domain walls the average velocity can be found by dividing the single domain wall velocity found in equation (VI.3) by the number of 180° domain walls in a leg.

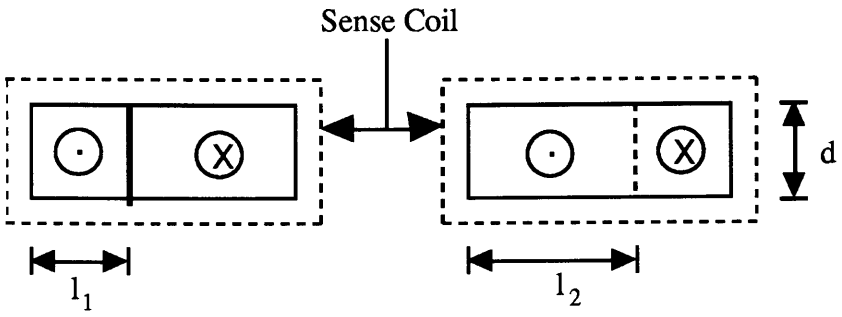

Figure VI.6 As the 180° degree domain wall moves to the left, there is a magnetization reversal of 2 M_s. Assuming $\partial H/\partial t$ is small, the change in flux is just the area where the reversal takes place $v_y d$ where $v_y = (l_1 - l_2)/\Delta t$.

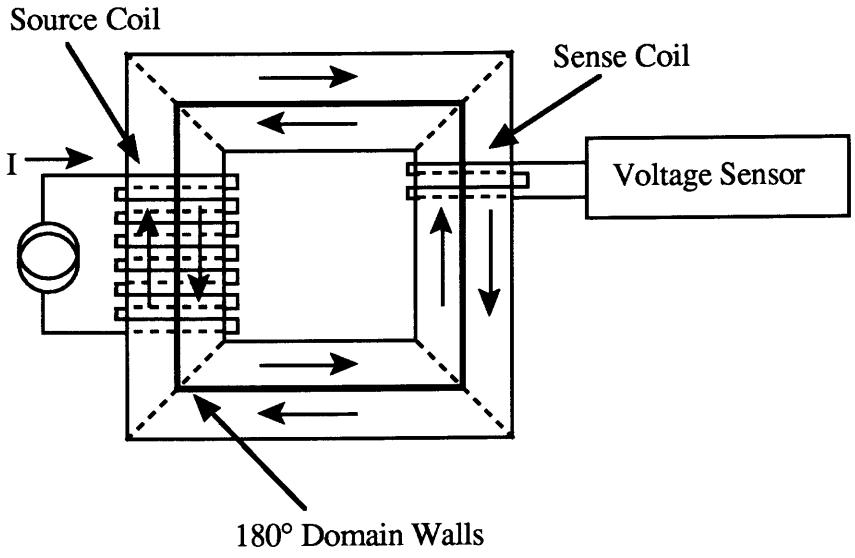

Figure VI.7 Source and sense coil configuration on SiFe picture frame. Sense coil can be placed on any leg of the picture frame. The current source used is a pulse source with controllable duty cycle (see Figure VI.13).

The actual experimental setup used to measure the domain wall velocity is shown in Figure VI.7. The sense coil is a ten turn coil on one leg of the picture frame. The source coil is a 30 turn coil on a different leg. The output from the sense coil is similar for placement on any of the four legs of the picture frame. H field coupling between the

source and sense coil has been ruled out by tests on both insulating and conducting non-magnetic samples.

Domain wall velocity is determined for magnetic field pulses produced by the source coil. The field values range from 0.01 to 3.5 Oe. The applied field pulses have a rise time of approximately 250ns and a controllable length. For the velocity measurements the magnetic field is applied in one single pulse. The sense coil is attached directly to the input of a high input impedance, low noise, Ithaco 1201 Preamplifier with a 400kHz bandpass. The output from the preamplifier is feed directly into a Philips PM3550 Digital Storage Oscilloscope so that the output can be transferred to a computer. Figures VI.8a and VI.8b show typical domain wall velocity versus time curves observed in the picture frame for two applied magnetic fields. The average velocity is calculated assuming six domain walls, as is shown in Figure VI.4 and a saturation magnetization for 3% SiFe of approximately 2.0 Tesla [Chen 1986]. The voltage induced in the sense coil is assumed to be produced by 180° domain wall motion.

At the beginning and the end of the magnetic field pulse the voltage output from the sense coil exhibits a relative positive and negative spike respectively, which is depicted as velocity in Figures VI.8. The spiking is an order of magnitude greater than the maximum size possible for direct coil coupling. In addition the spiking remains about the same magnitude no matter which leg of the picture frame the sense coil is placed on. The spiking is probably caused by the complicated motion of the "tree" domains at the surface. Similar spiking has been observed by Dillon and Earl [1959] and Gyorgy [1960]. Dillon and Earl and Kittel and Galt [1956] suggest that the velocity spiking at the beginning of the field pulse is caused the depinning of the domain walls from pinning sites at the surface. The inverse velocity spike present at the end of the field pulse is a result of rearrangement of the domain walls to an equilibrium position.

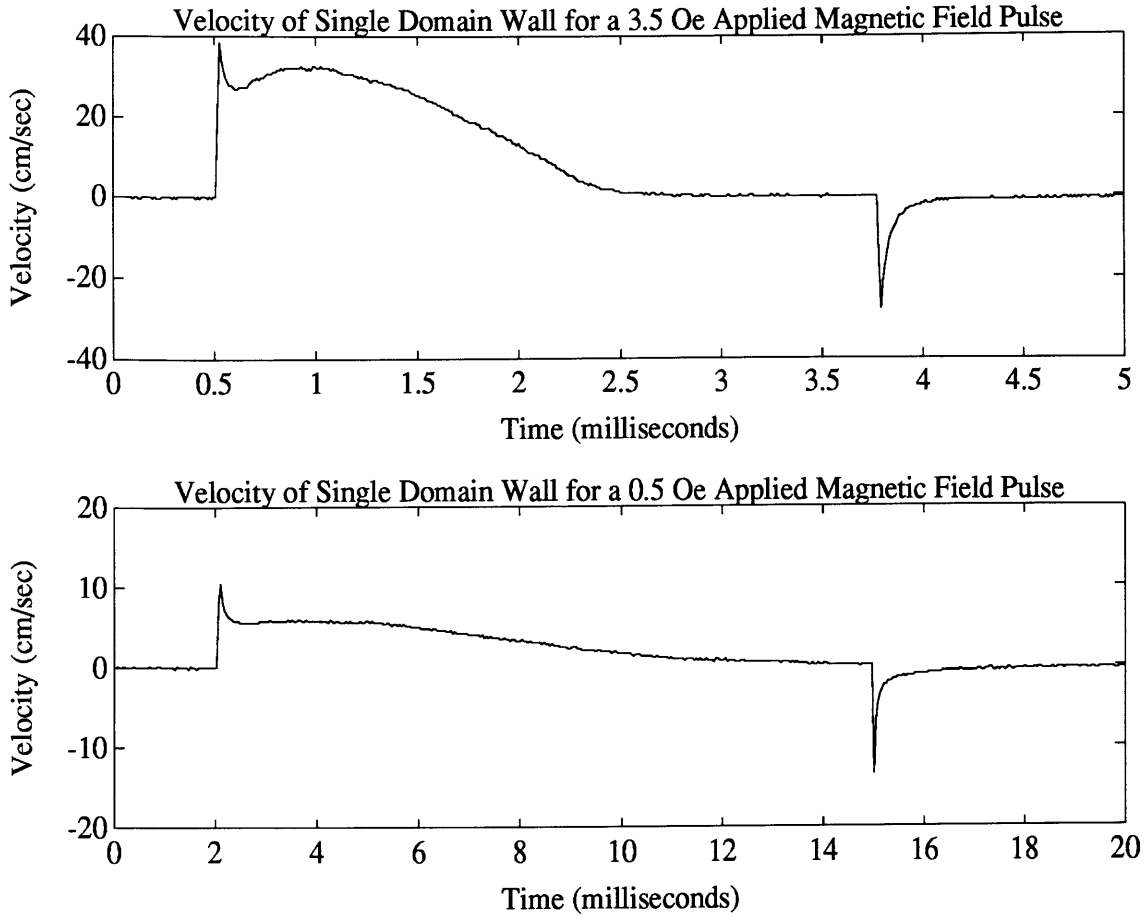

Figures VI.8 The domain wall velocity measured on the 3% SiFe picture frame. a) The applied field is 3.5 Oe. The length of the field pulse is approximately 3.5ms. b) The applied field is 0.5 Oe. The length of the field pulse is approximately 11ms. The large velocity spiking at the beginning and the end of the field pulse is related to motion of the "tree" domains.

The shape of the velocity curve is similar to those reported by Stewart [1951] and differs significantly from the profile reported by Kittel and Galt [1956] for a ferrite sample. The velocity curves found by Kittel and Galt show the initial and final spiking, but are flat, i.e., the wall moves at constant velocity, at constant field levels consistent with equation (VI.1). Since the domain walls do not appear to move with constant velocity in the SiFe picture frame, effects other than eddy current loss must be present. The decaying nature of the velocity profile is attributed to the interaction of the multiple

domain structure. In a perfectly oriented material two 180° domain walls on opposite sides of a domain magnetized antiparallel to the applied field will annihilate each other. In a misaligned material annihilation is opposed by the resulting increase in surface poling energy. Thus the two 180° domain walls are compressed together, but not annihilated until a much larger field is applied. Instead as they approach each other they repel in order to minimize poling. When the applied magnetic field is turned off, each 180° domain wall and its associated "tree" domains repel the other causing rearrangement of the domains in the material.

So far the discussion of the velocity curve has assumed that the domain wall motion is responsible for the magnetization, and thus produce the observed velocity curve. Proof that the magnetization measured by the sense coil is related to domain wall motion can be found by using an interrupted applied magnetic field pulse [Gyorgy 1960, 1963, 1993]. Since in the SiFe, the 180° domain wall moves through a highly damped system, when the applied field is turned off the domain wall should come to rest quickly. Gyorgy [1960 and 1963] shows that for soft ferromagnetic materials if the applied field is pulsed with high duty cycle and a pulse length shorter than the time required to move the wall across the sample, the domain wall will trace the same velocity profile including the interrupts. Figure VI.9 shows an interrupt test results from the SiFe picture frame used in this thesis.

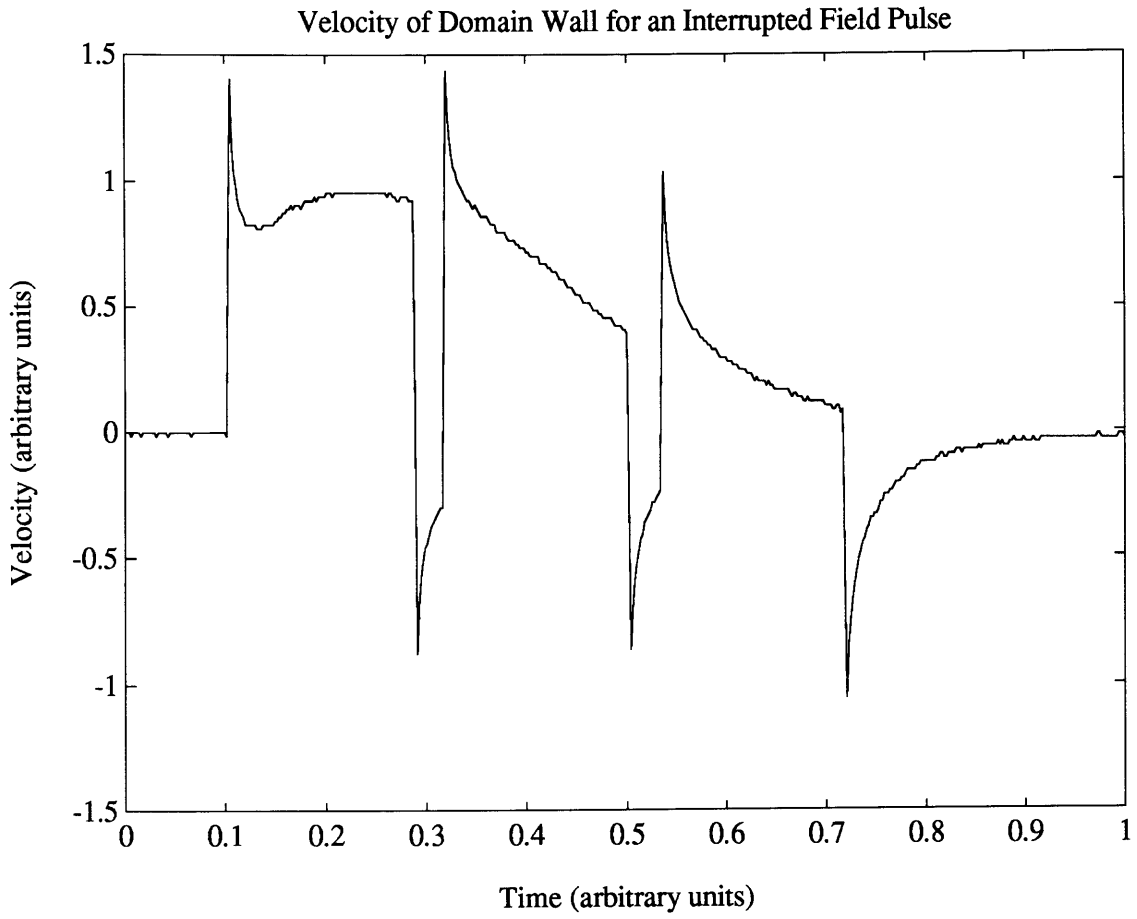

Figure VI.9 Velocity of domain wall for an interrupted field pulse. The duty cycle is 0.87. The velocity drops quickly after the field level drops to zero. The spiking is a result of the depinning and domain wall rearrangement processes. The velocity profile follows a similar path to the uninterrupted pulse, excluding the interrupts.

Again the spiking is caused by depinning and rearrangement processes. Integrating the velocity curve over time results in an effective length traveled by the domain walls. The effective length of travel, which is calculated to be 0.13cm, for the interrupted pulses differs from that of the uninterrupted pulse by less than 1%. Thus interruption of the magnetic field cause a slight rearrangement seen in the spiking, in addition to net translation of 180° domain walls.

An effective domain wall velocity as a function of applied magnetic field is shown in Figure VI.10. The effective velocity is taken to be the velocity measured at the flat portion of the velocity curve for larger applied fields (see Figures VI.8). For smaller applied fields the velocity curve does not flatten, but does exhibit an inflection point which is taken as the effective velocity. The resulting velocity versus applied magnetic field relationship is linear as expected in equation (VI.1) with the constant c = 9.2cm/(sec Oe). This value is larger than that measured by William et al. [1950], see Table IV.1, but the picture frame in those experiments was 0.114cm thick compared to 0.017cm for the picture frame used in this thesis. The difference in eddy current damping and possibly the more complex domain structure of the picture frame used in this thesis account for the differences.

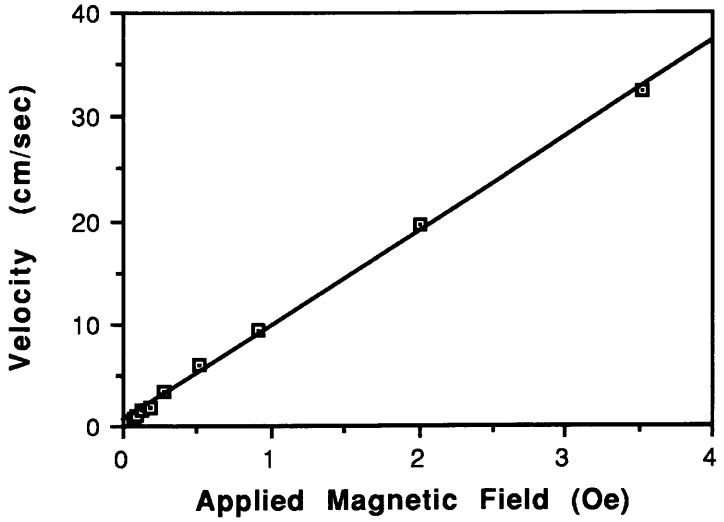

Figure VI.10 Effective domain wall velocity versus applied magnetic field. Velocity is linear in applied magnetic field with a slope of 9.2cm/(sec Oe).

VI.4 Tunneling Background for the SiFe Picture Frame Single Crystal

A number of types of experiments were performed on the picture frame. Surface motion caused by low frequency magnetization of the picture frame was measured using both a standard scanning tunneling microscope, and an atomic force microscope (For background on atomic force microscopy see Sarid [1991]). The two types of microscopes were used to verify that no direct magnetic coupling between the sample and the tunneling transducer exists. The magnetoacoustic emission experiments were performed using the high frequency tunneling transducer to investigate the motion surface of the picture frame during magnetization by a pulsed applied magnetic field.

VI.4a Experimental Setup and Apparatus for Tunneling Measurements

The fixture used to hold the tunneling transducer, and also the atomic force microscope, is shown in Figure VI.11. The fixture permits XY control to approximately 13μm and Z-direction control to 1μm. X-direction control is not used in these experiments. The tunneling transducer fixture is placed inside a styrofoam and foam rubber acoustic shield to minimize external acoustic noise. The acoustic shield also has a faraday cage built in to minimize tunneling transducer RF noise pickup. The tunneling tip is manipulated into position at the picture frame by the micrometers. The tip is then lowered externally using one micrometer while the piezoelectric feedback loop is operational (see Chapter V). The tip is brought down at approximately 1μm/sec with the micrometer. As the tip approaches the picture frame surface and tunneling begins (an approximate separation of 10Å), the feedback loop retracts the piezoelectric tube keeping the tunneling current at a constant level. At this point the external mechanical engagement ceases, and the tunneling transducer is engaged with the picture frame surface, resulting in a tunneling current.

A magnetic field is applied to the picture frame by the source coil shown in Figure VI.7. It was found that the source coil electrostatically couples into both the tunneling

transducer and the SiFe picture frame itself. The coupling into the picture frame directly causes interference since the picture frame is an electrically active part of the tunneling circuit. To reduce this effect the source coil is enclosed within an grounded copper shield on the picture frame (Figure VI.12).

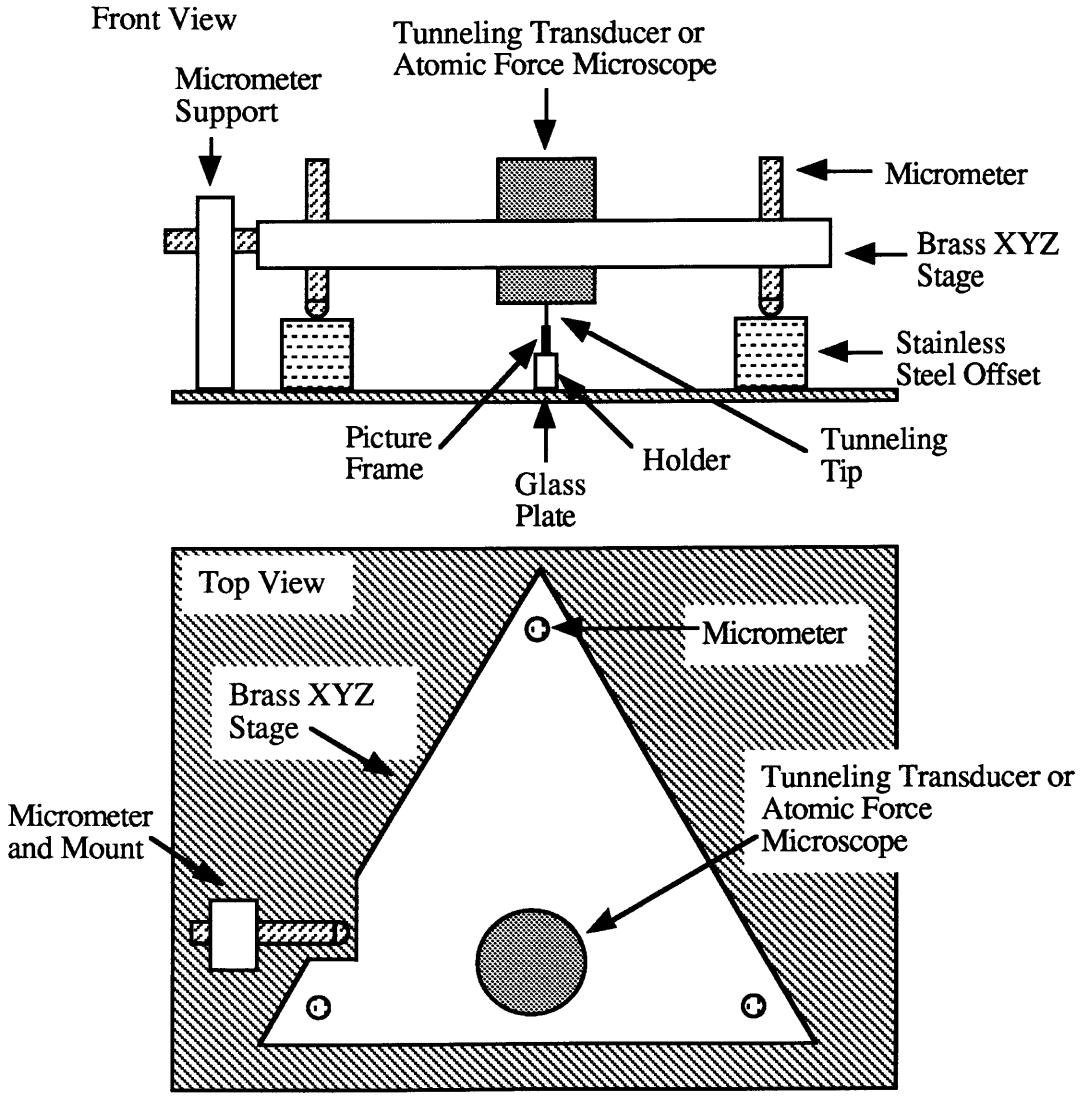

Figure VI.11 Front and side views of tunneling transducer fixture. The triangular XYZ stage permits control of placement of the tunneling tip to within 13μm in XY plane and 1μm in the Z-direction. The glass plate is mounted on vibration isolation pedestals. The entire setup is placed in a styrofoam and foam rubber acoustic shield to minimize external vibrational noise and vibration isolate the tunneling apparatus.

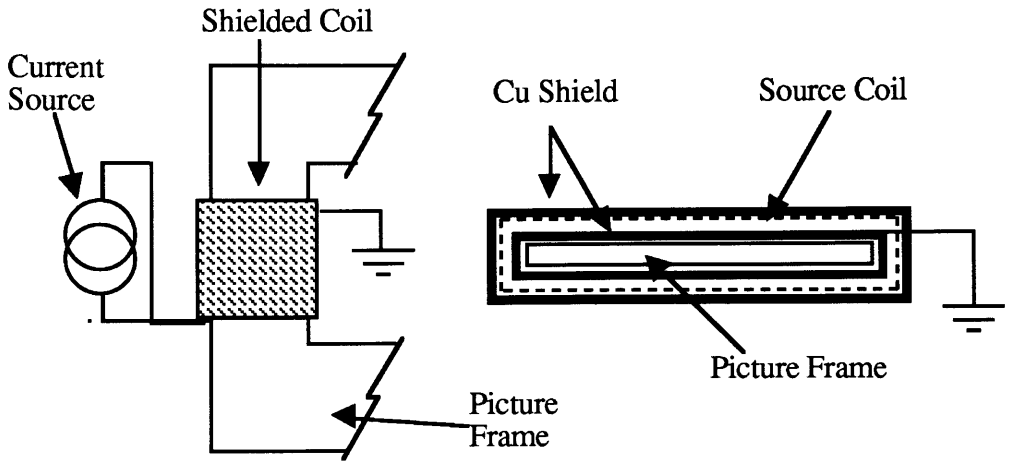

Figure VI.12 Copper shield configuration on the picture frame. The grounded copper shield is wound in a serpentine manner. The current source can either be DC, pulsed or AC.

Several current sources were used to produce the magnetic field of the source coil. For low frequency AC fields a Philips PM5192 Digital Function Generator in series with a resistor was used. For pulsed fields a pulsed current source (Figure VI.13) was designed and built. The current supplied to the source coil is controlled by R_{set}, where $I_{out} \approx 0.6\text{Volts}/R_{set}$, with a 250ns risetime. The compliance is set by the voltage supply, V_o which has a typical level between 20 and 30 volts to maximize the risetime of the current pulse while reducing the introduction of ring at the leading edge of the current pulse.

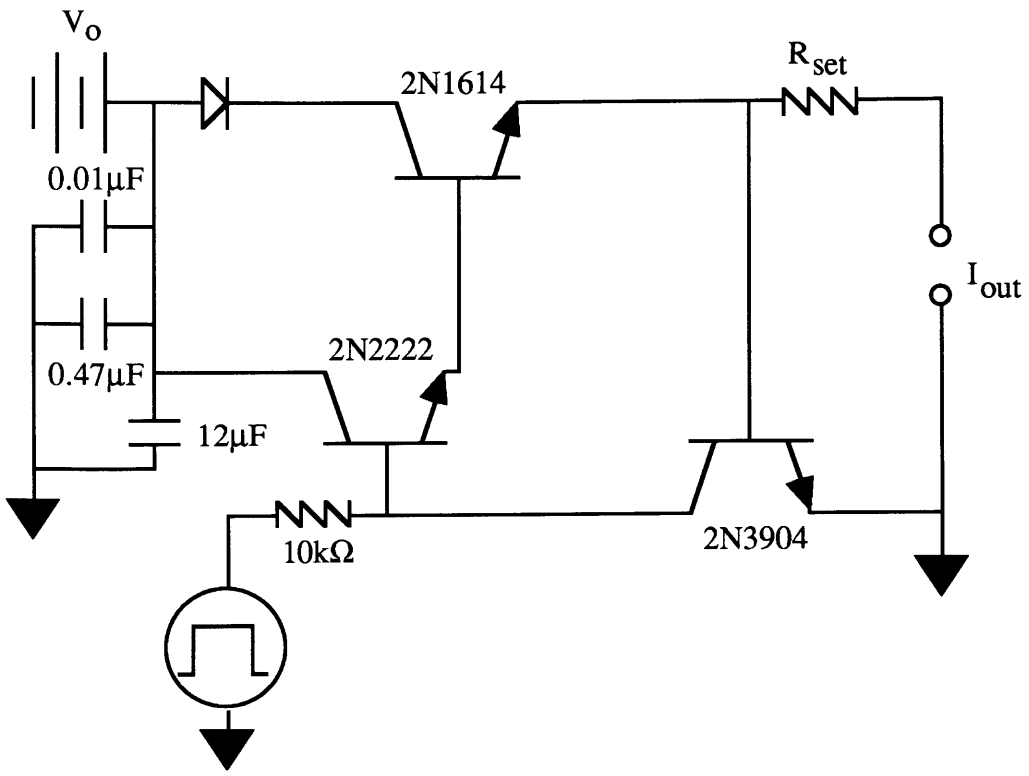

Figure VI.13 Pulsed current source to drive the source coil. The current is controlled by R_{set}. Pulse length is controlled by a General Radio 1340 Pulse Generator.

All tunneling and atomic force microscope measurements were made using a Digital Instruments, Inc. Nanoscope III. These measurements where made at the Advanced Materials Laboratory, Concord, Massachusetts. For low frequency magnetization, where measurement of magnetoacoustic emission is not the goal, the output from the tunneling transducer and the atomic force microscope can be analyzed directly by the instrumentation and software available with the Nanoscope III. For the magnetoacoustic emission measurements the output from the tunneling transducer is fed directly into a Philips PM3550 Digital Oscilloscope to then be transferred to computer for analysis.

VI.4b Picture Frame/Tunneling Transducer Configuration

The design of the tunneling transducer fixture permits the tunneling tip, or atomic force microscope tip to be placed at different points on the picture frame surface. For magnetoacoustic emission from a 180° domain wall, the shear components of the emitted radiation are the largest. The tunneling tip configuration to be used to measure the surface deflection of these transverse waves is discussed in Chapter V (see Figure V.11). The best placement of the tunneling tip on the picture frame for shear wave detection is near a corner on the narrow edge, Figure VI.14. For plane wave emission from the domain wall source shown in Figure VI.14, the maximum surface displace exists near the tunneling tip.

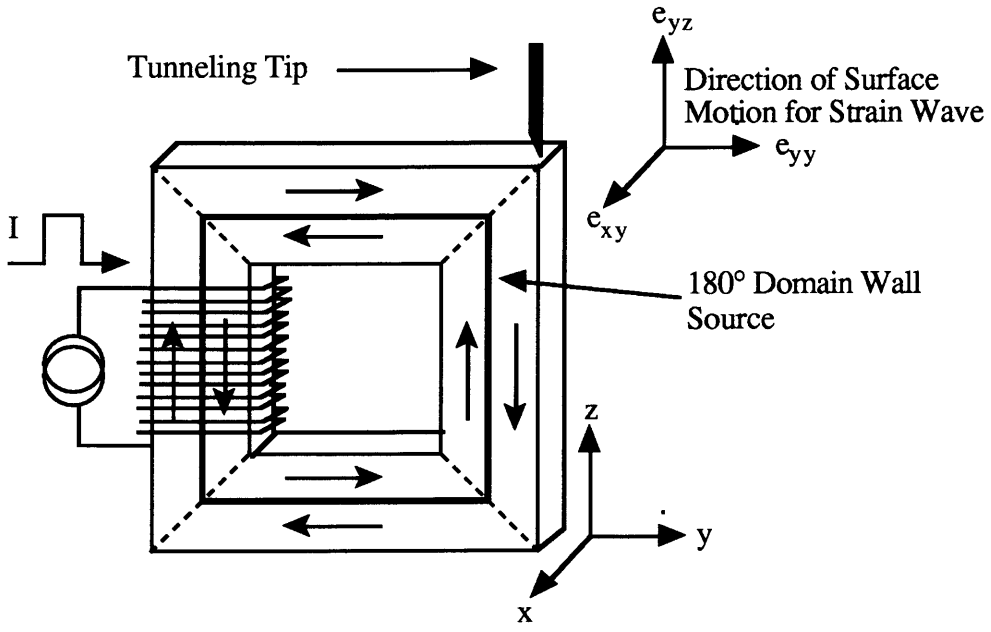

Figure VI.14 Tunneling tip placement for a transverse wave emitted from the 180° domain wall marked as the source. Maximum shear radiation exists on the narrow face for an accelerating planar domain wall.

The magnitude of the surface displacement is given by the product of the amplitude of the strain waves (equations (IV.48)) and the length of the domain wall in the corresponding direction:

$$\begin{aligned} \delta_x &= l_x\, e_{xy}, \\ \delta_y &= 2\,\Delta\, e_{yy}, \\ \delta_z &= l_z\, e_{yz}, \end{aligned} \qquad \text{(VI.4)}$$

where l_x and l_z are the lengths of the domain wall in the x- and z-directions respectively and Δ is the domain wall width parameter. In 3% SiFe the expected shear strain is $O(10^{-10})$, and thus the expected surface displacement for a magnetoacoustic emission from a planar 180° domain wall 0.017 cm thick and 1cm long is $\delta_x = O(10^{-12}$ cm) and $\delta_z = O(10^{-10}$ cm). This value of δ_x is below detectability, but δ_z is just below the limit of detection for the tunneling transducer as described in Chapter V. Thus the tunneling tip placement in Figure VI.14 maximizes the possibility of detection of the surface displacement, δ_z, caused by the passing of the shear wave under the tunneling tip. The longitudinal wave emitted from the 180° domain wall calculated by the model in Chapter IV, is also below the limit of detection of the tunneling transducer.

VI.4c Surface Displacement for Low Frequency Magnetization

The surface displacement associated with low frequency magnetization was measured using both a tunneling transducer and an Atomic Force Microscope (AFM). The AFM was used to assure that the motion detected was related to real surface motion not direct magnetic coupling into the tunneling transducer. The frequency of the applied magnetic field was kept <20 Hz so that large surface motion could be tracked by either the tunneling transducer or the AFM. The slew rate of both the tunneling transducer and AFM are limited by the response of the piezoelectric manipulator and controller which translate the tips for each device.

The tunneling tip, or AFM tip, was placed at a number of points in the surface of picture frame, Figure VI.15. At all points the surface was observed to move periodically in phase with the applied magnetic field.

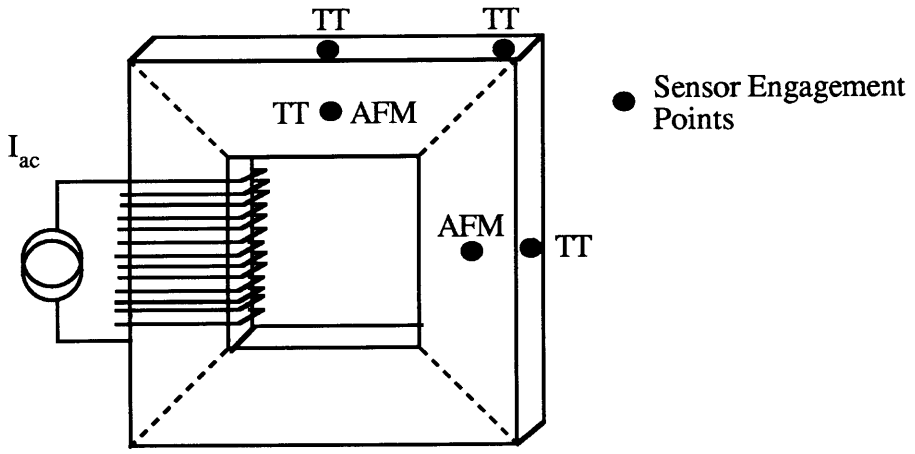

Figure VI.15 Depiction of points where the tunneling transducer was engaged to monitor low frequency motion of the surface. The spots marked with TT indicate points where the tunneling transducer was used. The spots marked AFM indicate points where the atomic force microscope was used.

The amplitude of surface motion is dependent on the magnitude of the applied magnetic field, and independent of the frequency of the applied field. The surface motion for 2.4 Oe peak to peak sinusoidal applied magnetic field is shown in Figures VI.16 and VI.17. The measurements were made using the AFM on the side furthest from the source coil. The AFM was raster scanned over a 100μm x 100μm area at a rate of 200 μm/sec and 0.4μm per line. Figure VI.16 shows a surface plot of the surface motion for the magnetic field at frequencies of 1, 2 , 4, 8, and 16 Hz. The relative amplitude of the surface motion is qualitatively depicted by gray scale. Surface displacement is shown in Figure VI.17 for the 2 Hz applied field with vertical displacement of ≈ 1000Å peak to peak. The same order of magnitude of surface displacements was found at all other points on the crystal investigated for a given applied magnetic field.

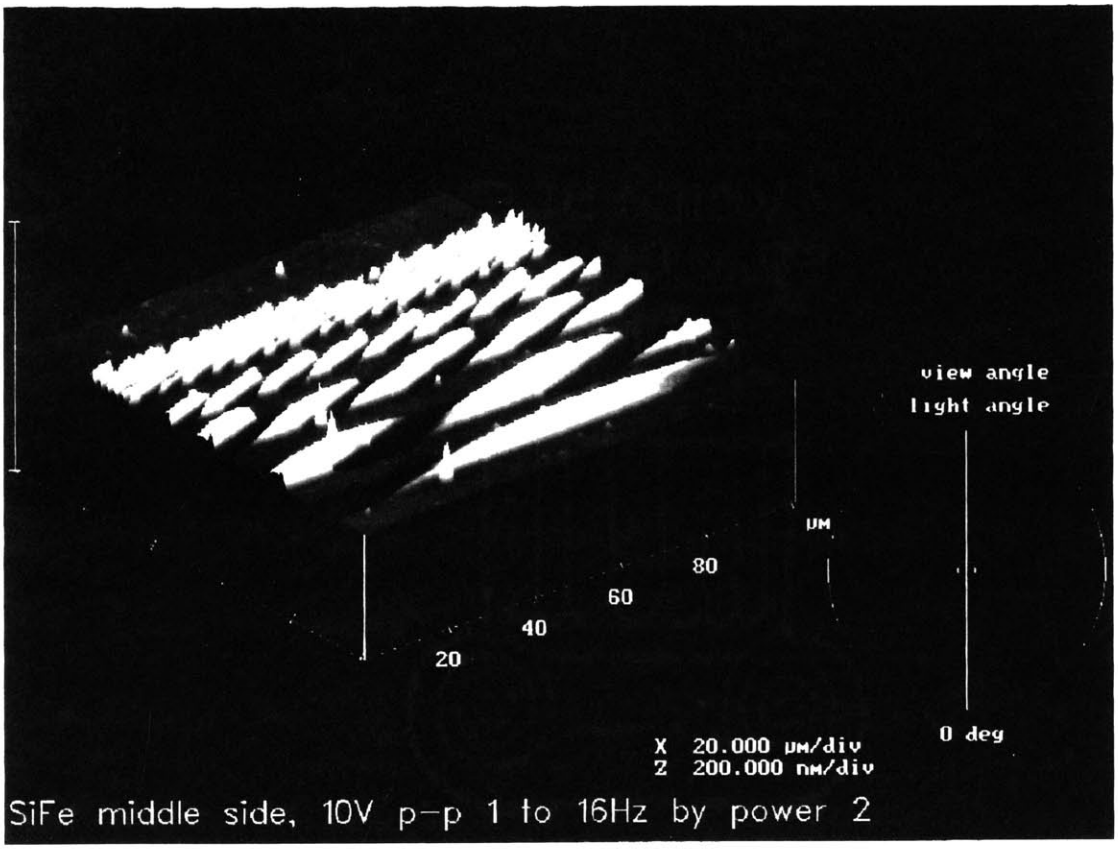

Figure VI.16 A gray scale surface plot of surface displacement of the SiFe picture frame measured by an atomic force microscope. The plot is a raster scan 100μm x 100μm in area. Lines are scanned at 200μm/sec, 0.4μm per scan line. The applied magnetic field is a 2.4 Oe peak to peak sinusoidal field at 5 different frequencies. The flat portions of the surface plot are periods with no applied magnetic field. The amplitude of oscillation is constant for all frequency values.

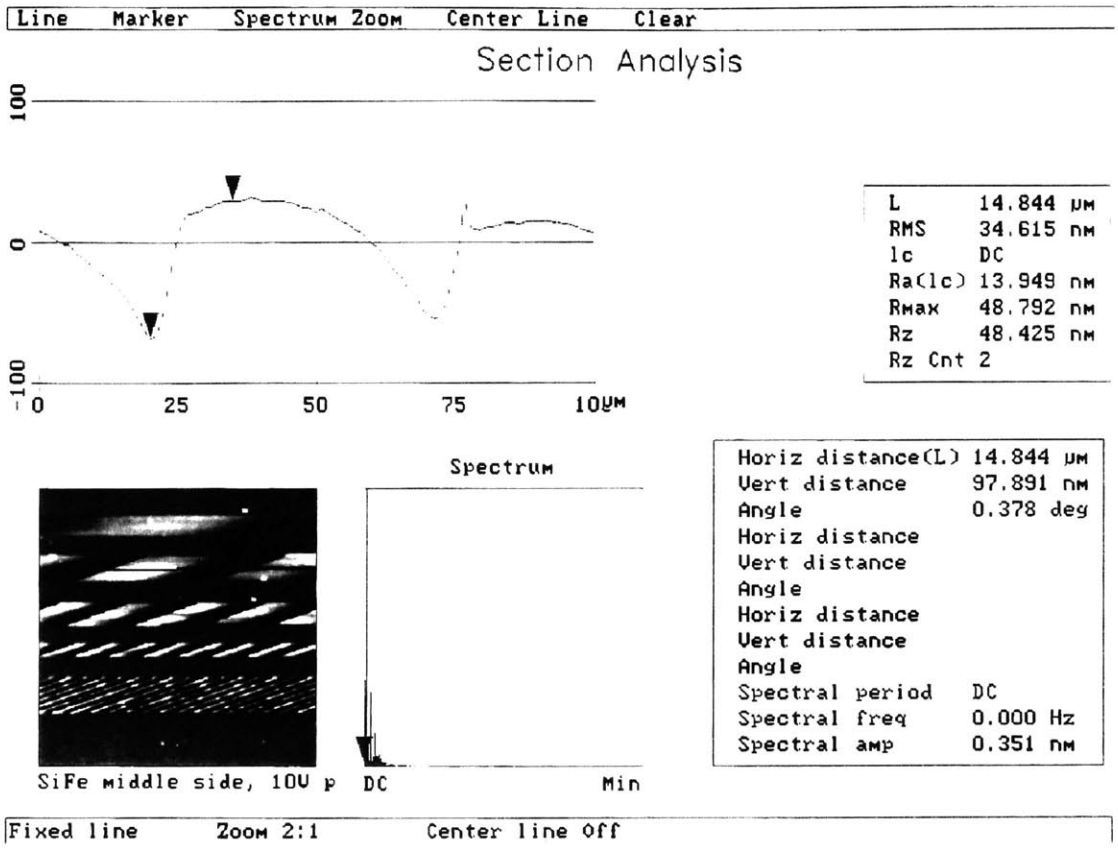

Figure VI.17 Cross-section of surface plot in Figure VI.16 for the 2Hz, 2.4 Oe applied magnetic field. Surface displacement is approximately 1000Å peak to peak.

Similar surface raster scans were made to look at the effect of applied magnetic field on the surface displacement. Figure VI.18 show a gray scale surface plot of a 5Hz sinusoidal applied magnetic field with peak to peak amplitude between 0.47 and 4.7 Oe. The measurements were taken with the AFM at the same place on the crystal as previously discussed. The magnitude of the surface displacement scales with the applied magnetic field.

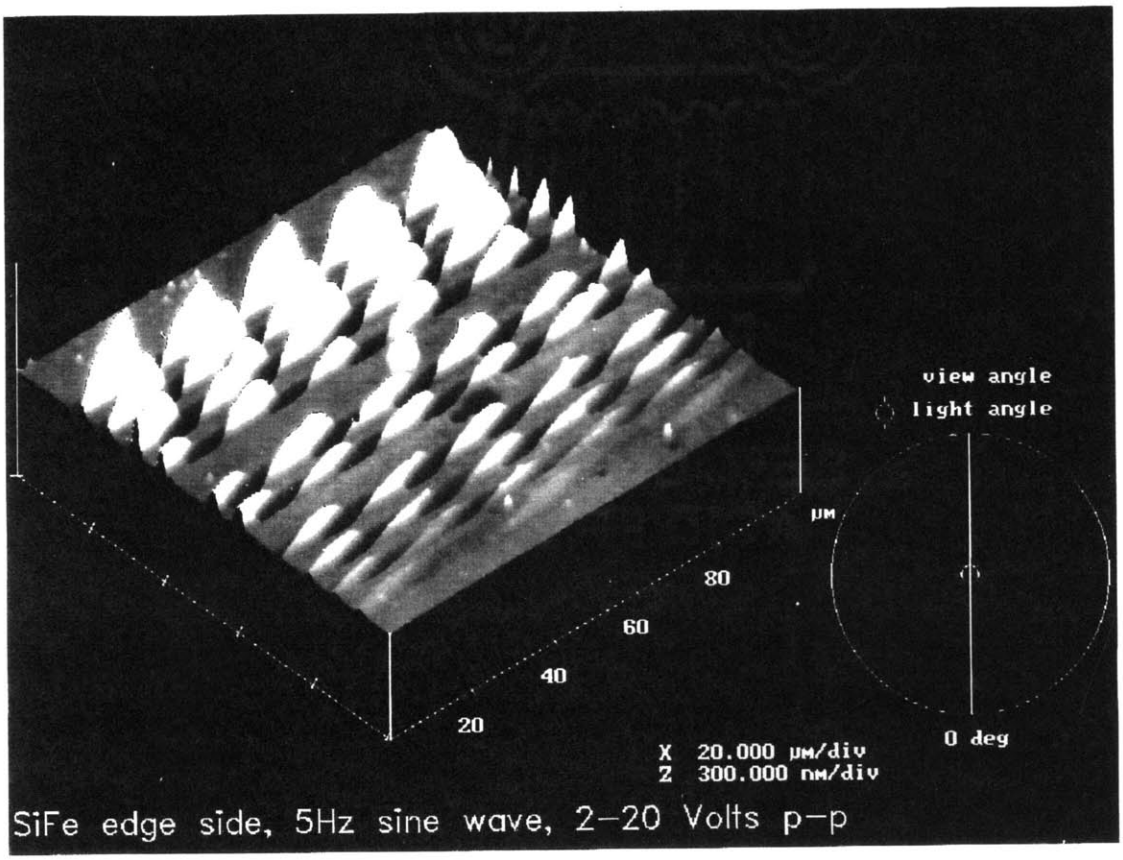

Figure VI.18 A gray scale surface plot of surface displacement of the SiFe picture frame measured by an atomic force microscope. The plot is a raster scan 100μm x 100μm in area. Lines are scanned at 200μm/sec, 0.4μm per scan line. The applied magnetic field ranges from 0.47 to 4.7 Oe peak to peak sinusoidal field, by 0.47 Oe. The frequency of the applied magnetic field is 5Hz. The flat portions of the surface plot are periods with no applied magnetic field. The amplitude of surface motion increases with increased applied magnetic field.

A cross-section of the amplitude of the surface displacement is shown in Figure VI.19 for a sinusoidal applied magnetic field of 4.7 Oe peak to peak. At this field the surface displacement is approximately 360μm peak to peak. The value of the peak to peak surface displacement has been determined by measurement from the data shown in Figure VI.18. The surface displacement versus applied magnetic field is plotted in Figure VI.20.

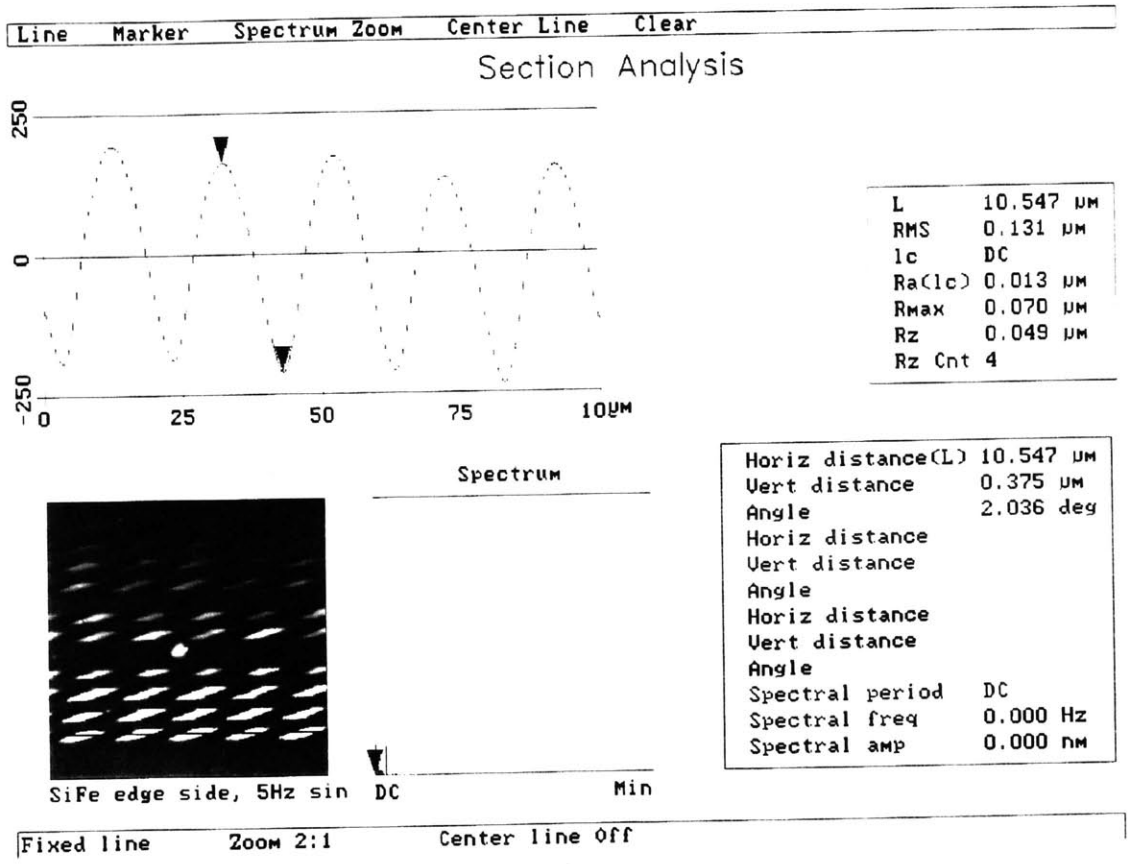

Figure VI.19 Cross-sectional plot of the surface displacement shown in Figure VI.18 for an applied magnetic field of 4.7 Oe. Surface displacement is approximately 360μm peak to peak.

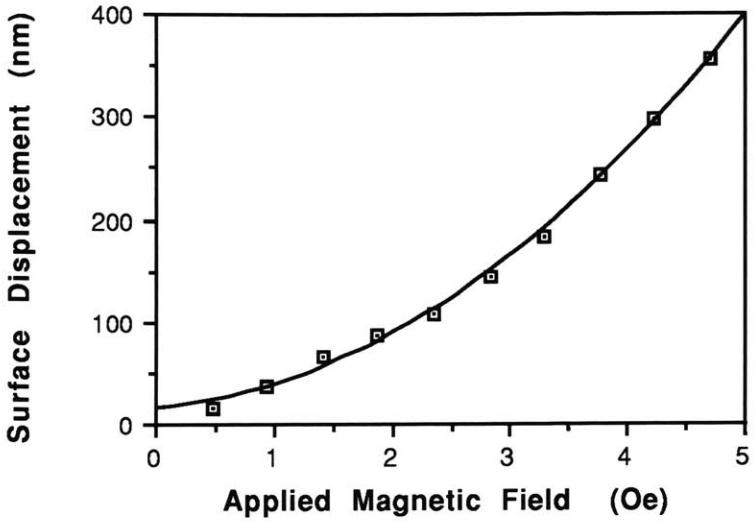

Figure VI.20 Peak to peak surface displacement versus peak to peak applied magnetic field for picture frame. Measurement made by atomic force microscope. The amplitude of the surface displacement is approximately given by a second order polynomial in applied magnetic field.

The observed surface motion is O(1000Å) at all points measured on the SiFe picture frame. For a perfect picture frame, see Figure VI.1, there should be no magnetostriction of the crystal. As is pointed out by Jiles [1991], there is no bulk magnetostriction associated with 180° domain wall motion. Since only 180° domain walls are mobile in the perfect picture frame, the surface should not move. The picture frame used in this thesis has a much more complicated domain structure including many "tree" domains. This could lead to magnetostriction. The order of magnitude of strain required to produce the observed surface displacements, along the length of a leg of the picture frame, 2cm long, and through the thickness of the crystal, 0.017cm, is estimated. For a 1000Å surface displacement the strain along the leg is $O(10^{-5})$, and through the thickness is $O(10^{-4})$. Magnetostriction strains along the legs on the order of 10^{-5} are possible for SiFe, ($\lambda_s = O(10^{-5})$). But pure strain produced by magnetostriction cannot

produce the surface displacement observed on the large surface of the picture frame. One possible explanation of the observed strain could be magnetostrictive induced bending. If there is strain mismatch on the two faces of the crystal, because of differences in the surface domain patterns, the legs of the picture frame will bend. This will cause significant surface motion. The maximum strain mismatch between the two faces of the crystal needed to cause the surface motion observed is 2.5×10^{-6}. This strain is possible with magnetostriction.

The observed surface motion of the picture frame during low frequency magnetization complicates the measurement of magnetoacoustic emission from 180° domain wall motion. The tunneling transducer is highly sensitive to surface displacement. But at high frequencies its dynamic range is limited. Once the surface of the sample moves an appreciable distance, more than a couple of angstroms in the time range of 1 millisecond, the piezoelectric feedback loop of the tunneling transducer responds to that motion. This causes significant tunneling current noise. If the surface moves such faster than the slew rate of the tunneling transducer over a distance much greater than 10Å, the picture frame surface will either touch the tunneling tip or move sufficiently far away that tunneling ceases. In both cases the piezoelectric feedback loop of the tunneling transducer is disturbed. Thus measurements must be made in a manner to assure that the picture frame - tunneling tip configuration is constant except for small high frequency transient motion.

VI.5 Magnetoacoustic Emission Measurements

Magnetoacoustic emission measurements have been made on the 3% SiFe picture frame single crystal using the tunneling transducer described in Chapter V. To best approximate the step change in velocity of the 180° domain wall used in the model presented in Chapter IV, a pulsed magnetic field was used. The time required for the

picture frame to respond to a pulsed magnetic field with a risetime of 250ns, and exhibit a maximum in the time rate of change of magnetization, as measured by the voltage induced in the sense coil, is approximately 2.0μs. There is a 0.5μs delay between the start of the current pulse in the source coil and the initial response in the sense coil. At that point a 1.5μs risetime is exhibited. As is discussed in Chapter VI.3b, the voltage induced in the sense coil is attributed to domain wall motion. The period of time directly after the rise of magnetic field pulse exhibits the largest average acceleration of the domain walls in the picture frame. This period where the domain walls are accelerating should be magnetoacousticly active. The level of emission is highly dependent on the exact acceleration process of the domain walls. The model derived in this thesis assumes that a 180° domain wall moves as a plane. This is only an approximation to the real motion of domain walls in magnetic materials. Still the model is proposed as a foundation for magnetoacoustic emission from 180° domain walls.

VI.5a Magnetoacoustic Emission Measurement: Experimental Results

Once the picture frame is placed in the tunneling transducer fixture the tunneling transducer is placed over the point on the picture frame where the surface measurement is to be performed. In this experiment the tunneling tip is placed such that the measurements are made on the edge of the picture frame, see Figure VI.14. The tunneling bias voltage is applied directly to the picture frame at a DC level O(100mvolts) above ground. The tunneling tip is lowered towards the picture frame until the tip engages and tunneling initiates. The DC tunneling current and the bias voltage can be adjusted, within the limits of the Nanoscope III, to maximize sensitivity to high speed surface motion, and the resulting high speed fluctuation in the tunneling current expect for magnetoacoustic emission from the 180° domain wall motion. The tunneling transducer is used in a mode that maintains a constant DC tunneling current by displacement of the tunneling tip with the piezoelectric control system. The high speed

fluctuation in tunneling current is monitored by the current voltage converting amplifier (see Figure V.5).

As a test of the tunneling transducer, the high frequency component of the tunneling current was monitored during application of a small, low frequency applied field (approximately 5 Oe peak to peak). No significant high frequency components to the tunneling current where detected above the noise level shown in Figure V.7 during this test. But surface motion was observed associated with magnetostrictive effects (see Chapter VI.4c). The magnetoacoustic emission from the 180° domain wall is a result of the acceleration process. A small, low frequency sinusoidal applied field may cause significant domain wall motion. But the acceleration of the domain wall is small compared to that required to achieve appreciable magnetoacoustic emission. Previous reports [Kwan 1983, Gorkunov et al. 1986, and Kim and Kim 1989] show magnetoacoustic emission in SiFe single crystals (not picture frames) is present at large magnetic field levels.

The tunneling current set point, the tunneling current level controlled by the piezoelectric feedback, used in the experimentation ranged from 1 to 40nA, the limit of the instrumentation. Since the major source of the noise at the output of the tunneling transducer is the current to voltage converter, the noise level is insensitive to the tunneling current set point. Thus maximum sensitivity is attained at with a DC tunneling current of 40nA (see equation (V.6)). For tunneling current set points of 10nA or less the tunneling biasing voltage was 100mV. For tunneling current set points above 10nA, the following biasing voltage - tunneling current set point relation was used: 10mV/nA.

The effect of a 5.8 Oe applied magnetic field pulse on the picture frame was investigated. Smaller field pulses were also used, but results for the smaller fields are similar to those shown here. Figure VI.21 shows the sense coil response to a 5.8 Oe magnetic field pulse 5μsec in length as well as the response of tunneling current between the picture frame and the tunneling transducer. In this test the tunneling current set point

was 10nA. The effective surface motion as a function of measured change in tunneling current, from equation (V.6), is 0.3Å/nA. The resulting tunneling current fluctuation shown in Figure VI.21b is similar to the background noise level of the tunneling transducer (see Figure V.7). At a 10nA DC tunneling current any surface motion caused by magnetoacoustic emission induced by the magnetic field pulse is below the background noise.

The noise in the tunneling transducer can be reduced by averaging the tunneling current response of the tunneling transducer over a large number of field pulses. The process used to make this measurement is to pulse the source coil using the pulse current source, then pulse the source coil with the opposite polarity current pulse. The drive voltage for the current pulse remains the same polarity, but the magnetic field reverses direction. The resulting tunneling current response to the magnetic field pulse is averaged over 32 magnetic field pulses all of the same polarity. This was done for tunneling current set points of 10, 20, and 40nA. The assumption is that by stepping the domain walls back and forth in the same general area of the picture frame similar shear elastic waves of opposite signs should be produced, see equations (IV.48). The reversibility of the magnetization process is evident from the domain wall velocity data presented in Chapter VI.3b.

The results of the experiments described above are shown in Figures VI.22 through VI.24. In each the tunneling transducer response to a 5.8 Oe pulsed magnetic field of approximately 3.5 microseconds in length is presented. In Figure VI.22a the average effective surface displacement of the two different polarity magnetic field pulses are shown. One polarity is represented by the solid line. The opposite polarity is represented by the dotted line. For each polarity magnetic field pulse there is a ring at the beginning and end of the pulse. The ringing is shown to be electrostatic coupling between the source coil and the tunneling transducer. The electrostatic coupling is independent of the polarity of the applied magnetic field pulse, but is dependent on the

polarity of the voltage across the source coil. The electrostatic coupling effect can be removed from the data by subtracting the two opposite polarity magnetic field results. Since the shear component of the elastic radiation emitted by the moving 180° domain wall switches polarity with the polarity change in the applied magnetic field, the surface displacement caused by this elastic radiation should add constructively. The subtracted data is shown in Figure VI.22b . Similar results are presented in Figures VI.23a and VI.23b for a tunneling current set point of 20nA, and Figures VI.24a and VI.24b for a tunneling current set point of 40nA.

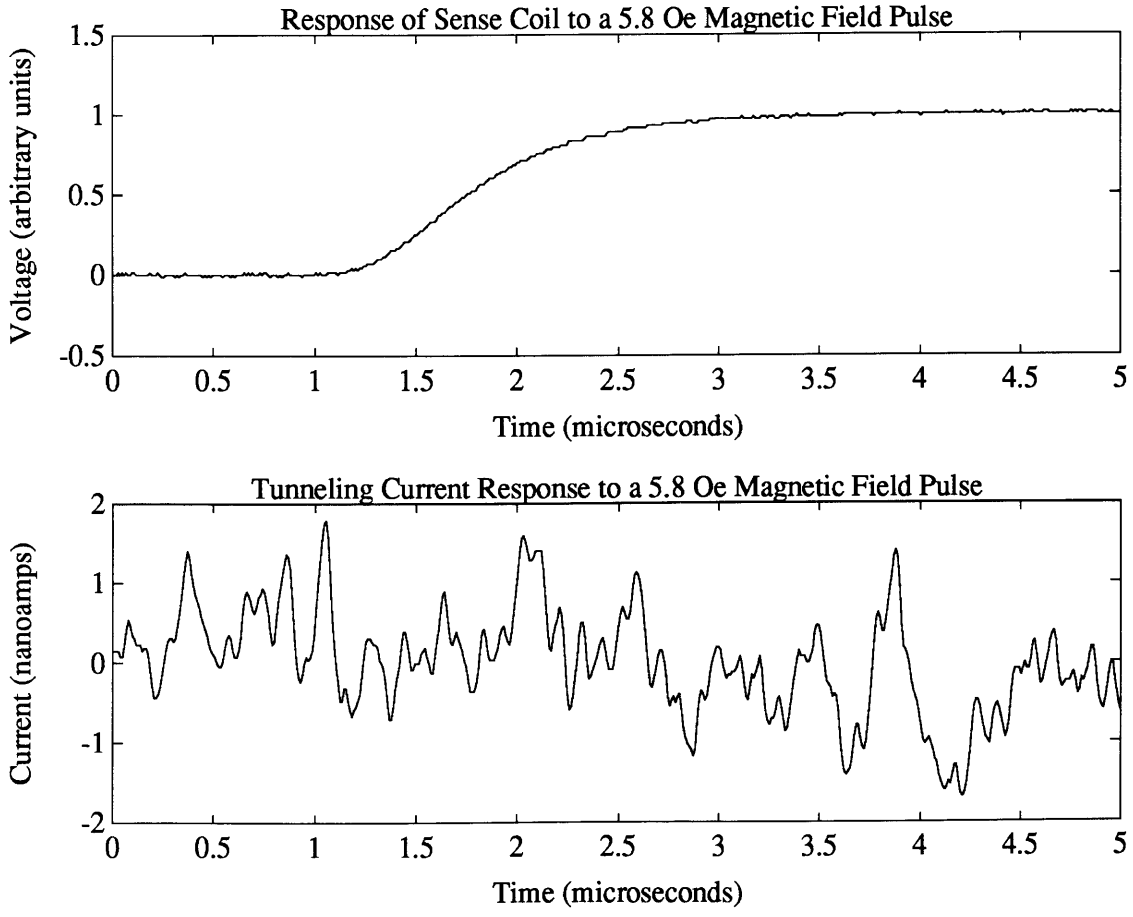

Figures VI.21 Response of a 5.8 Oe magnetic field pulse on the picture frame. a) The voltage induced on the sense coil versus time. b) The AC response of the tunneling current to the magnetic field pulse. The tunneling current set point is 10 nA. The effective surface motion for this tunneling current fluctuation is 0.3Å/nA.

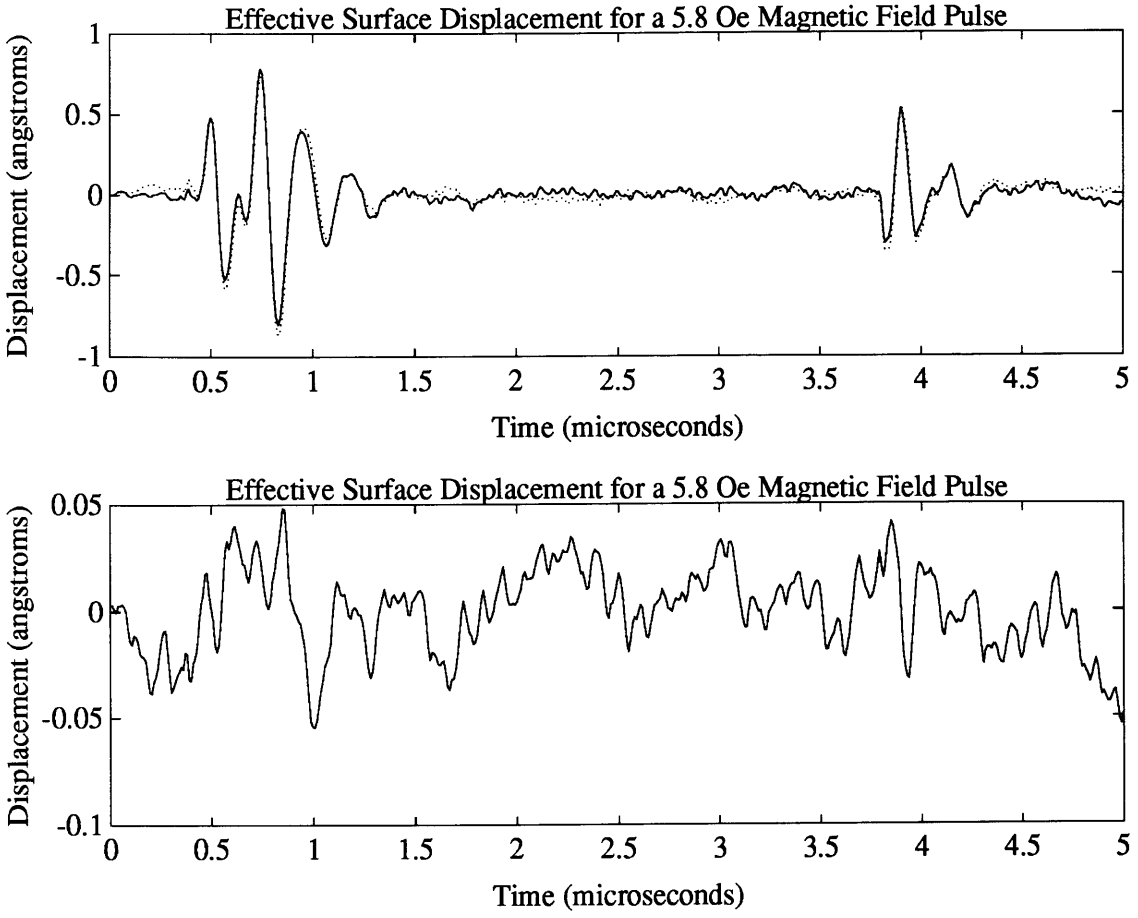

Figure VI.22 Average AC response of the tunneling current to 5.8 Oe magnetic field pulse (32 averages). The magnetic field pulse length is approximate 3.5μs. The tunneling current set point is 10 nA. a) One polarity magnetic field pulse is represented by a solid line. The other is represented by a dotted line. The AC response from 0.5 to 1.5μs and from 3.75 to 4μs is electrostatic coupling between the source coil and the tunneling transducer. b) Averaging of the two polarity responses in a). The electrostatic artifact cancels. Equivalent surface motion for the background noise is < 0.1Å. No magnetoacoustic emission is conclusively observed.

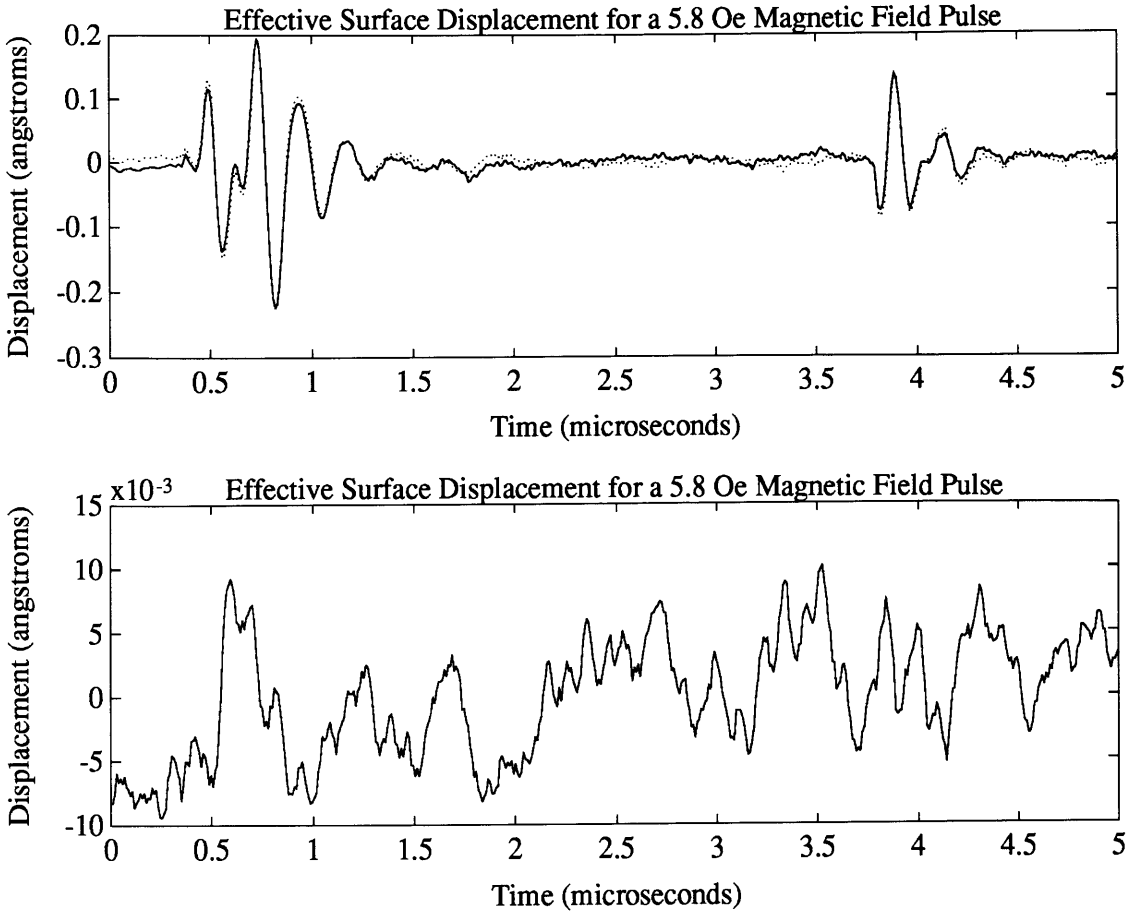

Figure VI.23 Average AC response of the tunneling current to 5.8 Oe magnetic field pulse (32 averages). The magnetic field pulse length is approximate 3.5μs. The tunneling current set point is 20 nA. a) One polarity magnetic field pulse is represented by a solid line. The other is represented by a dotted line. The AC response from 0.5 to 1.5μs and from 3.75 to 4μs is electrostatic coupling between the source coil and the tunneling transducer. b) Averaging of the two polarity responses in a). The electrostatic artifact cancels. Equivalent surface motion for the background noise is < 0.02Å. No magnetoacoustic emission is conclusively observed.

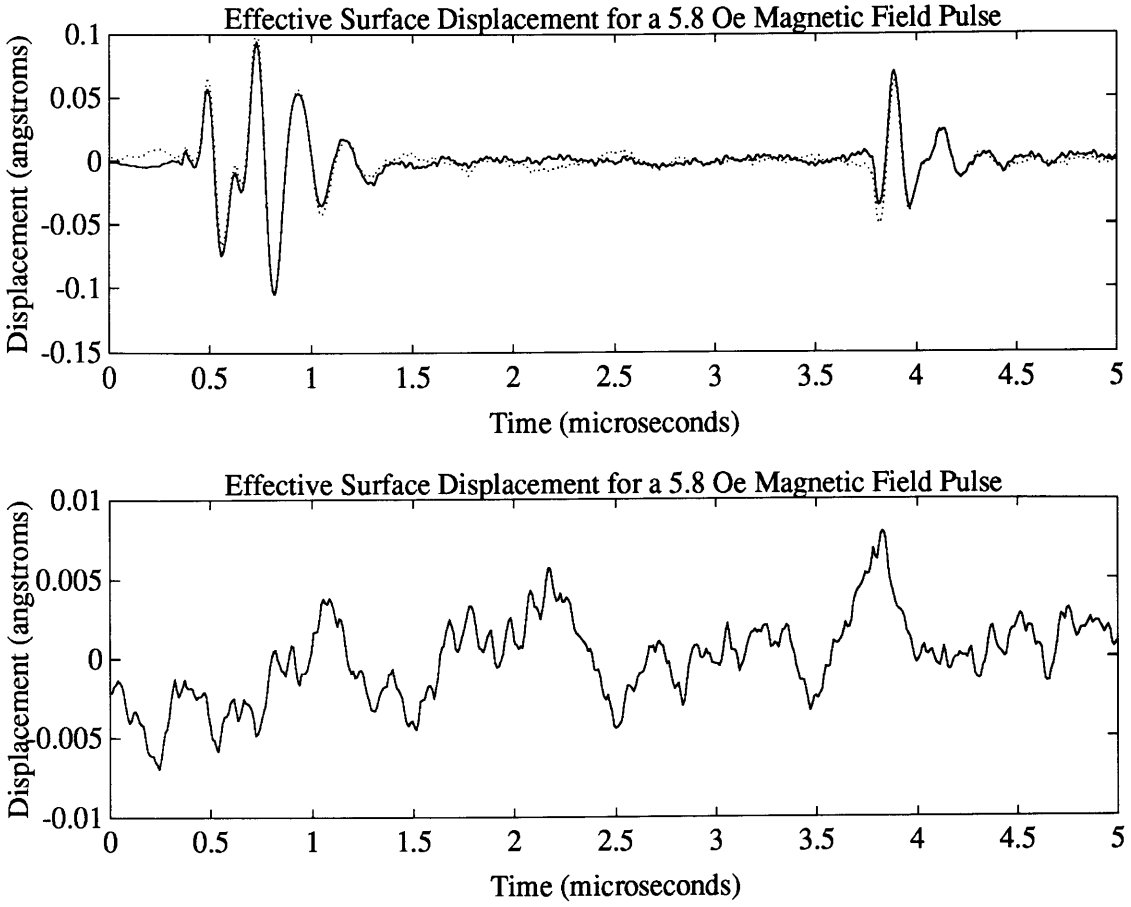

Figure VI.24 Average AC response of the tunneling current to 5.8 Oe magnetic field pulse (32 averages). The magnetic field pulse length is approximate 3.5μs. The tunneling current set point is 10 nA. a) One polarity magnetic field pulse is represented by a solid line. The other is represented by a dotted line. The AC response from 0.5 to 1.5μs and from 3.75 to 4μs is electrostatic coupling between the source coil and the tunneling transducer. b) Averaging of the two polarity responses in a). The electrostatic artifact cancels. Equivalent surface motion for the background noise is < 0.01Å. No magnetoacoustic emission is conclusively observed.

The sensitivity to surface motion is better than 0.01Å with the averaging and a DC tunneling current of 40nA. This level of sensitivity is similar to that predicted by Moreau and Kitterson [1992]. Even with this level of sensitivity there is no direct evidence of surface motion that could be a result of magnetoacoustic emission for a moving 180° domain wall.

The effect of longer magnetic field pulses on the surface motion of the picture frame was also investigated. As the magnetic field pulse length is increased motion of the picture frame surface is detected. The surface of the picture frame either moves enough in one direction to cause the surface of the picture frame to touch the tunneling tip or the surface pulls away from the tunneling tip and causes the tunneling process to cease. In either case an accurate measure of the size of the motion is impossible because of the small dynamic range of the tunneling transducer in this bandwidth. Once the tunneling process is interrupted, the piezoelectric feedback loop attempts to re-establish the tunneling current set point. This process takes a number of seconds to stabilize. The large surface motion for the longer magnetic field pulses is expected because the large magnetostrictive effects observed for low frequency magnetic fields (see Chapter VI.4c).

VI.5b Magnetoacoustic Emission Measurements: Discussion

The 180° domain wall as a source of magnetoacoustic emission in the SiFe picture frame has been investigated experimentally using a tunneling transducer. The evidence found suggests that any emission from 180° domain walls is smaller than the noise level in the tunneling transducer used as the detector. The model presented in Chapter IV predicts that the level of emission for a planar 180° domain wall should be $O(10^{-2}\text{Å})$, which is barley detectable using the tunneling transducer. There are a number of assumptions made in the model that exist only in the best case scenario. Relaxing these assumptions can result in a decreased observed amplitude of magnetoacoustic emission from a 180° domain wall.

The assumption that is most suspect is the domain wall moving as a plane over the whole length of crystal. In real material the domain wall interacts with the surfaces and crystal defects. This results in discontinuous motion of small segments of the domain wall in an applied magnetic field [Chikazumi 1986]. For the SiFe crystal the

entire domain wall must move in unison to introduce enough shear strain to be detectable by the tunneling transducer. As soon as the wall motion is segmented the level of emission is reduced. In addition the elastic radiation emitted from these smaller segments of 180° domain wall is no longer a plane wave further reducing the amplitude of the radiation far away from the source. Since the picture frame used in the experiments is not ideal, as evident in the complicated "tree" domains observed, the probability of moving a single 180° domain wall as a plane is unlikely. Thus the inability to detect magnetoacoustic emission from the single crystal for the small fields used is not surprising.

In Chapter IV it is noted that SiFe is not an ideal test vehicle for the model. The high level of damping caused by eddy currents limits the acceleration of the domain wall. Since the model predicts that elastic radiation is emitted only during the acceleration of the domain wall, a material in which domain walls are able to reach high velocities quickly is a much better candidate for verification of the model.

Chapter VII: Conclusions and Recommendations

VII.1 Conclusions

A model is presented in this thesis which predicts that accelerating 180° domain walls are possible sources of magnetoacoustic emission. This predictions runs contrary to the accepted theory that only non-180° domain walls and possibly domain wall creation/annihilation can produce magnetoacoustic emission. The model is an extension, with corrections, of earlier models where 180° domain walls were considered sources of magnetoacoustic emission [Lord 1967, and Kuleev et al. 1986]. An experimental methodology based on a Scanning Tunneling Microscope is developed for detection of magnetoacoustic emission from isolated domain walls. The experimental method is tested on a 3% SiFe picture frame single crystal where the maximum size of the predicted elastic radiation is about the same magnitude as the equivalent surface deflection noise of the tunneling transducer $O(10^{-12}\text{Å})$. In this sample no magnetoacoustic emission is observed.

The development of the model results in the following additions to the theory of magnetic domain walls:

1) In a material with cubic symmetry and thus cubic anisotropy the 180° domain wall is a stable domain wall configuration because of magnetostatic self energy, not magnetoelastic energy. This is true even in the limit of an infinite material.

2) For small domain wall velocities an approximate analytic solution to the Landau and Lifshitz equations of motion has been developed which gives a realistic description of the magnetization distribution within a 180° domain wall. This magnetization distribution is energetically more favorable than the commonly used Walker solutions to the Landau and Lifshitz equations of motion.

These two facts are used to develop the model for elastic radiation from an accelerating 180° domain wall. Even though a number of assumptions about the 180°

domain wall are made to facilitate an analytic expression for the elastic radiation, relaxation of those approximations will not eliminate the 180° domain wall as a source of magnetoacoustic emission. This is true because the model is based on the elastic interaction of the domain wall itself with the crystal lattice.

The model predicts that insulating materials should exhibit larger amplitude emission from 180° domain walls than metallic ferromagnets, assuming the same magnetoelastic constants. This is a direct result of the domain wall damping mechanisms in each class of material. For the same applied field the domain wall in an insulating material accelerates more quickly to a significantly higher velocity than does the domain wall in the metallic ferromagnet.

The experimental method for detection of the magnetoacoustic emission has been developed which utilizes an electron tunneling transducer. The tunneling transducer designed for this thesis has a equivalent surface deflection noise level of approximately 0.01Å peak to peak, after signal processing. This tunneling transducer is highly sensitive to local surface motion. The tunneling transducer should be a valuable addition to the standard tools used to measure acoustic emission in all materials.

VII.2 Recommendation

An experimental method has been developed that can be used to test the theoretical results of this thesis. But a different test vehicle is needed. The choice should be made to permit isolation of 180° domain walls from non-180° domain walls. A number of experiments could be performed that might verify the existence of the of elastic radiation emitted from a 180° domain wall:

1) Tests on highly oriented picture frame single crystals made of ferrite materials are a natural extension of this thesis. The ferrite material is ideal because of the low loss. This permits the domain walls to remain planar at higher velocities than those of metallic ferromagnets. In addition, in most ferrite materials the velocity of the 180° domain wall

produced by a pulsed applied magnetic field better approximates the step function used in the theoretical calculations. The major limitation is preparation of the picture frame.

2) A test method using a geometry which is easily fabricated, but permits isolation of a single 180° domain wall is also a good avenue. One possibility is a rectangular rod geometry such that the difference in the time of flight of the radiation from the closure domains and the plane wave radiation pulse from the 180° domain wall permits temporal separation of the effects from the 180° and non-180° domain walls.

3) Measurement on hexagonal ferrite materials. These materials offer an excellent opportunity because they are uniaxial and thus contain mostly 180° domain walls. Kusanagi et al. [1979a] used their results from experimentation on Co, also uniaxial, to help conclude that 180° domain walls do not emit elastic radiation. But Co has the same inherent weakness as a test vehicle as other metallic ferromagnets, the eddy current loss limits the acceleration of the domain walls, making it a poor source of 180° domain wall produced magnetoacoustic emission.

The model developed for magnetoacoustic emission from accelerating 180° domain walls contains a number of approximations to facilitate an analytic solution. There are a number of modifications to the model that would improve the model for application to real materials.

1) The model needs to be extended so that the driving magnetic field is given instead of assuming a velocity function and ignoring the applied magnetic field.

2) Planar motion of the 180° domain wall is assumed in the model. The result is a plane wave solution to the elastic equations of motion. In most real ferromagnetic materials where the early stage of magnetization takes place by small discontinuous jumps of domain walls (which are called Barkhausen jumps). A plane model is inaccurate. A improved approach would look at the elastic radiation field from a small source. In such a model the radiation in the near field and far field should be considered.

3) Additional terms in the magnetoelastic energy should be included. Contribution from exchange elastic energy, and possible rotational effects should be incorporated.

4) The model should be extended to domain wall velocities up to and above the speed of sound in a material.

5) The reciprocal response of the domain wall and elastic radiation, i.e. absorption, should also be considered. This could enhance the understanding of the dynamics of magnetization in a multidomain material. The existence of both domain wall emission and absorption of elastic radiation could be used to produce a controlled cascaded acoustic source.

Additional work is required to explore the consequences of the magnetization distribution proposed for a moving 180° domain wall. This should include numerical micromagnetic modeling of the magnetic system starting with the magnetization distribution developed in this thesis. The methodology should be similar to the approach used by Scheinfein et al. [1989 and 1991].

Finally experiments which can utilize the development of the tunneling transducer should be pursued. One interesting experiment is the direct measurement of the local strain field in the vicinity of the domain wall. This could be done by moving the domain wall underneath the tip of the tunneling transducer. For a 1000Å domain wall in SiFe (assuming 1 Oe applied magnetic field) the time for traversal under the tunneling tip is greater than 1μs.

Appendix A: Magnetic Energy Terms Used for Domain Wall Modeling

A.1 Introduction

The modeling in this thesis requires the use of magnetic energy in a ferromagnetic material. This appendix present a brief review of three of these contributing terms; exchange, magnetocrystalline anisotropy and magnetoelastic energies. A number of reviews are referenced that contain more in depth presentations of the energies discussed here.

A.2 Magnetic Exchange Energy

In Chapter II the exchange energy is introduced. Although this energy (equation (II.4)) is often called the exchange energy it is more accurately referred to by Landau and Lifshitz [1982] as the "non-uniformity energy" because it is reflects the change in the exchange energy as magnetic moment non-uniformity is introduced into the ordered magnetic system. Equation (II.4) is a continuous classical representation of the Heisenberg ferromagnet [Akhiezer et al. 1968, Ashcroft and Mermin 1976, and Gubanov et al. 1992]. The Heisenberg ferromagnet is based on the quantum mechanical description of the non-relativistic hydrogen molecule.

For the hydrogen molecule one assumes can assume that the nuclei are fixed and a non-relativistic Hamiltonian exists for the electron system (see Akhiezer et al.[1968] for a good introduction applicable to the ferromagnetic system). The wave function of the electron system must be antisymmetric under exchange on the spin variable and the coordinates according to the Pauli principle [Schiff 1955]. Since the wave function for the nonrelativistic Hamiltonian can be written as a product of the space and spin functions, the symmetry of the space function restricts the symmetry of the spin system. For the hydrogen molecule the antisymmetric spin wave function yields the lowest energy state. In this system the exchange energy is defined as the matrix element for the electron

electrostatic interaction under exchange of electrons between nuclei. This interaction is short range.

The Heisenberg ferromagnet extends the hydrogen molecule to a crystal lattice, assuming that each atom in the crystal lattice has a localized spin **S**. In the ferromagnet the space function is antisymmetric. Thus the spin function must be symmetric, or the lowest energy state is when the spins, **S**, are aligned. The exchange contribution to the Hamiltonian for the entire system is given by

$$\mathcal{H} = -\frac{1}{2} \sum_{n \neq m} J(R_{nm})\, \mathbf{S}_n \cdot \mathbf{S}_m, \tag{A.1}$$

when $J(R_{nm})$ is the exchange integral [Ashcroft and Mermin 1976], R_{nm} is the distance between nearest neighbors which in a rigid ferromagnet is assumed to be fixed, and the summation is over nearest neighbors because of the short range nature of the exchange interaction. The exchange integral for the ferromagnetic system is positive. The Heisenberg ferromagnet is isotropic. Thus the exchange energy is sometimes referred to as isotropic exchange.

The Heisenberg ferromagnet assumes that the electrons associated with the exchange interaction are localized at the lattice site. Such a model is a reasonable picture for insulating ferromagnets, but entirely inaccurate in metallic ferromagnets. In the case of the metallic ferromagnets the itinerant electrons are involved in the exchange interaction. Attempts to use the Heisenberg ferromagnetic model to determine the magnitude and sign of the exchange integral for metallic ferromagnets has been unsuccessful [Gubanov et al. 1992]. But the exchange Hamiltonian can be used to accurately describe magnetic phenomena in metallic ferromagnets if the exchange integral is replaced by an experimentally determined exchange constant. This thesis uses the exchange energy to calculate magnetic phenomena associated with the formation and motion of domain walls. In such calculations the Heisenberg ferromagnetic approach is very successful..

The Heisenberg ferromagnet still requires a quantum mechanical approach to investigate the energy states of the magnetic system. As is point out by Kittel and Galt [1956] and Martin [1967] when dealing with a large number of lattice sites there are a large number of energy states close to the ground state of the magnetic spin system. In the ground state all spins are aligned. The energy states can be approximated by a macroscopic continuum where the spin associated with each lattice site is replaced by a continuous magnetization distribution. Here the magnetization has a constant magnitude M_s, but can rotate continuously is space. This continuum classical approach has been shown to be very successful in prediction of magnetic phenomenon including long wavelength magnetic spin waves, and domain wall properties.

The replacement of the Heisenberg ferromagnet Hamiltonian (A.1) with a continuum model results in an exchange energy:

$$f_{ex} = -\sum_{n \neq m} 2\, J_{nm}\, \mathbf{M}_n \cdot \mathbf{M}_m, \tag{A.2}$$

where $\mathbf{M}_i$ is the magnetization vector at a i-th lattice site, and J_{nm} is the exchange integral. The summation is over nearest neighbor sites. Since $\mathbf{M}$ is a continuous spatial function, $\mathbf{M}_m$ can be expanded in as a function of $\mathbf{M}_n$. For a material with cubic symmetry the summation over nearest neighbors results in and exchange energy density of

$$E_{t-ex} = E_o - \frac{2A}{M_s^2}\, \mathbf{M} \cdot \nabla^2 \mathbf{M}, \tag{A.3}$$

where A is the exchange constant. The constant term can be ignored because it is independent of local changes in the direction of magnetization. Thus the resulting exchange energy density, or the non-uniformity energy density, is written as

$$E_{ex} = -\frac{2A}{M_s^2}\, \mathbf{M} \cdot \nabla^2 \mathbf{M}. \tag{A.4}$$

A.3 Magnetocrystalline Anisotropy Energy

The magnetocrystalline anisotropy energy is a combination of a number of different contributions all of which are dependent on the crystal symmetry and the direction of the magnetization relative to the crystal lattice. The standard magnetocrystalline anisotropy energy used in domain wall theory is a classical phenomenological representation of all the anisotropic electromagnetic and quantum mechanical contributions to the magnetic energy. The form of the magnetocrystalline anisotropy is expressed to accurately represent the symmetry of the crystal lattice of the material under consideration. For this reason the forms of the magnetocrystalline anisotropy differ for cubic and uniaxial material.

A number of different sources exist for anisotropy in ferromagnetic materials. For most materials the largest source of magnetocrystalline anisotropy energy is spin-orbit coupling at a single ion [Kanamori 1963, van den Berg 1984, and O'Handley 1991]. As long as the crystal field is not perfectly symmetric [O'Handley] the orbital angular momentum can interact with the crystal field and the spin couples into the crystal symmetry via the spin-orbit interaction [Chen 1986]. Additional contributions to the magnetocrystalline anisotropy can include dipole-dipole, quadrupole-quadrupole, pseudipolar interactions and spin-orbit couple between different lattice sites. In most cases these contributions are much smaller than the single ion spin-orbit coupling.

A continuum classical model for magnetocrystalline anisotropy is typically used in domain wall calculations. In this approach the crystal symmetry restricts the form of the anisotropy energy. The two crystal symmetries used in this thesis are the cubic and the uniaxial. For the cubic case the anisotropy energy can be expanded in term of the direction cosines (α_1, α_2, α_3) of the magnetization vector relative to the crystal axes. Utilizing the fact that any change in sign of the magnetization, i.e. a rotation of 180°, should leave the energy unchanged, all odd powers of the direction cosines vanish.

Since all three direction (1, 2, 3) are equal in the cubic material the magnetocrystalline anisotropy energy density for a cubic material can be written:

$$E_a = K_1[\alpha_1^2 \alpha_2^2 + \alpha_1^2 \alpha_3^2 + \alpha_2^2 \alpha_3^2] + K_2[\alpha_1^2 \alpha_2^2 \alpha_3^2] + ..., \quad (A.5)$$

where K_1 and K_2 are anisotropy constants. The dominant term is usually K_1. If K_1 is positive then the [100], [010], and [001] directions are called easy directions because E_a is a minimum when the magnetization points in these directions. If K_1 is negative than the [111] directions are called easy directions because E_a is a minimum when the magnetization points in these directions [Chikazumi 1986].

For the uniaxial material there is only one easy axis. The expansion of the magnetocrystalline anisotropy energy density is in terms of one angle:

$$E_a = K_{u1} \sin^2 \theta + K_{u2} \sin^4 \theta + ..., \quad (A.6)$$

where K_{u1} and K_{u2} are uniaxial anisotropy constants and θ is a measure of the direction of the magnetization vector relative to the easy direction. Again the requirement that rotation through 180° leaves the energy unchanged is used.

A.4 Magnetoelastic Energy

Both the exchange energy density and the anisotropy energy density are derived assuming the crystal lattice is rigid. If this constraint is relaxed, then as the crystal lattice is strained both of these energy contributions will change [Kittel and Galt 1956, Callen and Callen 1973, Brown 1966 and 1967, Turov 1965]. This results in two magnetoelastic energies which are called magnetostriction energy, referred to a magnetoelastic energy in this thesis, and exchange elastic energy. Rotation effects [Brown 1965 and 1966, and Auld 1968] are not included in this treatment.

The magnetostriction energy comes from the strain modification of the crystal field- spin orbit couple responsible for magnetocrystalline anisotropy energy [Kanamori 1963]. If the cubic magnetocrystalline anisotropy energy is expanded to first order in strain the resultant energy can be written

$$f_{mag-el} \approx E_a + G_{ij}\, e_{ij}\, \alpha_k\, \alpha_l, \tag{A.7}$$

where E_a is the anisotropy energy density and the terms in Gij are the magnetostriction energy. The magnetostriction energy can be rewritten as

$$\begin{aligned} f_{mag} = B_1 \left[e_{xx} \left(\alpha_1^2 - \frac{1}{3} \right) + e_{yy} \left(\alpha_2^2 - \frac{1}{3} \right) + e_{zz} \left(\alpha_3^2 - \frac{1}{3} \right) \right] \\ + 2\, B_2 \left[\alpha_1\, \alpha_2\, e_{xy} + \alpha_2\, \alpha_3\, e_{yz} + \alpha_1\, \alpha_3\, e_{xz} \right], \end{aligned} \tag{A.8}$$

where B_1 and B_2 are magnetoelastic constants [Kittel and Galt 1956, and Chikazumi 1986].

The exchange integral in equation (A.1) is dependent on the separation of the nearest neighbors, and is thus sensitive to strain in the crystal lattice. A formulation of the effect of strain on the classical continuum model for exchange energy can be found by expanding equation (A.4) in terms of the strain tensor [Brown 1966]:

$$f_{ex-el} = b_{jklm}\, e_{jk} \left[\frac{\partial \alpha_i}{\partial x_l} \frac{\partial \alpha_i}{\partial x_m} \right], \tag{A.9}$$

where b_{jklm} are the exchange elastic constants, and e_{jk} is the strain tensor. This type of exchange elastic energy, sometime called exchange striction, is normally considered small compared to the magnetostrictive energy, because in most cases the spatial rotation of the magnetization vector is small. Within a domain wall the spatial rotation of the domain wall is quite large. This results in an exchange energy density which is on the same order of magnitude as the magnetocrystalline anisotropy energy density. Still the current work in elastic phenomenon associated with domain wall excludes exchange elastic energy [Maugin and Miled 1986, and How et al. 1989]. Estimate of the effect of exchange

striction are beyond the scope of this thesis. But inclusion of this effect in domain wall elastic theory is needed.

Appendix B: Magnetoelastic Strain in a Cubic Material

Lifshitz [1944] investigated the magnetic domain wall structure of cubic materials, including the effects of magnetostriction on the total energy of the magnetic system. In his paper, the magnetization within the domain wall is determined by minimizing the four energy contributions: exchange, anisotropy, magnetoelastic and elastic strain. The magnetostatic self energy is assumed to be zero and there is no external field. Lifshitz asserts that if one postulates the existence of a planar domain wall, then the magnetization is only a function of the normal to that plane (here the y-direction). Likewise he suggests that the strain tensor must also depend only on that normal direction. From these assumptions, and using the equilibrium conditions on the stress tensor, Lifshitz concluded that the strain within the infinite material must be constant and equal to the strain in the uniformly magnetized regions of the material.

The suggestion that the strain field is constant throughout the material presupposes and implies that the domain wall does not influence the strain field within the material. This appendix presents Lifshitz' argument, but carries out the complete calculations for the strain field. It is shown below that the approximations made by Lifshitz are invalid and lead to an actual strain field with an infinite limiting value as the infinite boundaries are approached. In addition, a brief discussion is presented in which an exchange magnetoelastic term is included with the energy terms.

Starting with the assumption that the domain wall is x-z planar and infinite it is concluded that the magnetization, strain and stress fields are functions of y only. Lifshitz has employed the infinitesimal strain approximation, the strains are all first order in the spatial derivatives of the displacement vector,

$$e_{ij} = \frac{1}{2}\left(u_{i,j} + u_{j,i}\right), \tag{B.1}$$

where the use of the subscript i,j implies the derivative of the i-th component with respect to the j-th direction [Landau and Lifshitz 1970]. General functions for the diagonal components of the strain tensor are given by

$$\begin{aligned} e_{xx} &= f_1(y), \\ e_{yy} &= f_2(y), \\ e_{zz} &= f_3(y). \end{aligned} \tag{B.2}$$

Upon integration of these general strain functions using the infinitesimal strain approximation the three components of the displacement vector are derived:

$$\begin{aligned} u_x &= f_1(y)\, x + g_1(y, z), \\ u_y &= \int f_2(y)\, dy + g_2(x, z), \\ u_z &= f_3(y)\, z + g_3(x, y). \end{aligned} \tag{B.3}$$

From these expressions one can calculate the off diagonal components of the strain tensor:

$$\begin{aligned} 2\, e_{xy} &= \frac{\partial\, g_1(y, z)}{\partial\, y} + x\, \frac{d\, f_1(y)}{d\, y} + \frac{\partial\, g_2(x, z)}{\partial\, x}, \\ 2\, e_{yz} &= \frac{\partial\, g_3(x, y)}{\partial\, y} + z\, \frac{d\, f_3(y)}{d\, y} + \frac{\partial\, g_2(x, z)}{\partial\, z}, \\ 2\, e_{xz} &= \frac{\partial\, g_3(x, y)}{\partial\, x} + \frac{\partial\, g_1(y, z)}{\partial\, z}. \end{aligned} \tag{B.4}$$

Since the strains are only a function of y, using the expression for e_{xz} one can determine the dependence of $g_1(y, z)$ and $g_3(x, y)$ on both x and z.

$$g_1(y, z) = g_1(y)\, z + h_1(y) \quad \text{and} \quad g_3(x, y) = g_3(y)\, x + h_3(y). \tag{B.5}$$

Thus one can rewrite the strains e_{xy} and e_{yz} as

$$2\,e_{xy} = z\,\frac{d\,g_1(y)}{d\,y} + \frac{d\,h_1(y)}{d\,y} + x\,\frac{d\,f_1(y)}{d\,y} + \frac{\partial\,g_2(x,\,z)}{\partial\,x},$$
$$2\,e_{yz} = x\,\frac{d\,g_3(y)}{d\,y} + \frac{d\,h_3(y)}{d\,y} + z\,\frac{d\,f_3(y)}{d\,y} + \frac{\partial\,g_2(x,\,z)}{\partial\,z}. \tag{B.6}$$

The strains e_{xy} and e_{yz} can only be functions of y. In order to satisfy this requirement $g_2(x, z)$ must be written as

$$g_2(x,\,z) = \alpha\,x^2 + \beta\,z^2 + \gamma\,x\,z + k_1\,x + k_2 + k_3\,z. \tag{B.7}$$

Note that α, β, γ, and k_i's are unknown constants. Substituting this into the expressions B.6 for e_{xy} and e_{yz} it can be shown that

$$\frac{d\,f_1}{d\,y} = -\,2\,\alpha, \quad \frac{d\,g_1}{d\,y} = -\,\gamma, \tag{B.8a}$$

and

$$\frac{d\,f_3}{d\,y} = -\,2\,\beta, \quad \frac{d\,g_3}{d\,y} = -\,\gamma. \tag{B.8b}$$

This results in expressions for the g_i and f_i functions as follows:

$$\begin{aligned}
g_1(y,\,z) &= -\,\gamma\,y\,z + d_1\,z + h_1(y) + \delta_1,\\
g_2(x,\,z) &= \alpha\,x^2 + \beta\,y^2 + \gamma\,x\,z + O(x,\,z)) + \delta_2,\\
g_3(x,\,y) &= -\,\gamma\,y\,x + d_3\,x + h_3(y) + \delta_3,\\
f_1(y) &= -\,2\,\alpha\,y + \delta_4,\\
f_2(y) &= f_2(y),\\
f_3(y) &= -\,2\,\beta y + \delta_6,
\end{aligned} \tag{B.9}$$

where d_i and δ_i are constants.

The strain tensor can now be determined to be

$$\begin{aligned} e_{xx} &= -2\,\alpha\, y + c_1, \\ e_{yy} &= f_2(y), \\ e_{zz} &= -2\,\beta\, y + c_3, \\ e_{xy} &= \frac{1}{2}\frac{d\,h_1(y)}{d\,y} + c_4, \\ e_{xz} &= -2\,\gamma\, y + c_5, \\ e_{yz} &= \frac{1}{2}\frac{d\,h_2(y)}{d\,y} + c_6, \end{aligned} \tag{B.10}$$

where c_i are constants.

Contrary to what Lifshitz states the e_{xx}, e_{zz} and e_{xz} are not necessarily constants. If it is assumed that α, β, and γ are zero then the conclusion by Lifshitz that e_{xx}, e_{zz} and e_{xz} are constants is accurate. The argument used to equate α, β, and γ to zero is the need to prevent the strain from becoming infinite as y approaches $\pm\infty$. It is apparent that if α, β, and γ are non-zero then the infinitesimal strain approximation is invalid for the infinite material. The strain tensor must be determined using finite strain theory.

There are still a number of restrictions on the strain and stress field in a material in equilibrium. These constraints can be used to further determine the strain field within the magnetic material. The next condition is the force equilibrium condition, $\sigma_{ij,j} = 0$ [Landau and Lifshitz 1970]. If it is assumed that $\sigma_{ij}(y)$ is a function of y only. Then the force equilibrium condition yields that $\sigma_{ix,x} + \sigma_{iy,y} + \sigma_{iz,z} = 0$, or σ_{iy} is a constant for i = x, y, and z. This give a stress tensor with m_i constant:

$$\boldsymbol{\sigma} = \begin{bmatrix} \sigma_{xx} & m_1 & \sigma_{xz} \\ m_1 & m_2 & m_3 \\ \sigma_{xz} & m_3 & \sigma_{zz} \end{bmatrix}. \tag{B.11}$$

The final condition on the stress tensor, that does not employ a direct model for the magnetic-elastic coupling, is the requirement that at the surfaces the normal component of the stress tensor is zero when the materials is subject to no external forces [Landau and Lifshitz 1970]:

$$\boldsymbol{\sigma} \cdot \mathbf{n}_s = 0. \tag{B.12}$$

Here an additional restriction on the system is imposed. As is discussed in Chapter II in a finite material, on a surface orthogonal to the x- and z-directions, the magnetization distribution is a function of both x and z. These surfaces contain the closure domains and surface Néel walls [Scheinfein et al. 1989 and 1991]. For the infinite material these effects are still present, they are just ignored because of the assumption that the domain wall is investigated an arbitrarily large distance from all surfaces. Thus the symmetry assumed in the earlier stages of the model for the strain and stress fields in the material is invalid near the closure domains and surface Néel walls. For this reason it is valid to assume $\sigma_{ij}(y)$ holds only on the two surfaces orthogonal to the y-direction. On these surfaces, at $y = \pm \infty$, it is possible to evaluate (B.12) using the stress tensor given in (B.11). This gives

$$\boldsymbol{\sigma} = \begin{bmatrix} \sigma_{xx} & 0 & \sigma_{xz} \\ 0 & 0 & 0 \\ \sigma_{xz} & 0 & \sigma_{zz} \end{bmatrix}. \tag{B.13}$$

The dependence of σ_{xx}, σ_{xz} and σ_{zz} cannot be determined without more restrictions on the stress and strain tensors.

Th effect the domain wall has on the strain and stress fields within the material can be determined by modeling the magnetic-elastic interaction in the material. The model will assume that the only coupling is through the standard magnetoelastic energy, the energy based on magnetocrystalline anisotropy. If this is assumed for the cubic material, then the total energy density within the material, dependent on strain, is:

$$
\begin{aligned}
f = B_1\left[e_{xx}\left(\alpha_1^2-\frac{1}{3}\right)+e_{yy}\left(\alpha_2^2-\frac{1}{3}\right)+e_{zz}\left(\alpha_3^2-\frac{1}{3}\right)\right] \\
+ B_2\left[\alpha_1\,\alpha_2\,e_{xy}+\alpha_2\,\alpha_3\,e_{yz}+\alpha_1\,\alpha_3\,e_{xz}\right] \\
+\frac{1}{2}c_{11}\left(e_{xx}^2+e_{yy}^2+e_{zz}^2\right)++\frac{1}{2}c_{44}\left(e_{xy}^2+e_{yz}^2+e_{xz}^2\right) \\
c_{12}\left(e_{xx}\,e_{yy}+e_{yy}\,e_{zz}+e_{xx}\,e_{zz}\right),
\end{aligned}
\tag{B.14}
$$

where α_i are the direction cosines relative to the easy directions of magnetization in the crystal, B_1 and B_2 are the magnetoelastic coefficients and c_{11}, c_{12}, and c_{44} are the elastic moduli [Chikazumi 1986]. The relationship between the stress and strain tensor is given by [Landau and Lifshitz 1970],

$$\sigma_{ij}=\frac{\partial f}{\partial e_{ij}}. \tag{B.15}$$

For the domain wall in which the magnetization is restricted to rotate only in the x-z plane, the direction cosine $\alpha_2 = 0$. The stress tensor can then be determined using (B.13), (B.14) and (B.15):

$$
\begin{aligned}
\sigma_{xx} &= B_1\left(\alpha_1^2-\frac{1}{3}\right)+c_{11}\,e_{xx}+c_{12}\left(e_{yy}+e_{zz}\right), \\
\sigma_{yy} &= 0 = -\frac{1}{3}B_1\ +c_{11}\,e_{yy}+c_{12}\left(e_{xx}+e_{zz}\right), \\
\sigma_{zz} &= B_1\left(\alpha_3^2-\frac{1}{3}\right)+c_{11}\,e_{zz}+c_{12}\left(e_{xx}+e_{yy}\right), \\
\sigma_{xy} &= 0 = c_{44}\,e_{xy}, \\
\sigma_{yz} &= 0 = c_{44}\,e_{yz}, \\
\sigma_{xz} &= B_2\,\alpha_1\,\alpha_3+c_{44}\,e_{xz}.
\end{aligned}
\tag{B.16}
$$

The conclusion from this is that e_{xy} and e_{yz} are zero. Also solving for e_{yy} one finds that

$$e_{yy}=-\frac{c_{12}}{c_{11}}\left(e_{xx}+e_{zz}\right)+\frac{B_1}{3\,c_{11}}. \tag{B.17}$$

This implies that e_{yy} is also a linear function of y (equation (B.10)).

It is apparent that components of the strain and stress tensors approach infinity in the limit of y approaching infinity. The flaw in the argument is that an infinite material, in which the region being investigated is far from the closure domains and surface Néel walls, cannot be modeled using the infinitesimal strain approximation to determine the strain tensor. It may be possible to use the infinitesimal strain approximation in the vicinity of the domain wall. But this does not permit the extension of the conditions to infinity.

It is apparent that Lifshitz' [1944] conclusion that all the components of the strain tensor in a cubic material with a single planar domain wall are constants is not valid for the magnetic material. The implication that the domain wall does not affect the strain distribution within the magnetic material is incorrect. In order to determine the strain field in the vicinity of the domain wall a different approach is required.

The correct method for determining the strain distribution within the material requires that the strain tensor be determined from the local stress requirements. This is then substituted into the total energy of the material, and that energy is minimized. Since the actual value of the magnetoelastic energy is quite small, relative to the anisotropy and exchange energy in the vicinity of the domain wall, it is possible to approach this using perturbation theory. This perturbation approach is used in Chapter III of this thesis to determine the elastic emission from a moving 180° domain wall. The actual strain distribution in the vicinity of the domain wall is not calculated in this thesis.

Appendix C: Magnetization Comparison with Walker Solution

The elastic radiation from a moving 180° domain wall calculated in this thesis is determined postulating the component of magnetization normal to the direction of motion (see Chapter IV). In addition, the applied magnetic field and damping are assumed to exactly cancel yielding the simple differential equations (IV.17) and (IV.27). The major difference between the results obtained in Chapter IV and the Walker solution for the moving domain wall [Dillon 1963 and Schryer and Walker 1974] is that in this thesis the magnetization in the direction of motion is not assumed to be constant as it is in the Walker solution. It is shown in this appendix that for low domain wall velocity the non-constant cant angle solution yields the same linear relationship between velocity and applied magnetic field. In addition, the energy density is lower than that of the Walker solution. Thus the magnetization distribution derived in this thesis is considered better solution.

A complete set of magnetic field equations for the 180° domain wall in a cubic material can be written as follows:

$$H_x = -\frac{2K_1}{M_s}\sin\theta + \frac{2A}{M_s}\frac{\partial^2 \sin\theta}{\partial y^2} - \frac{\lambda}{|\gamma|}\cos\theta\frac{\partial\theta}{\partial t}, \tag{C.1a}$$

$$H_y = -\left(\frac{2K_1}{M_s} + \frac{M_s}{\mu_o}\right)\phi + \frac{2A}{M_s}\frac{\partial^2\phi}{\partial y^2} - \frac{\lambda}{|\gamma|}\frac{\partial\phi}{\partial t}, \tag{C.1b}$$

$$H_z = \frac{2A}{M_s}\frac{\partial^2\cos\theta}{\partial y^2} + H_o + \frac{\lambda}{|\gamma|}\sin\theta\frac{\partial\theta}{\partial t}, \tag{C.1c}$$

where the applied field, H_o, is in the z-direction. These equations use an "effective" uniaxial anisotropy for the cubic material as discussed in Chapter II. The last term in each field expression is an effective field to account for the Gilbert damping term [Gilbert 1955, and How et al. 1989], where λ is the Gilbert damping parameter which accounts

for the *viscous* damping in the magnetic material. The behavior of M can be investigated using the magnetic field expressions (C.1) and the Landau Lifshitz equation of motion:

$$\frac{1}{|\gamma|}\frac{\partial \mathbf{M}}{\partial t} = -\mathbf{M}\times\mathbf{H}. \tag{C.2}$$

The y component of equation (C.2) is used to find the velocity versus applied magnetic field relationship. The magnetization can be written in terms of the direction cosines (equations (IV.11)), assuming, as is done throughout this thesis, that the cant angle is small. Thus the resulting differential equation for the time rate of change of ϕ is given by

$$\frac{M_s}{2K_1|\gamma|}\frac{\partial \phi}{\partial t} = \frac{M_s \lambda}{2K_1|\gamma|}\frac{\partial \theta}{\partial t} + \frac{H_o M_s}{2K_1}\sin\theta + \sin\theta\cos\theta - \Delta^2\frac{\partial^2\theta}{\partial y^2}. \tag{C.3}$$

In Chapter IV it is postulated that the component of magnetization normal to the direction of motion of the domain wall is not a constant, but given by

$$\phi = \phi_{max}\sin\theta, \tag{C.4}$$

resulting in equation (IV.14) being satisfied for the following direction cosine relations:

$$\begin{aligned}
\sin\theta &= \pm\,\mathrm{sech}\left(\frac{y(t)}{\Delta'}\right),\\
\phi &= \frac{v_y \mu_o}{M_s|\gamma|\Delta'}\,\mathrm{sech}\left(\frac{y(t)}{\Delta'}\right),\\
\cos\theta &= -\tanh\left(\frac{y(t)}{\Delta'}\right),
\end{aligned} \tag{C.5}$$

where $M_s|\gamma|\Delta'/\mu_o = 2v_w$. Equation (C.3) can now be simplified using these solutions yielding

$$-\frac{\lambda}{|\gamma|}\frac{\partial\theta}{\partial t} = H_o\sin\theta. \tag{C.6}$$

Equation (C.6) can be solved for the steady state case, $y(t) = y - v_y t$, using equation (C.5) where

$$\frac{\partial \theta}{\partial t} = \frac{v_y}{\Delta'} \sin \theta, \tag{C.7}$$

resulting in a linear velocity field relationship:

$$v_y = -\frac{\Delta' |\gamma|}{\lambda} H_o. \tag{C.8}$$

This is identical to that determined by Dillon [1963] and Schryer and Walker [1974] for the case of a small cant angle. But in this solution the component of magnetization in the direction normal to the direction of motion is not a constant cant angle. This linear applied magnetic field-velocity relationship is observed experimentally [Williams et al. 1950 and Chikazumi 1986]. The two other components of equation (C.2) can be reduced to equation (C.7) to $O(v_y)$. Thus for small velocity the solution to the Landau and Lifshitz equation derived in this thesis is self consistent.

A comparison between the Walker solution and the model presented in this thesis can be made by comparing the magnetic energy density for the two cases. The general energy density expression for the system can be written [Schryer and Walker 1974] as

$$f = -H_o M_z + \frac{1}{2\mu_o} |\mathbf{M}|^2 + \frac{K_1}{M_s^2}\left(M_x^2 + M_y^2\right) + \frac{A}{M_s^2}\left|\frac{\partial \mathbf{M}}{\partial y}\right|^2. \tag{C.9}$$

Since the only terms that differ between the Walker solution and equation (C.5) involve M_y, all terms independent of M_y are identical in both models and can be ignored in the comparison. The energy density for the Walker solutions is given by

$$f_w = \frac{M_s^2}{2\mu_o} \phi_o^2 + K_1 \phi_o^2 + A\left(\frac{\partial \phi_o}{\partial y}\right)^2. \tag{C.10}$$

ϕ_o is the constant cant angle. Using the expression for ϕ_o derived by Schryer and Walker, the Walker solution energy density can be written as

$$f_W = \frac{\mu_o H_o^2}{2\lambda^2}\left(1 + \frac{2K_1\mu_o}{M_s^2}\right). \tag{C.11}$$

Thus the energy density is constant. This is compared on a point by point basis to the energy density calculated using the magnetization distribution derived in this thesis.

For the solution given in equation (C.5) the energy density is given by

$$\begin{aligned} f_A = {} & \frac{v_y^2\mu_o^2}{2\mu_o(|\gamma|\Delta')^2}\operatorname{sech}^2\left[\frac{y(t)}{\Delta'}\right] + K_1\left(\frac{v_y\mu_o}{M_s|\gamma|\Delta'}\right)^2\operatorname{sech}^2\left[\frac{y(t)}{\Delta'}\right] \\ & + A\left(\frac{v_y\mu_o}{M_s|\gamma|\Delta'^2}\right)^2\operatorname{sech}^2\left[\frac{y(t)}{\Delta'}\right]\tanh^2\left[\frac{y(t)}{\Delta'}\right] \end{aligned} \tag{C.12}$$

This can be rewritten using the expression for the velocity of the domain wall, (C.8)

$$f_A = \frac{\mu_o H_o^2}{2\lambda^2}\operatorname{sech}^2\left(\frac{y(t)}{\Delta'}\right)\left(1 + \frac{2K_1\mu_o}{M_s^2}\left(1 + \tanh^2\left(\frac{y(t)}{\Delta'}\right)\right)\right). \tag{C.13}$$

f_A is not a constant, but is a function of the spatial variable y. The maximum value of f_A exists when

$$\tanh^2\left(\frac{y(t)}{\Delta'}\right) = -\frac{4K_1\mu_o}{M_s^2}. \tag{C.14}$$

This can be substituted into (C.13) yielding

$$f_A = \frac{\mu_o H_o^2}{2\lambda^2}\operatorname{sech}^2\left(\frac{y(t)}{\Delta'}\right)\left(\frac{1}{2} + \frac{2K_1\mu_o}{M_s^2}\right). \tag{C.15}$$

The hyperbolic secant function is not substituted since it is always less than or equal to 1.

Using expression (C.15), f_A can be compared to f_W given in equation (C.11). The comparison reveals that $f_A < f_W$ for all values of y. Thus the energy density of the magnetization distribution determined in this thesis is always less than the Walker solution. Although a domain wall with non-constant cant angle produces in increase in exchange energy density compared to the Walker solutions, both the anisotropy and magnetostatic self energies densities are much smaller for the non-constant cant angle. This results in the lower energy density. The lower energy density suggests that the magnetization distribution derived in this thesis is more energetically favorable than the Walker solution for small 180° domain wall velocity. In addition the distribution derived in this thesis is consistent with the velocity versus applied magnetic field relation observed for the domain wall.

References

Aharoni, A., and Jakubovics, J.P., (1991), "Magnetic Domain Walls in Thick Iron Films", *Physical Review B*, **43**; (1) 1290.

Akhiezer, A.I., Bar'yakhtar, V.G., and Peletminskii, (1968), Spin Waves, translated by Chomet, S., North Holland Publishing Company, Amsterdam.

Amazigo, J.C., and Rubenfeld, L.A., (1980), Advanced Calculus, John Wiley and Sons, New York.

Ashcroft, N.W., and Mermin, N.D., (1976), Solid State Physics, Saunders College, Philadelphia.

Auld, B.A., (1968), "Nonlinear Interaction of Spin Waves and Elastic Waves", Advances in Microwaves, Volume III, Young, L. editor, Academic Press, New York.

Auld, B.A, (1971), "Magnetostatic and Magnetoelastic Wave Propogation in Solids", Applied Solid State Science: Advances in Materials and Device Research, Volume II, Wolfe, R. editor, Academic Press, New York, 347

Auld, B.A., (1990), Acoustic Fields and Waves in Solids, Volume I, Robert E Krieger Publishing Company, Malabar, Florida, 1.

Binning , G., and Rohrer, H., (1986), "Scanning Tunneling Microscopy", *IBM Journal of Research and Development*, **30**; (4) 355.

Binning , G., and Rohrer, H., (1982), "Scanning Tunneling Microscopy", *Helvetica Physica Acta*, **55**; 726.

Breckenridge F.R., Tschiegg, C.E., and Greenspan, M., (1975), "Acoustic Emission: Some Applications of Lamb's Problem", *Journal of Acoustical Society of America*, **57**; (3) 626.

Brizzolara, R.A., and Colton, R.J., (1990), "Magnetostriction Measurements Using a Tunneling-Tip Strain Detector", *Journal of Magnetism and Magnetic Materials*, **88**; 343.

Brizzolara, R.A., and Colton, R.J., (1992), "The Magnetostriction of CoFeNiMo Metallic Glasses Measured with a Tunneling Transducer", *Journal of Magnetism and Magnetic Materials*, **103**; 111.

Brown Jr., W.F., (1962), Magnetostatic Principles in Ferromagnetism, North-Holand Publishing Company, Amsterdam.

Brown Jr., W.F., (1963), Micromagnetics, Interscience Publishers, New York.

Brown Jr., W.F., (1965), "Theory of Magnetoelastic Effects in Ferromagnetism", *Journal of Applied Physics*, **36**; (2) 994.

Brown Jr., W.F., (1966), Magnetoelastic Interactions, Springer-Verlag, Berlin.

Burkhardt, G.L., Beissner, R.E., Matzkanin, G.A., and King, J.D., (1982), "Acoustic Methods for Obtaining Barkhausen Noise Stress Measurements", *Materials Evaluation*, **40**; (5) 669.

Buttle, J.D., Briggs, G.A.D., Jakubovics, J.P., Little, E.A., and Scruby, C.B., (1986), "Magnetoacoustic and Barkhausen Emission in Ferromagnetic Materials", *Philosophical Transactions of the Royal Society of London A*, **320**; 363.

Buttle, D.J., Scruby, C.B., Jakubovics, J.P., and Briggs, G.A.D., (1987), "Magneto-acoustic and Barkhausen Emission: Their Dependence on Dislocations in Iron", *Philosophical Magazine A*, **55**; (6) 717.

Buttle D.J., Dalzell, W., Scruby, C.B., and Langman, R.A., (1990), "Comparison of Three Magnetic Techniques for Biaxial Stress Measurements", Review of Progress in Quantitative Nondestructive Evaluation, Volume 9B, Thompson, D.O., and Chimenti, D.E., editors, Plenum Press, New York, 1879.

Callen E., and Callen H.B., (1963) "Magnetostriction, Forced Magnetostriction, and Anomalous Thermal Expansion in Feromagnets", *Physical Review*, **139**, (2A) A457.

Callen E., and Callen H.B., (1965) "Static Magnetoelastic Coupling in Crystals", *Physical Review*, **129**, (2) 578.

Callen, H.B., and Goldberg, N., (1965), "Magnetostriction of Polycrystalline Aggregates", *Journal of Applied Physics*, **36**; (3-II) 976.

Chen, C.W., (1986), Magnetism and Metallurgy of Soft Magnetic Materials, Dover Publications, Incorporated, New York.

Chen, C.J., (1993), Introduction to Scanning Tunneling Microscopy, Oxford University Press , New York.

Chikazumi, S., (1986), Physics of Magnetism, Robert E. Krieger Publishing Co., Malabar, Florida.

Cullity, B.D., (1972), Introduction to Magnetic Materials, Addison-Wesley Publishing Company, Reading Massachusetts.

Dillon, J.F., Jr., (1963), "Domains and Domain Walls", Magnetism, Volume III, Rado, G.T., and Suhl, H., editors, Academic Press, New York, 415.

Dillon, J.F., Jr. and Earl, E.H., Jr., (1959), "Domain Wall Motion and Ferrimagnetic Resonance in a Manganese Ferrite", *Journal of Applied Physics*, **30**; (2) 202.

Dionne, G.F., and Goodenough, J.B., (1972), "Effects of Co^{2+} and Mn^{3+} Ion Substitution on the Anisotropy and Magnetostriction Constants of $Y_3Fe_5O_{12}$", *Materials Research Bulletin*, **7**; 749.

Duke, C.B., (1969), "Tunneling in Solids", Solid State Physics: Advances In Research and Applications, Supplement 10, Seitz, F. and Turnbull, D., editors, Academic Press Inc., New York.

Edward, C., and Palmer, S.B., (1987), "The Effect of Stress and Sample Shape on the Magnitude and Frequency of Magnetomechanical Acoustic Emission", *Journal of the Acoustical Society of America*, **82**; (2) 534.

Eschenfelder, A.H., (1980), Magnetic Bubble Technology, Springer-Verlag, Berlin.

Evans, A.G., and Linzer, M., (1977), "Acoustic Emission in Brittle Materials", Annual Review of Materials Science, Volume VII, Huggins, R.A., Bube, R.H., and Roberts, R.W., editors, Annual Reviews, Inc., Palo Alto, 179.

Galt, J.K., (1952), "Motion of a Ferromagnetic Domain Wall in Fe_3O_4", *Physical Review*, **85**; (4) 664.

Gilbert, T.L., (1955), "A Lagrangian Formulation of the Gyromagnetic Equation of Motion of the Magnetization Field", *Physical Review*, **100**; 1243.

Gradshteyn, I.S., and Ryzhik, I.M., (1980), Table of Integrals, Series and Products, Academic Press, New York, (integral number 2.584.68) 165.

Gorkunov, E.S., Bartenev, O.A., and Khamitov, V.A., (1986), "Magnetoelastic Acoustic Emission in Ferrosilicon Single Crystals", *Soviet Physics Journal*, **29**; (1) 56.

Gubanov, V.A., Liechtenstein A.I., and Postnikov, A.V., (1992), Magnetism and Electronic Structure of Crystal, Springer-Verlag, Berlin.

Guyot, M., Merceron, T., and Cagan, V., (1987), "Acoustic Emission, Domain Walls and Hysteresis in YIG", *Physics Letters A*, **120**; (2) 64.

Guyot, M., Merceron, T., and Cagan, V., (1988), "Acoustic Emission alon the Hysteresis Loops of Various Ferro- and Ferrimagnets", *Journal of Applied Physics*, **63**, (8) 3855.

Guyot, M., Merceron, T., and Cagan, V., (1990a), "Does the Magnetostriction Control the Acoustic Emission?", *Journal of Magnetism and Magnetic Materials*, **83**; 217.

Guyot, M., Merceron, T., Renaudin, P., and Cagan, V., (1990b), "Thermal Investigation of the Acoustic Emission in Polycrystalline Ferrimagnets", *IEEE Transactions on Magnetics*, **26**; (5) 1828.

Guyot, M., and Cagan, V., (1991), "The Acoustic Emission along the Hysteresis Loop of Various Ferro and Ferrimagnets", *Journal of Magnetism and Magnetic Materials,* **101**; 256.

Guyot, M., and Cagan, V., (1993), "The Magneto-acoustic Emission", *Journal of Applied Physics,* **73**; (10) 5348.

Gyorgy, E.M., [1993], Bell Telephone Laboratories, Inc., Murray Hill, New Jersey, private communications.

Gyorgy, E.M., (1963), "Magnetization Reversal in Nonmetallic Ferromagnets", Magnetism, Volume III, Rado, G.T., and Suhl, H., editors, Academic Press, New York. 525.

Gyorgy, E.M., [1960], "Computer and Switching", *Journal of Applied Physics*, **31**; (5) 100S.

Higgins, F.P., and Carpenter, S.H., (1978), "Sources of Acoustic Emission Generated during the Tensile Deformation of Pure Iron", *Acta Metallurgica*, **26**; 133.

How, H., O'Handley, R.C., and Morgenthaler, F.G., (1989), "Soliton Theory for Realistic Magnetic Domain Wall Dynamics", *Physical Review B*, **40**; (7) 4808.

Jacobsen, E.H., (1960), "Sources of Sound in Piezeoelectric Crystals", *The Journal of the Acoustical Society of America*, **32**; (8) 949.

James, D.R., and Carpenter, S.H., (1971), "Relationship between Acoustic Emission and Dislocation Kinetics in Crystalline Solids", *Journal of Applied Physics*, **42**; (12) 4685.

Jiles, D., (1988), "Review of Magnetic Methods for Nondestructive Evaluation", *NDT International*, **21**; (5) 311.

Jiles, D., (1991), Introduction to Magnetism and Magnetic Materials, Chapman and Hall, London.

Kanamori, J., (1963), "Anisotropy and Magnetostriction of Ferromagnetic and Antiferromagnetic Material", Magnetism, Volume 1, Rado, G.Y. and Suhl, H., editors, Academic Press, New York.

Känzig, W., "Ferroelectrics and Antiferroelectrics", (1957), Solid State Physics: Advances In Research and Applications, Volume 4, Seitz, F. and Turnbull, D., editors, Academic Press Inc., New York, 5.

Kim, H.C., and Kim C.G., (1989), "Effect of Magnetising Frequency and Stress on Magneto-acoustic Emission for 3% Si-Fe Crystals", *Journal of Physics D: Applied Physics*, **22**; 192.

Kittel, C., (1949), "Physical Theory of Ferromagnetic Domains", *Review of Modern Physics*, **21**; (4) 541.

Kittel, C. and Galt., J.K., (1956), "Ferromagnetic Domain Theory", Solid State Physics: Advances In Research and Applications, Volume 3, Seitz, F. and Turnbull, D., editors, Academic Press Inc., New York, 437.

Kolsky, H., (1963), Stress Waves in Solids, Dover Publishing, Inc., New York.

Krause, R.F., (1992), Magnetics International, Inc., Burns Harbor, Indiana, private communications.

Krinchik G.S. and Benidze, O. M., (1974), "Magneto-Optic Investigation of Magnetic Structures under Micron Resolution Conditions", *Soviet Physics JETP*, **40**; (6) 1081.

Kuleev, V.G., Shcherbinin, V.E., Zhakov, S.V., Subbotin, Y.S., and Men'shikov, N.M., (1986), "Effect of Physical Differences between the Barkhausen Effect and Barkhausen Acoustic Emission on Their Application in Nondestructive Inspection", *Soviet Journal of NDT*, **22**; 573.

Kusanagi, H., Kimura, H., and Sasaki, H., (1979a), "Acoustic Emission Characteristics During Magnetization of Ferromagnetic Materials", Fundamentals of Acoustic Emission, Ono, K., editor, the Joint Meeting of the Acoustical Societies of America and Japan, 309.

Kusanagi, H., Kimura, H., and Sasaki, H., (1979b) "Stress Effect on the Magnitude of Acoustic Emission During Magnetization of Ferromagnetic Materials", *Journal of Applied Physics*, **50**; (4) 2985.

Kwan, M.M, (1983), "Magnetomechanical Acoustic Emission (MAE) of Ferromagnetic Materials", Ph.D. Thesis, University of California, Los Angeles.

Kwan, M.M., Ono, K., and Shibata, M., (1984), "Magnetomechanical Acoustic Emission of Ferromagnetic Materials at Low Magnetization Levels (Type I Behavior)", *Journal of Acoustic Emission*, **3**; (3) 144.

Landau, L., and Lifshitz, E., (1935), 'On the Theory of the Dispersion of Magnetic Permeability in Ferromagnetic Bodies', *Phys. Z. SowjUn.*, **8**; 153. Reprinted in L.D. Landau: Collected Papers, D. ter Haar, editor, Gordon and Breach, Scientific Publisher, New York, 101 (1965).

Landau, L.D., and Lifshitz, E.M., (1982), Electrodynamics of Continuous Media, Pergamon Press, Oxford.

Landau, L.D., and Lifshitz, E.M., (1986), Theory of Elasticity, Pergamon Press, Oxford.

LeCraw, R.C., and Comstock, R.L, (1965), "Magnetoelastic Interactions in Ferromagnetic Insulators", Physical Acoustics, Volume III-Part B, Mason, W.P. editor, Academic Press, New York, 127.

Lifshitz, E., (1944), "On the Magnetic Structure of Iron", *Journal of Physics U.S.S.R.*, **8**; (6) 337.

Lin, C.C., Segel, L.A. and Handelman, G.H., (1974), Mathematics Applied to Deterministic Problems in the Natural Sciences, Macmillan Publishing Company, Incorporated, New York.

Lord, Jr., A.E., (1967), "Elastic Wave Radiation from Simply-Vibrating 180° Magnetic Domain Walls", *Acustica*, **18**; (4) 187.

Lord, Jr., A.E., Usatschew, R., and Robinson, M., (1974), "Acoustic Emissions Associated with Changes of Magnetization in Thin Nickel Rods", *Letters in Applied and Engineering Sciences*, **2**; 1.

Lord, Jr., A.E., (1981), "Acoustic Emission-An Update", Physical Acoustics, Volume XV, Mason, W.P., and Thurston, R.N., editors, Academic Press, New York, 289.

Lord, Jr., A.E., (1975), "Acoustic Emission", Physical Acoustics, Volume XI, Mason, W.P., and Thurston, R.N., editors, Academic Press, New York, 295.

Love, A.E.H., (1944), A Treatise on the Mathematical Theory of Elasticity, Dover Publications, Incorporated, New York.

Malén, K., and Bolin, L., (1974), "A Theoretical Estimate of Acoustic-Emission Stress Amplitude", *Physica Status Solidi B,* **61**; 637.

Malozemoff, A.P., (1979), and Slonczewski, J.C., Magnetic Domain Walls in Bubble Materials, Academic Press, New York.

Martin, D.H., (1967), Magnetism in Solids, Iliffe Books, Ltd., London.

Maugin, G.A., (1979), "Classical Magnetoelasticity in Ferromagnetic with Defects", Electromagnetic Interaction in Elastic Solids, Parkus, H., editor, Springer-Verlag, Wien, 243.

Maugin, G.A, and Miled, A., (1986), "Solitary Waves in Elastic Ferromagnets", *Physical Review B*, **33**; (7) 4839.

Melcher, J.R., (1981), Continuum Electromechanics, The M.I.T. Press, Cambridge, Massachusetts.

Mihara, A., (1992), "X-Ray Topographic Observation of Magnetic Domain Structures and 180° Walls in a (100) Crystal of Pure Iron under an External Magnetic Field", *Japanese Journal of Applied Physics*, **31**; (6A) 1793.

Mohamad, I.J., Zammit Mangion, L., Lambson, E.F., and Saunders, G.A., (1982), "Acoustic Emission from Domain Wall Motion in Ferroelectric Lead Germanate", *Journal of Physics and Chemistry of Solids*, **43**; (8) 749.

Moreau, A., and Ketterson, J.B., (1992), "Detection of Ultrasound Using a Tunneling Microscope", *Journal of Applied Physics*, **72**; (3) 861.

Morse, P.M., and Feshbach, H., (1953), Methods of Theoretical Phyics, McGraw-Hill Book Compnay, Inc., New York.

Motogi, S., and Maugin, G.A., (1984a), "Effects of Magnetostriction on Vibrations of Bloch and Néel Walls,", *Physica Status Solidi (a)*, **81**; 519.

Motogi, S., and Maugin, G.A., (1984b), "Magnetoelastic Oscillations of a Bloch Wall in Ferromagnets with Dissipation", *Japanese Journal of Applied Physics*, **23**; (8) 1026.

Namkung, M., DeNale, R., Kushnick, P.W., Grainger, J.L., and Todhunter, R.G., (1989), "Uniaxial Stress Effects on Magnetoacoustic Emission", Proceedings of the 1989 IEEE Ultrasonics Symposium, Volume 2, McAvoy, B.R., editor, IEEE Publishing Service, New York, 1167.

Namkung, M., Utrata, D., DeNale, R., and Grainger, J.L., (1991), "Effects of Uniaxial Stress on Magnetoacoustic Emission Spectra of Steel", Review of Progress in Quantitative Nondestructive Evaluation, Volume 10B, Thompson, D.O., and Chimenti, D.E., editors, Plenum Press, New York, 1959.

Ng, D.H.L., Jakubovics, J.P., Scruby, C.B., and Briggs, G.A.D., (1992a), "Effect of Stress on Magneto-acoustic Emission from Mild Steel and Nickel", *Journal of Magnetism and Magnetic Materials*, **104-107**; 355.

Ng, D.H.L., Jakubovics, J.P., Scruby, C.B., and Briggs, G.A.D., (1992b), "Effect of Biaxial Stress on Magnetoacoustic Emission from Nickel", *IEEE Transactions on Magnetics*, **28**; (5) 2214.

O'Dell, T.H., (1981), Ferromagnetodynamics, John Wiley and Sons, New York.

O'Handley, R.C., (1991), Magnetism and Magnetic Materials, unpublished.

Ono, K., (1979), "Acoustic Emission Arising from Plastic Deformation and Fracture", Fundamentals of Acoustic Emission, Ono, K., editor, the Joint Meeting of the Acoustical Societies of America and Japan, 167.

Ono, K. and Shibata, M., (1980), "Magnetomechanical Acoustic Emission in Iron and Steel", *Materials Evaluation*, **38**; (1) 55.

Ono, K., and Shibata, M., (1981), "Magnetomechanical Acoustic Emission for Residual Stress and Prior Strain Determination", Advances in Acoustic Emission, Dunegan, H.L., and Hartman, W.F., editors, Dunhart, Knoxville, 154.

Ono, K., (1986), "Magnetomechanical Acoustic Emission - A Review", Progress in Acoustic Emission III, The Japanese Society of NDI, 200.

Ott, H.W., (1976), Nosie Reduction Techniques in Electronic Systems, John Wiley and Sons, New York.

Privorotskii, I.A., (1971), "Theory of Domain Structure of Uniaxial Ferromagnets", *Soviet Physics JETP*, **32**; (5) 964.

Privorotskii, I., (1976), Thermodynamic Theory of Domain Structure, John Wiley and Son, New York.

Sarid, D., (1991), Scanning Force Microscopy, Oxford University Press, New York.

Scheinfein, M.R., Unguris, J., Celotta, R.J., and Priece, D.T., (1989), "Influence of the Surface on Magnetic Domain-Wall Microstructure", *Physical Review Letters*, **63**; (6) 668.

Scheinfein, M.R., Unguris, J., Blue, J.L., Coakley, K.J., Pierce, D.T., Celotta, R.J., and Ryan, P.J., (1991), "Micromagnetics of Domain Walls at Surfaces", *Physical Review B*, **43**; (4) 3395.

Schryer, N.L., and Walker, L.R., (1974), "The Motion of 180° Domain Walls in Uniform DC Magnetic Fields", *Journal of Applied Physcis*, **45**; (12) 5406.

Segel, L.A., (1977), Mathematics Applied to Continuum Mechanics, Macmillan Publishing Co., Inc., New York.

Shibata, M. and Ono, K., (1981), "Magnetomechanical Acoustic Emission - A New Method for Non-Destructive Stress Measurement", *NDT International*, **14**; 227.

Schiff, L.I., (1955), Quantum Mechanics, McGraw-Hill Book Company, New York.

Simmons, J.G., (1963), "Generalized Formula for the Electric Tunnel Effect between Similar Electrodes Separated by a Thin Insulating Film", *Journal of Applied Physics*, **34**; (6) 1793.

Spanner, J.C., (1974), Acoustic Emission Techniques and Applications, Intex Publishing Company, Evanston, Illinois.

Stewart, K.H., (1951), "Experiments on a Specimen with Large Domains", *Le Journal De Physique et le Radium*, **12**, 22.

Takata, Y., (1963), "Observation od Domain Structure and Calculation of Magnetostatic Energy on the c-Plane of Cobalt Single Crystals", *Journal of the Physical Society of Japan*, **18**; (1) 87.

Tukov, E.A., (1965), Physical Properties of Magnetically Ordered Crystals, Academic Press, New York.

van der Berg, H.A.M., (1984), Micromagnetics and Domains in Soft-Ferromagnetic Media, Delft University Press.

Weinstock, R. (1974), Calculus of Variations, Dover Publications, Incorporated, New York.

Williams, R.V., (1980), Acoustic Emission, Adam Hilger Ltd., Bristol, United Kingdom.

Williams, H.J., (1937), "Magnetic Properties of Single Crystal Silicon Iron", *Physical Review*, **52**; 747.

Williams, H.J., and Shockley, W., (1949), "A Simple Domain Structure in an Iron Crystal Showing a Direct Correlation with the Magnetization", *Physical Review*, **75**; (1) 178.

Williams, H.J., Bozorth, R.M., and Schockley, W., (1949), "Magnetic Domain Patterns on Single Crystals of Silicon Iron", *Physical Review*, **75**; (1) 155.

Williams, H.J., Schockley, W., and Kittel, C., (1950), "Studies of the Propagation Velocity of a Ferromagnetic Domain Boundary", *Physics Review*, **80**; (6) 1090.

Zammit-Mangion, L.J., and Saunders, G.A., (1984), "Acoustic Emission and Domain Wall Dynamics in Ferroelectric - Ferroelastic Gadolinium and Terbium Molybdate", *Journal of Physics C: Solid State Physics*, **17**; 2825.